NASA Contractor Report 4228

Probabilities and Statistics for Backscatter Estimates Obtained by a Scatterometer With Applications to New Scatterometer Design Data

Willard J. Pierson, Jr.
CUNY Institute of Marine and Atmospheric Sciences
The City College of New York
New York, New York

Prepared for
National Aeronautics and Space Administration
Oceanic Processes Branch
under Grant NAGW-690

NASA
National Aeronautics and
Space Administration
Office of Management
Scientific and Technical
Information Division

1989

TABLE OF CONTENTS

		page
	ABSTRACT	vi
1.	INTRODUCTION	
	1.1 Historical review	1
	1.2 Scatterometer design features	2
	1.3 Probability concepts	5
2.	DEFINITIONS	
	2.1 The quantities involved	8
	2.2 The probability density function	8
3.	THE MEANING OF σ^o_M	
	3.1 Backscatter theories	10
	3.2 The specification of the wind	11
4.	PROPERTIES OF EQUATION 4	
	4.1 Monte Carlo methods	13
	4.2 K_p The normalized standard deviation .	14
	4.3 The normalized expected value	14
5.	POINT ESTIMATES OF POPULATION PARAMETERS AND RANDOM INTERVALS FOR POPULATION PARAMETERS	
	5.1 The concepts	16
	5.2 Probabilities	17
	5.3 Point estimates	18
	5.4 Interval estimates	21
6.	SIMPLIFIED RESULTS FOR LARGE VALUES OF σ^o_M .	26
7.	THE SOLUTION FOR ALL VALUES OF σ^o	28

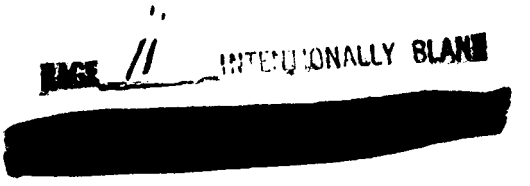

8. EXAMPLES BASED ON A NEW SCATTEROMETER DESIGN

8.1 Theoretical considerations 32

8.2 A noise only model..... 35

8.3 Position, velocity and attitude errors 35

8.4 Time correlated random variables 40

8.5 Model errors, synoptic scales and meso-scales 41

8.6 A test for t_R constant over short orbit segments 43

8.7 The Amazon rain forest 46

9. EXAMPLES BASED ON TABLE 2 FOR RANDOM INTERVALS AND RESULTS FOR A CANDIDATE MODEL FUNCTION

9.1 Assumptions 47

9.2 Random intervals 47

9.3 Interpretation in terms of a candidate model 64

9.4 The effect of constant orbit errors for fairly long times 77

10. MAXIMUM LIKELIHOOD ESTIMATES FOR $\bar{U}$ AND χ

10.1 Wind speed and direction conventions. 78

10.2 Theories and models 78

10.3 Maximum likelihood estimates of $\bar{U}$ and χ 80

11. SYSTEM AND MODEL VALIDATION .....

11.1 Comparison with conventional wind measurements 84

11.2 Comparison of maximum likelihood estimates when conventional data are unavailable 88

11.3 Detecting large wind speed discrepancies between models for vertically and horizontally polarized data 89

11.4 Detecting model errors that result from incorrect upwind-crosswind and downwind-crosswind differences 98

11.5 Additional considerations 103

11.6 Additional applications of the random intervals 106

11.7 Applications to the SEASAT-SASS data . 109

12 RESOLUTION AND WAVENUMBER ALIASING

12.1 Twenty five kilometer resolution 110

12.2 Fifty kilometer resolution 110

12.3 One hundred kilometer resolution 110

12.4 Wave number aliasing and filtering .. 112

13 FURTHER CONSIDERATION OF THE MAXIMUM LIKELIHOOD ESTIMATES

13.1 Discussion 113

13.2 Maximum likelihood estimates for a wider range of σ^o 113

14 SUMMARY

14.1 The probability density function for backscatter as a random variable ... 118

14.2 Recovering wind speed and direction estimates 119

15 ACKNOWLEDGEMENTS 120

16 REFERENCES 121

ABSTRACT

The values of the NRCS, σ^o, obtained by a scatterometer a random variables. They are random variables with the property th the variance is a known function of the expected value (or the me in a loose sense). The probability density function has featur that allow required probabilities to be obtained from the norm distribution. Models for the expected value obtain it as a functi of the properties of the waves on the ocean and the winds th generated the waves with the goal of obtaining wind speeds a directions.

A scatterometer presently in the design stage has improved fe tures compared to the SASS on SEASAT in that the backscatter valu are closely located on a well defined grid. Also the requir parameters are known from the design features of the instrument.

Point estimates of the expected value, σ^o_M, are found fr various statistics given the parameters that define the probabili density function for each value. Random intervals are derived wi a preassigned probability of containing the value, σ^o_M. statistical test to determine whether or not successive values σ^o are truly independent is derived.

Ways to correct for certain kinds of errors in a model sole by means of backscatter data are derived. Ways to use convention measurements from the National Data Buoy network to interpr backscatter models more thoroughly and to either improve them validate them are found.

The maximum likelihood estimates for wind speed and direction are found, given a model for backscatter as a function of the properties of the waves on the ocean. These estimates are biased as a result of the terms in the equation that involve natural logarithms, and calculations of the point estimates of the maximum likelihood values are used to show that the contributions of the logarithmic terms are negligible and that the terms can be omitted.

1. INTRODUCTION

1.1 Historical review. The term "scatterometer" was coined by R. K. Moore (Personal Communication, 1986) and used in the description of a radar-radiometer by Moore and Ulaby (1969). A scatterometer differs from other radars in that estimates both of the received signal power plus the receiver noise power and of the receiver noise power alone are obtained. The latter is then subtracted from the former to obtain an estimate of the received signal power alone. Both of these randomly varying quantities are measurable and of course, by definition, positive. However, if the randomly varying received signal power is very small compared to the randomly varying receiver noise power, subtracting the randomly varying noise power from the randomly varying signal plus the noise power can produce a negative value for the randomly varying estimate of the received power.

Scatterometer data are used to attempt to determine the speeds and directions of the winds over the ocean by means of backscatter estimates obtained from a scatterometer on a polar orbiting spacecraft at an altitude of about 800 km. The first attempt to do this globally was by means of the SASS on SEASAT. At first it was believed that the wind speeds and directions obtained from the backscatter estimates were quite good as in Duffy and Atlas (1986), Pierson, et al. (1984), and Woiceshyn, et al. (1985). Further studies have revealed various kinds of systematic errors in the wind recoveries, most noteably as described by Woiceshyn, et al. (1986).

1.2 Design features. Schematic versions of a new scanning pattern are shown in Figs. 1 and 2. If to scale, each square would represent an area of the ocean surface that is 25 by 25 km. Two possibilities for obtaining backscatter data for each of these areas are under consideration.

The scanning pattern as in Fig. 1 consists of 25 by 25 km squares oriented both parallel to the subsatellite track at nearly a constant, but different, incidence angle for each of the four measurements over considerable distances and normal to the track for incidence angles that vary from about 15^{o} to 59^{o}. The along track variation of the parameters associated with each backscatter value is small over distances of several hundred km, but the cross track variation is rather large. There are 24 areas, each 25 by 25 km, for a total distance of 600 km normal to the subsatellite track on each side of the track. The incidence angle, including the beam at 115^{o}, varies from about 15.6^{o} to 59.1^{o}.

One possibility, as shown in Fig. 2, is to have one vertically polarized and one horizontally polarized value for the backscatter estimates obtained from forward looking antennas at 45^{o} to the subsatellite track to the right side. A third estimate would be obtained by means of an antenna at 115^{o} to the track, quite possibly for horizontal polarization. The fourth for vertical polarization would be at 135^{o} to the track.

The second possibility is a vertically polarized estimate at 45^{o}, both vertically and horizontally polarized estimates at 115^{o} and a vertically polarized estimate at 135^{o}. The first of these

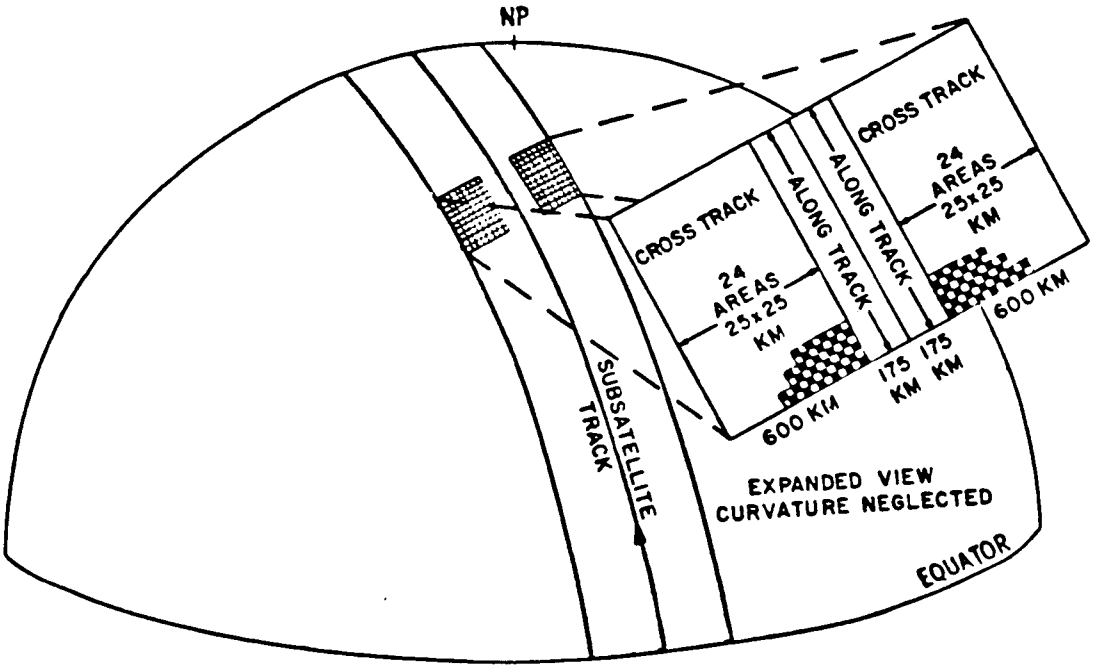

Fig. 1 Schematic Drawing of Large Scale Grid of 25 by 25 Km Areas. The Chessboard Pattern in the Expanded View Actually Fills the Entire Area. All Squares Provide Data.

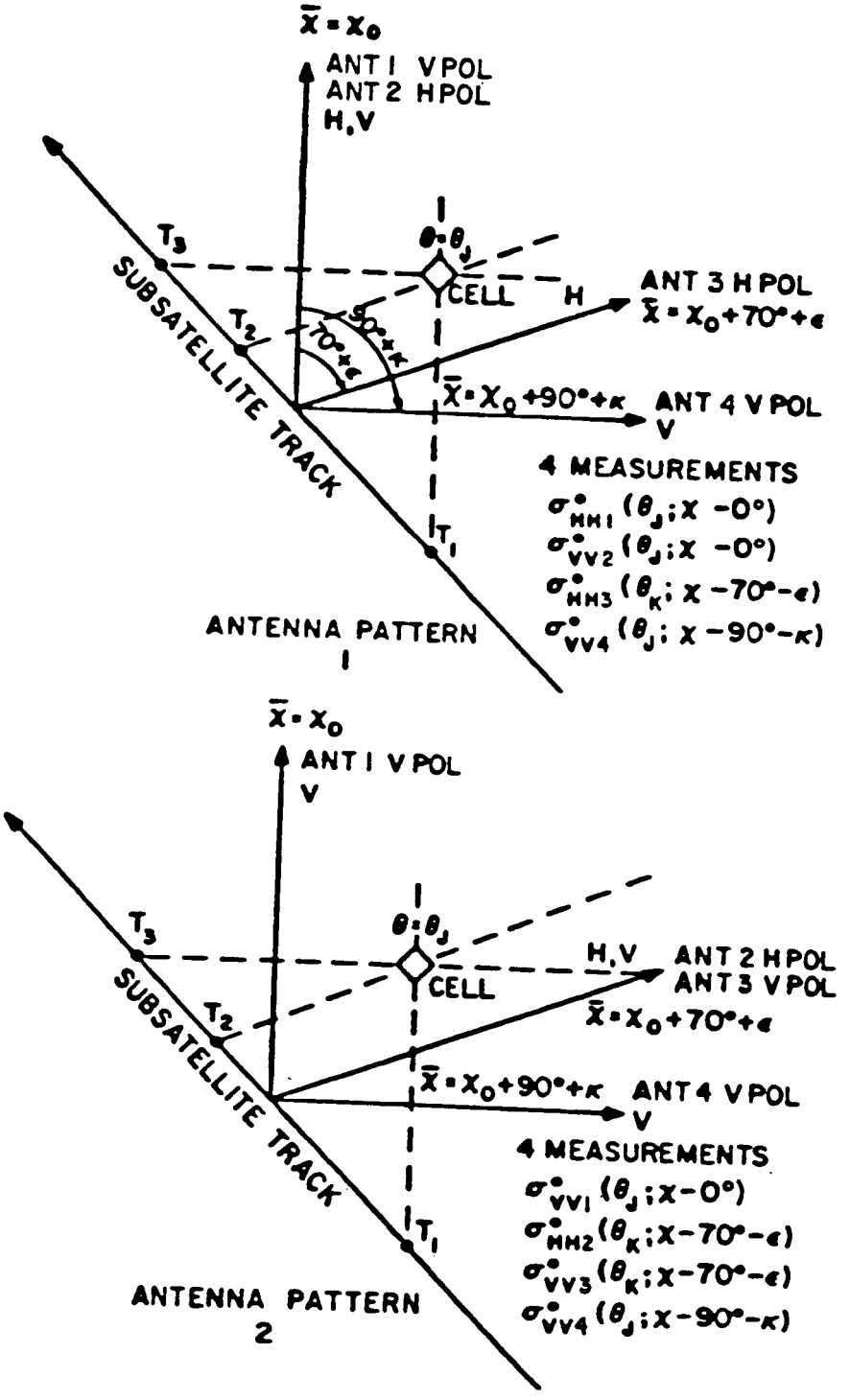

Fig. 2 Two Possible Combinations of Four Backscatter Estimates for the Right Side Looking Forward.

two possibilities seems to offer the surest opportunity to recover unique values for the wind speed and direction because of the apparent marked difference between upwind backscatter estimates and downwind backscatter estimates when vertically and horizontally polarized values are compared for high winds and high incidence angles. The first of these two possibilities will be used in a subsequent section. The changes required for the second possibility are easy to make.

Fig. 2 illustrates a feature of the actual data in that the pointing directions of the radar beams are not exactly 70^{o} and 90^{o} behind the lead beam. This produces minor shifts in the various inverse curves that result and complicates the recovery of the winds from a computational point of view. This aspect of the problem will be neglected in the analyses and discussions to follow.

This new design as in Chi, et al. (1986) and Chi, et al. (1987) and in terms of various other sources of variability for the estimates, such as attitude errors, orbital errors, and squint, is a vast improvement over the SASS. The major difficulty will be to obtain a correct theory, or model, to relate the backscatter estimates to the waves on the ocean and then the winds that generated the waves.

1.3 Probability concepts. Both the backscattered signal from the waves on the ocean and the receiver noise are incoherent, which means that the envelopes of the time varying signal plus the noise as, say, voltages can be described instantaneously by a Rayleigh probability density and that the power

has an exponential distribution. Successive values from these envelopes are correlated for short time intervals.

The Doppler shift as a function of the position of a given small area of the ocean and of the velocity of the spacecraft allows successive small areas as in Figs. 1 and 2 to be sampled and estimates of the backscatter to be obtained for each one. The new feature of the present design is that digital data processing and filtering will make the precise alignment of the areas illustrated in these two figures possible.

Probability theory and statistical methods are involved in the design of a scatterometer as described by Chi, et al. (1986) and Chi, et al. (1987). The design involves combining a large number of quasi independent estimates of the random variables obtained by the instrument so as to obtain a much more stable, less randomly varying, estimate of the backscatter.

Although the theory of sampling from a normal distribution with an unknown expected value for the first moment about the origin, conventionally, μ, and an unknown variance, $\mathcal{E}\,(\chi - \mu)^2 = \sigma^2$ (note this is not σ^o), does not quite apply, a scatterometer essentially obtains a large number of estimates of a random variable, say, X_1, X_2, X_3, ... X_n and finds the average as in

$$\bar{X} = \frac{1}{N} \sum_{1}^{N} X_i \qquad (1)$$

It then, in a way, follows that the expected value of $\bar{X}$ is given by

$$\mathcal{E}\,(\bar{X}) = \mu \qquad (2)$$

and that the variance of $\bar{X}$ is

$$\mathcal{E}(\bar{X} - \mu)^2 = \sigma^2/N \qquad (3)$$

The single number that is obtained from one of the four different estimates of the backscatter from the waves in a given 25 by 25 km area on the ocean is thus analogous to the $\bar{X}$ in Eqn. (1), and the variance of the estimate (i.e. $\bar{X}$) is analogous to the expected value given in Eqn. (3). The analogy is not exact. Therein lies both the value of a scatterometer and the difficulty in interpreting the estimates of the backscatter. One purpose of this paper is to explain this difficulty and to provide a correct theory for the interpretation of the backscatter estimates.

2. DEFINITIONS

2.1 The quantities involved. For the analysis to follow, certain definitions are needed. These are:

σ^o is a random variable.

σ^o_M is the expected value of σ^o.

$VAR(\sigma^o) = \alpha(\sigma^o_M)^2 + \beta\ \sigma^o_M + \gamma$ is the variance of σ^o.

$SD(\sigma^o) = (VAR(\sigma^o))^{\frac{1}{2}}$ is the standard deviation of σ^o.

Since the variance is a known function of σ^o_M, $VAR(\sigma^o)$ and $SD(\sigma^o)$ will be replaced by $VAR(\sigma^o_M)$ and $SD(\sigma^o_M)$ throughout.

α, β and γ are known design parameters for the scatterometer for a known 25 by 25 km cell and polarization.

In these definitions, σ^o is the value of the normalized radar backscattering cross section obtained by a scatterometer, and σ^o_M is its expected value. The purpose of the definitions is to tie together concepts used in the theory of probability and statistics with those used in scatterometery and to avoid confusion between the notations used in the two different subject areas.

2.2 The probability density function. With these definitions, the probability density function for σ^o is given by

$$f(\sigma^o) = (2\pi)^{-\frac{1}{2}}(SD(\sigma^o_M))^{-1} \exp\left(-\frac{1}{2}(\sigma^o - \sigma^o_M)^2/VAR(\sigma^o_M)\right) \qquad (4)$$

as first obtained by Fischer (1972). It is not usually necessary to designate the polarization of the backscatter in the following analysis so that the appropriate subscripts will be omitted until they are needed. There is only one unknown parameter in Eqn. (4). It is σ^o_M, and if it is known, both the expected value of σ^o and the variance of σ^o are known. The range of definition for σ^o is

$$-\infty < \sigma^o < \infty \tag{5}$$

but the range of definition of σ^o_M is

$$0 \leq \sigma^o_M < \infty \tag{6}$$

because the theory for backscatter from any target does not admit negative values. It is conceivable, however, that there could be no backscatter at all from certain kinds of targets, or that the value of σ^o_M could be so low that it could be virtually indistinguishable from zero. Eqn. (4) still has a meaning if σ^o_M is zero. For the derivation of Eqn. (4), it is assumed that both the expected value of the receiver noise and the variance of the noise are constant. The backscatter estimates recovered by the SEASAT SASS for some incidence angles ranged over 40 dB. For some theoretical purpose it may be necessary to show results in dB if σ^o is positive. For the practical uses of the data, there does not seem to be any reason to use dB for the recovery of winds.

3. THE MEANING OF σ_M^o

3.1 Backscatter theories. Theories for the calculation of radar backscatter from the ocean surface attempt to predict the value of σ_M^o from either the properties of the waves or the study of backscatter data. The most recent models are those of Wentz, et al. (1984) and Wentz, et al. (1986), Iwata (1985), Durden and Vesecky (1985), Plant (1986) and Donelan and Pierson (1987). These models do not treat separately some properties of the waves known to produce backscatter such as breaking waves (Banner and Fooks, 1985) and wedges (Lyzenka, et al. 1983, Kwoh and Lake, 1984). In general, σ_M^o is some function of the properties of the waves and thus indirectly some function of the winds (both past and present over the entire ocean) that generated the waves. More specifically, it should be possible to represent σ_M^o as dominantly a function of the wind speed and the direction of the wind (relative to the pointing direction of the radar beam) for the area being analyzed and to account for such effects as fetch, duration, swell, breakers, wedges, and water temperature in the process of estimating the winds. To do this requires the combined efforts of oceanographers, meteorologists and radar scientists. Numerous estimates of backscatter obtained by measurements from radars on platforms in oceans or lakes, on aircraft and on SEASAT have yielded data that can be compared with models for σ_M^o.

The last four models referenced above (there may be others) are based on the two scale theory reviewed by Valenzuela (1978). The separation of scales wavenumber is a matter of considerable

debate. Backscatter theories that claim to avoid the separation of scales assumption have both proponents and opponents as in Bahar (1987) and Guissard (1987) and the references contained therein.

One purpose of this paper is to find bounds on σ^o_M so that various models can be tested operationally. The value of σ^o_M for a particular sample value of σ^o from Eqn. (4) can be assumed to be known theoretically based on some model for backscatter from the waves on the ocean. For purposes of analysis in the material on maximum likelihood estimates and the use of various models it will be assumed that, with polarization included,

$$\sigma^o_{VV} = \sigma^o_{VV}(\bar{U}, \chi, \theta) \tag{7}$$

$$\sigma^o_{HH} = \sigma^o_{HH}(\bar{U}, \chi, \theta) \tag{8}$$

where θ the incidence angle, is known.

3.2 The specification of the wind. It is not necessary to specify the height at which the mean effective windspeed $\bar{U}$ for a neutrally stratified atmosphere is to be measured. Some investigators use u_* instead of $\bar{U}$. If the logarithmic wind profile for a neutrally stratified atmosphere is used and if the friction velocity is determined by one of the usual methods to be

$$\frac{u_*^2}{(\bar{U}(10))^2} = C_{DN}(\bar{U}(10)) \tag{9}$$

then u_* and z_o are both functions of $\bar{U}$ (10). The wind at 10 m, and the wind at any height, or u_* are all equivalent. In the Monin-Obukhov theory, all wind profiles are logarithmic close to the sea surface. There are differences as far as some backscatter theories are concerned, and there are many different versions for the right hand side of Eqn. (9). Also for other than neutral atmospheric stability, Monin-Obukhov theory is needed to interpret comparions of conventionally measured winds with backscatter data. The air-sea temperature difference is required from some other source to compute the actual wind at greater heights from the effective neutral wind. Hasse (1986) has discussed the various concepts that are involved. Donelan (1982) has provided an analysis to support the contention that the right hand side of Eqn. (9) is also a function of the waves on the ocean. The values of (7) and (8), or improved models for $\sigma^o_{M'}$ vary over many orders of magnitude in such a way that it should be possible to recover estimates of $\bar{U}$ and χ from the backscatter estimates.

4. PROPERTIES OF EQUATION 4

4.1 Monte Carlo methods. The transformation

$$t = (\sigma^o - \sigma_M^o)/(\alpha(\sigma_M^o)^2 + \beta\,\sigma_M^o + \gamma)^{\frac{1}{2}} \qquad (10)$$

changes Eqn. (4) to Eqn. (9).

$$f(t) = (2\pi)^{-\frac{1}{2}} \exp(-t^2/2) \qquad (11)$$

The random variable, t, is a sample value from a normal probability density function with an expected value of zero and a standard deviation of one. From (10) it follows that σ^o can be represented by Eqn. (12).

$$\sigma^o = \sigma_M^o + t \cdot SD(\sigma_M^o) \qquad (12)$$

The sampling variability of σ^o in Eqn. (4) is entirely equivalent to the values obtained fron Eqn. (12). If some model for σ_M^o is available, even if it is not fully correct, then σ_M^o can be used to generate random values of σ^o. These in turn can be used to obtain winds recovered from simulated σ^o estimates and test the algorithms designed to do this. The theoretical values of σ_M^o need not necessarily be correct for this to be done. The model values, σ_M^o, need not necessarily correspond to the best model values that would recover more nearly correct winds.

4.2 K_P The normalized standard deviation. Eqn. (12) can be used to obtain K_P as follows:

$$\sigma^o = \sigma_M^o \, (1 + t \cdot SD(\sigma_M^o)/\sigma_M^o) \tag{13}$$

$$= \sigma_M^o \, (1 + t \, K_P)) \tag{14}$$

As σ_M^o approaches 0, K_P approaches infinity. As σ_M^o approaches infinity, K_P approaches $\alpha^{\frac{1}{2}}$.

4.3 The normalized expected value. From Eqn. (10) if σ_M^o is known, a random variable can be defined by

$$Y = \sigma^o/SD(\sigma_M^o) \tag{15}$$

and its expected value is

$$\mathcal{E}\,(Y) = M = \sigma_M^o/SD(\sigma_M^o) \tag{16}$$

The probability density function is then

$$f(Y) = (2\pi)^{-\frac{1}{2}} \exp\,(-\tfrac{1}{2}(Y - M)^2) \tag{17}$$

The variance of Y is one. Eqn. (17) has the same shape as the graph of the unit variance zero mean normal distribution, but it is centered at the value, M. For $\sigma_M^o = 0$, $M = 0$. As σ_M^o becomes large, M asymptotically approaches $\alpha^{-\frac{1}{2}}$. Also M is the reciprocal of K_P defined as in Eqn. (18).

$$M = 1/K_P \tag{18}$$

Given σ_M^o, α, β and γ the probability that Y and hence σ^o will be negative can quickly be guessed, or computed, since M represents the number of standard deviations that the expected value lies away from zero. For large values of σ_M^o and for one of the areas that would be sampled, a possible value of α is 0.02 so that $\alpha^{-\frac{1}{2}}$ equals 0.14^{-1} or 7.07. The integral of the unit variance zero mean normal probability density function from $-\infty$ to -7 is a very small number. Thus a negative estimate of σ^o would be highly improbable. For σ_M^o equal to zero, M is zero, and the probability of a negative value of Y or σ^o is 0.50. The standard deviation of σ^o is then $\gamma^{\frac{1}{2}}$.

Although Eqn. (4) has a range for σ^o over all possible positive and negative values and for σ_M^o from zero to infinity, probability models are both unrealistic and unverifiable over their entire domain of definition. The actual instrument sets physical limits that constrain the random variables and unknown parameters in ways that are features of its design. A value of M equal to 4 or more is sufficient to ensure that the chance that σ^o will be negative is negligible.

5. POINT ESTIMATES OF POPULATION PARAMETERS AND RANDOM INTERVALS FOR POPULATION PARAMETERS

5.1 The concepts. Given an independent random sample of values from a population with a probability density function with a known form, but with one or more unknown parameters that define it more exactly, the classical statistical problem is to estimate the unknown parameters. An independent random sample from a normal distribution with an unknown expected value and an unknown variance provides the data from which various statistics can be computed so as to obtain point estimates of the two parameters and so as to construct intervals whose end points have a pre-assigned probability of enclosing the values of each of the two population parameters. The procedures are a part of the classical literature on the subject and the random intervals are constructed from statistics that involve the "student t" distribution and the Chi Square distribution. All terms and the methods that are used are carefully defined in, for example, Mood, et al. (1974), except that the intricate notation of this reference has been simplified in this paper.

For scatterometers in general and for any new design, a statistician is thus faced with the task of stating as much as possible about the unknown population parameter, σ^o_M, given at first a single value, i.e., a sample of size one, for the random variable, σ^o. Clearly the standard methods applied to a sample from a normally distributed population do not apply. As described above, the data from the scatterometer have already been processed extensively to the extent that the random variable, σ^o, is like the $\bar{X}$ in Eqn. (1) and the variance is like Eqn. (3) for

quite large N with the major difference being that the variance is a function of the first moment about the origin.

5.2 Probabilities. For purposes of further analysis the random variable t in Eqns. (10), (11), and (12) will be, at times, defined with subscripts so as to differentiate different values. Also at times the absolute value of these subscripted values will be assigned a sign to designate whether the subscripted value is positive or negative.

The integral of Eqn. (11) is often given in tabular form (pre-computer) from minus infinity to some positive value of t, say, $+|t_2|$, as in

$$\Phi(+|t_2|) = (2\pi)^{-\frac{1}{2}} \int_{-\infty}^{+|t_2|} \exp(-t^2/2)\,dt \qquad (19)$$

The definition can readily be extended to

$$\Phi(-|t_1|) = (2\pi)^{-\frac{1}{2}} \int_{-\infty}^{-|t_1|} \exp(-t^2/2)\,dt \qquad (20)$$

so that

$$\Phi(+|t_2| - \Phi(-|t_1|) = (2\pi)^{-\frac{1}{2}} \int_{-|t_1|}^{+|t_2|} \exp(-t^2/2)\,dt \qquad (21)$$

With these definitions, it follows that

$$P(\sigma_M^o - |t_1|SD(\sigma_M^o) < \sigma^o < \sigma_M^o + |t_2|SD(\sigma_M^o)) = \Phi(+|t_2|) - \Phi(-|t_1|) \qquad (22)$$

Where $P(\cdot)$ means that the probability that σ^o will fall in the interval defined by $-|t_1|$, σ_M^o, $SD(\sigma_M^o)$ and $+|t_2|$ is given by the right hand side of the equation.

5.3 Point estimates. Given a sample from a known probability density function, hereafter PDF, with unknown moments, the first moment about the origin can be estimated by the sample mean. The average of one number is that number itself so that

$$\sigma_M^o = \sigma^o \qquad (23)$$

is an estimate of σ_M^o. This estimate is not a particularly good one since, from Eqn. (22), it scatters by a considerable amount about the expected value of σ_M^o for, say $|t_1| = |t_2| = 1$. This point estimate was substituted into the equation for the standard deviation to estimate the scatter of σ^o for reduction of the SEASAT SASS data.

An alternative point estimate is the maximum likelihood estimate of σ_M^o. For a given sample σ^o is known, and the maximum likelihood estimate of σ_M^o is that value of σ_M^o that maximizes $f(\sigma^o)$ for the sample value of σ^o. Omitting the $(2\pi)^{-\frac{1}{2}}$, multiplying by, or adding, constants does not change the location of the maximum. Also since the natural logarithm of $f(\sigma^o)$ is more convenient to work with, the result can be put in the form of Eqn. (24).

$$\mathrm{MLE}(\sigma_M^o) = \mathrm{MAX}\left[-\tfrac{1}{2}\left(\frac{\sigma^o - \sigma_M^o}{\mathrm{SD}(\sigma_M^o)}\right)^2 - \tfrac{1}{2}\ell n\left(\frac{\mathrm{VAR}(\sigma_M^o)}{\alpha(\sigma^o)^2 + \beta\,\sigma^o + \gamma}\right)\right] \qquad (24)$$

as σ_M^o is varied. The constant in the denominator of the logarithmic term causes the function to be zero when $\sigma_M^o = \sigma^o$. The derivative of Eqn. (24) with respect to σ_M^o when set to zero gives the MLE if that part of the PDF is considered for which $\sigma_M^o \neq 0$. The result is a cubic equation. A simple search by a computer subroutine can generally locate MLE(σ_M^o). It is slightly less than σ_M^o. Values of the MLE will be given later based on newly available design parameters.

If both mesoscale variability from one 25 km resolution area to the next (Pierson, 1983a) and the sypnotic scale gradients can be neglected in the sense that both are small compared to the sampling variability of estimates of the backscatter (Pierson, et al. 1984) when various numbers of 25 km resolution cells are combined, it should be possible to average the estimates of σ^o to obtain more stable estimates.

Consider for example, n values of σ^o for a row parallel to the subsatellite track as in σ_1^o, σ_2^o, ... σ_n^o. The area sampled would be 25 km wide by 25·n km long. Then

$$\bar{\sigma}^o = \frac{1}{n}\sum_1^n \sigma_i^o = \frac{1}{n}\left(n\,\sigma_M^o + \sum_1^n t_i \mathrm{SD}(\sigma_M^o)\right) \qquad (25)$$

from Eqn. (12). The expected values of $\bar{\sigma}^o$ and $(\sigma^o - \sigma_M^o)^2$ are then

$$\mathcal{E}(\bar{\sigma}^o) = \sigma_M^o \tag{26}$$

and $$\mathcal{E}(\bar{\sigma}^o - \sigma_M^o)^2 = \left(\frac{1}{n}\sum_1^n t_i \, SD(\sigma_M^o)\right)^2$$

$$= \frac{1}{n^2} n \, VAR(\sigma_M^o)$$

$$= \frac{VAR(\sigma_M^o)}{n} \tag{27}$$

since $\mathcal{E}(t_i)^2 = 1$ and $\mathcal{E}(t_p, t_q) = 0 \ (p \neq q)$. Effectively, averaging n values of σ^o along a row reduces α, β and γ by n^{-1}.

Similarly, areas that are n long by n wide could be represented by

$$\sigma_{ij}^o = \sigma_{Mij}^o + t_{ij} \, SD(\sigma_{Mij}^o) \tag{28}$$

The average would be approximately

$$\bar{\sigma}^o = \frac{1}{n^2}\left(\sum_1^n \sum_1^n (\bar{\sigma}_M^o + t_{ij} \, SD(\bar{\sigma}_{Mij}^o))\right) \tag{29}$$

so that

$$\mathcal{E}(\bar{\sigma}^o) = \bar{\sigma}_M^o \simeq \text{effective value of the } \sigma_{Mij}^o \tag{30}$$

where $\bar{\sigma}_M^o$ could represent the effective model value at the center of the larger area.

The variance would be

$$\mathcal{E}(\bar{\sigma}^o - \bar{\sigma}_M^o)^2 = \frac{1}{n^4}\sum_1^n \sum_1^n VAR(\bar{\sigma}_M^o) \tag{31}$$

The α's, β's, and γ's for the n^2 areas could be summed to find an effective value for them. The variance would be reduced by n^{-2}. Further analysis is needed to decide on some of these steps.

5.4 Interval estimates. The concept of an interval estimate is described in Mood, et al. (1974). Fig. 3 is an illustration of this concept. The horizontal axis is σ_M^o and the vertical axis is σ^o for the ranges defined by (5) and (6). For, say, $|t_1| = |t_2|$, the two continuous curves in Eqn. (22) can be graphed. The range of σ^o for a particular σ_M^o is shown by the vertical line, and σ^o is a function of σ_M^o.

The probability that σ^o will equal a value somewhere on this vertical line is given by the right hand side of Eqn. (22). For any of these possible random values of σ^o that lie on the example vertical line, a horizontal line can be drawn between the upper and lower curves. Any one of these lines will intersect the vertical line for the example value of σ_M^o. Two examples, out of an infinite number are shown by a continuous line and a dashed line.

Essentially σ^o is a function of the chosen values of $|t_1|$, $|t_2|$ and σ_M^o as in (32a) and (32b).

$$\sigma^o = \sigma^o(\sigma_M^o, |t_2|) \tag{32a}$$

$$\sigma^o = \sigma^o(\sigma_M^o, |t_1|) \tag{32b}$$

If the two equations can be inverted so as to find (33a) and (33b)

$$\sigma_M^o = \sigma_M^o(\sigma^o, |t_2|) \tag{33a}$$

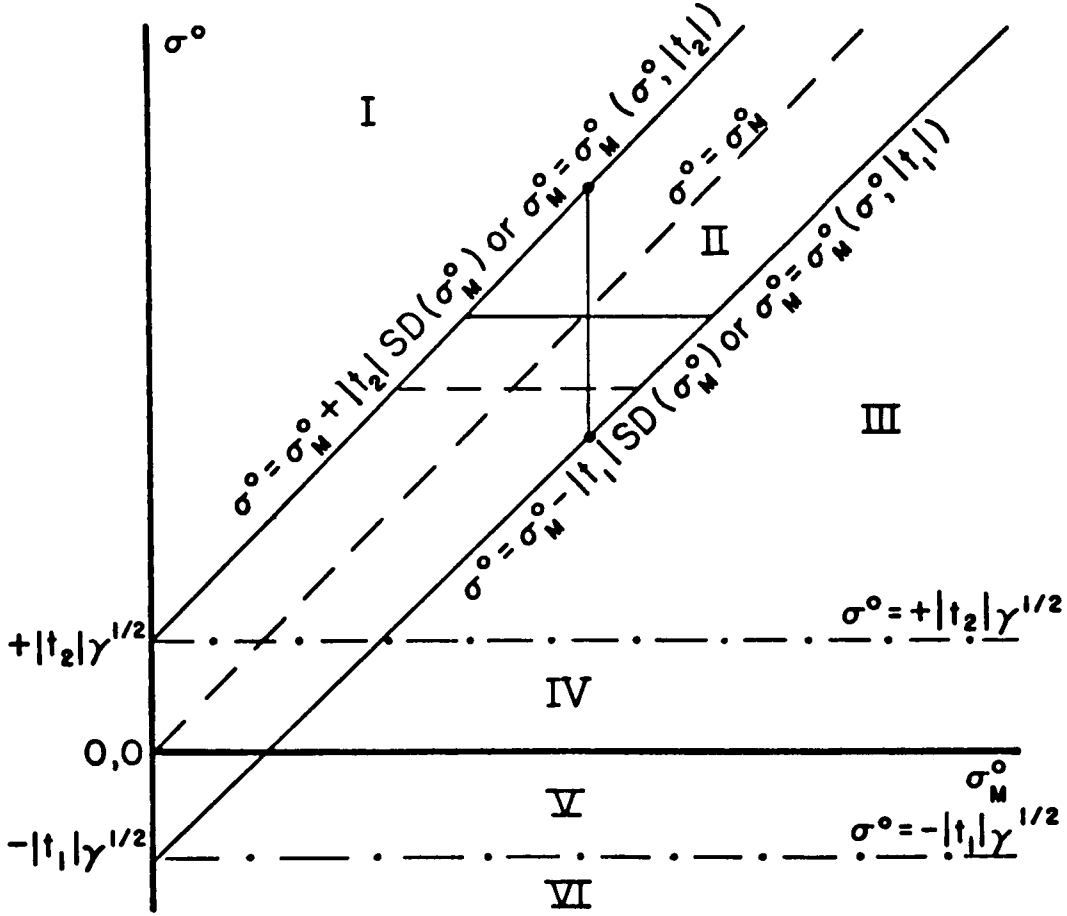

Fig. 3 An Illustration of the Concept of a Random Interval.

$$\sigma_M^o = \sigma_M^o(\sigma^o, |t_1|) \tag{33b}$$

,which is equivalent to interchanging the independent and dependent variables, then

$$P(\sigma_M^o(\sigma^o, |t_2|) < \sigma_M^o < \sigma_M^o(\sigma^o, |t_1|)) = \Phi(+|t_2|) - \Phi(-|t_1|) \tag{34}$$

if $\sigma_M^o(\sigma^o, |t_2|)$ is greater than zero.

Eqn. (34) describes an interval for this case with lower and upper bounds that are a function of the random variable, σ^o, i.e., the measurement made by a scatterometer, which is known. The value of σ_M^o is not known yet. The interval is consequently a statistic. It can be computed, given α, β and γ for each sample value. The parameter, σ_M^o , has the above probability of being contained in this random interval.

If $\sigma^o > + |t_2|\gamma^{\frac{1}{2}}$ as shown by a dash-dot line three additional probabilities can be found. The value

$$+ |t_3| = \sigma^o/\gamma^{\frac{1}{2}} \tag{35}$$

can be computed. Then

$$P(\sigma_M^o \equiv 0) = 1 - \Phi(+ |t_3|) \tag{36}$$

$$P(0 < \sigma_M^o < \sigma_M^o(\sigma, |t_2|)) = \Phi(+|t_3|) - \Phi(|t_2|) \tag{37}$$

and

$$P(\sigma_M^o(\sigma^o, |t_1|) < \sigma_M^o) = \Phi(- |t_1|) \tag{38}$$

The sum of the probabilities in (34), (36), (37), and (38) is one as a check. The equations divide the area above $\sigma^o = + |t_2| \gamma^{\frac{1}{2}}$ in the first quadrant into the line $\sigma_M^o \equiv 0$ and region I, region II and region III as shown.

If σ^o falls between $+ |t_2| \gamma^{\frac{1}{2}}$ and $- |t_1| \gamma^{\frac{1}{2}}$ as in Regions IV and V in Fig. 1 the value of, say,

$$t_4 = \sigma^o / \gamma^{\frac{1}{2}} \tag{39}$$

can be found even if σ^o is negative. Three probabilities can be defined as follows:

$$P(\sigma_M^o \equiv 0) = 1 - \Phi(t_4) \tag{40}$$

(and, in particular, if σ^o is zero, the probability that $\sigma_M^o \equiv 0$ is 0.5)

$$P(0 < \sigma_M^o < \sigma_M^o (\sigma^o, |t_1|)) = \Phi(t_4) - \Phi(- |t_1|) \tag{41}$$

$$P(\sigma_M^o(\sigma^o, |t_1|) < \sigma_M^o) = \Phi(- |t_1|) \tag{42}$$

Again the probabilities add to one.

If σ^o is less than $- |t_1| \gamma^{\frac{1}{2}}$ as in Region VI of Fig. 1, the quantity

$$t_5 = \sigma^o / \gamma^{\frac{1}{2}} \tag{43}$$

can be found. The two probabilities are

$$P(\sigma_M^o \equiv 0) = 1 - \Phi(t_5) \tag{44}$$

and

$$P(0 < \sigma_M^o) = \Phi(t_5) \tag{45}$$

It is important to be able to interpret negative values of the random variable, σ^o. The triangular area in Region V of Fig. 1 shows that there is a non-negligible probability for a random interval that will contain a positive value of σ_M^o even if σ^o is negative.

Two typical choices for $|t_2| = |t_1|$ are 1 and 1.645. For the value, 1, the right hand side of (34) equals 0.6826. For the value, 1.645, it equals 0.90. There is no particular reason why four different curves could not be graphed on Fig. 3 to delineate these other probabilities.

6. SIMPLIFIED RESULTS FOR LARGE VALUES OF σ_M^o

The standard deviation of σ^o can be re-written as Eqn. (46) where

$$SD(\sigma_M^o) = (\alpha(\sigma_M^o + \frac{\beta}{2\alpha})^2 + (\frac{4\alpha\gamma - \beta^2}{4\alpha}))^{\frac{1}{2}} \tag{46}$$

For large values of σ_M^o the first term in (46) dominates the second, and the second term can be neglected to obtain an approximate result as in Eqn. (47).

$$P(\sigma_M^o - |t_1|\ \alpha^{\frac{1}{2}}(\sigma_M^o + \beta/2\ \alpha) < \sigma^o < \sigma_M^o + |t_2|\ \alpha^{\frac{1}{2}}(\sigma_M^o + \beta/2\ \alpha)) \tag{47}$$

$$= \Phi(+|t_2|) - \Phi(-|t_1|)$$

The inequality,

$$\sigma_M^o(1 - |t_1|\ \alpha^{\frac{1}{2}}) - |t_1|\ \beta/2^{\frac{1}{2}} < \sigma^o \tag{48}$$

is equivalent to

$$\sigma_M^o < \frac{\sigma^o + |t_1|\ \beta/2\alpha^{\frac{1}{2}}}{1 - |t_1|\alpha^{\frac{1}{2}}} \tag{49}$$

with a corresponding result for the other one, so that

$$P\left\{\frac{\sigma^o - |t_2|\ \beta/2\alpha^{\frac{1}{2}}}{1 + |t_2|\ \alpha^{\frac{1}{2}}} < \sigma_M^o < \frac{\sigma^o + |t_1|\ \beta/2\ \alpha^{\frac{1}{2}}}{1 - |t_1|\ \alpha^{\frac{1}{2}}}\right\} = \Phi(+|t_2|) - \Phi(-|t_1|) \tag{50}$$

Eqn. (50) defines a random interval, by two statistics such that the probability that this random interval contains the population parameter, σ_M^o, is given by the right hand side of the equation. By assumption, the probability that σ_M^o is zero is negligible. Eqn. (36) is then equal to zero. Eqn. (37) equals $1 - \Phi(+ |t_2|)$ and so on.

7. THE SOLUTION FOR ALL VALUES OF σ^o

For the general solution, one needs to replace Eqn. (22) by inequalities as functions of σ^o that bound σ^o_M as in Eqns. (32a) to (34). The algebra is best carried out by setting the inequality sign to an equality sign, squaring an appropriate expression, solving the quadratic equation that results for σ^o_M as a function of σ^o, α, β, γ and $|t_1|$ or $|t_2|$ and picking the correct sign for the solution. The two results are

$$\sigma^o_M(\sigma^o,|t_2|) = \frac{\sigma^o+|t_2|^2\beta/2-((\sigma^o+|t_2|^2\beta/2)^2-(1-|t_2|^2\alpha)((\sigma^o)^2-|t_2|^2\gamma))^{\frac{1}{2}}}{1-|t_2|^2\alpha} \qquad (51)$$

and

$$\sigma^o_M(\sigma^o,|t_1|) = \frac{\sigma^o+|t_1|^2\beta/2+((\sigma^o+|t_1|^2\beta/2)^2-(1-|t_1|^2\alpha)((\sigma^o)^2-|t_1|^2\gamma))^{\frac{1}{2}}}{1-|t_1|^2\alpha} \qquad (52)$$

so that the terms in Eqn. (34) become known. Again the random values for the bounds for the inequalities are statistics that can be computed from the sample value of σ^o.

The terms $1-|t_1|^2\alpha$ and $1-|t_2|^2\alpha$ would cause difficulties if either one were to become negative. The mathematical model for the PDF then fails to be realistic. As discussed above the value of α is so small that this does not affect the usefulness of the results.

For Eqn. (51), if $\sigma^o = |t_2|\gamma^{\frac{1}{2}}$, $\sigma_M^o(\sigma^o|t_2|)$ is zero and is undefined if $\sigma^o < |t_2|\gamma^{\frac{1}{2}}$. For Eqn. (52) if $\sigma^o = -|t_1|\gamma^{\frac{1}{2}}$ the numerator becomes

$$-|t_1|\gamma^{\frac{1}{2}} + |t_1|^2\beta/2 + |t_1|\gamma^{\frac{1}{2}} - |t_1|^2\beta/2 = 0 \tag{53}$$

so that $\sigma_M^o(\sigma^o|t_1|)$ is undefined for $\sigma^o < -|t_1|\gamma^{\frac{1}{2}}$. Fig. 3 shows these points and illustrates the requirement that no value of σ_M^o can be negative.

These results have many applications to the interpretation of backscatter estimates from scatterometers, as will be illustrated by specific examples in following sections. An example of their implications is to consider some typical numerical values. Suppose that $\gamma = 10^{-6}$ and two estimates of σ^o have been obtained: one is equal to 10^{-5} and the other is equal to -10^{-5}. From Eqn. (39) for the first value of σ^o, $t_4 = 0.01$, and for the second, it equals -0.01.

For σ^o equal to 10^{-5}, the following probability statements concerning random intervals can be made if $|t_1| = |t_2| = 1$

$$P(\sigma_M^o \equiv 0) = 0.496 \tag{54a}$$

$$P(0 < \sigma_M^o < \sigma_M^o(\sigma^o, |t_1|)) = 0.3453 \tag{54b}$$

$$P(\sigma_M^o(\sigma^o, |t_1|) < \sigma_M^o) = 0.1587 \tag{54c}$$

The first probability statement would need to be interpreted here and when first described above quite carefully. This interpreta-

tion would be: Given a large number of sample values of σ^o equal to 10^{-5} such that γ equaled 10^{-6} and $|t_1|$ equalled 1, drawn from populations with unknown values of σ_M^o some of which were identically zero, then the probability that σ^o was drawn from a population such that σ_M^o was in fact zero is 0.496.

If on the other hand, the sample value of σ^o is -10^{-5} the probabilities become

$$P(\sigma_M^o \equiv 0) = 0.5040 \tag{55a}$$

$$P(0 < \sigma_M^o < \sigma_M^o(\sigma^o, |t_1|)) = 0.3373 \tag{55b}$$

$$P(\sigma_M^o\ (\sigma^o, |t_1|) < \sigma_M^o) = 0.1587 \tag{55c}$$

where, for known values of α, β and γ the numerical values of the statistics inside the probability statements have changed. It would obviously be difficult to distinguish possible values of σ_M^o one from the other, if successive sample values for σ^o were 10^{-5} and -10^{-5}.

If, to continue, σ^o were to equal $-1.645 \cdot 10^{-3}$ (the corresponding positive value would be about -29.8 db), and $|t_1|$ were 1.645, then the probability that σ_M^o would be greater than zero would be 0.05.

From Eqns. (25) to (31) an average of four values of σ^o effectively reduces the values of α, β and γ by a factor of four and the corresponding standard deviations by a factor of 2. The vertical line for the example value of σ_M^o would be half as long

in Fig. 1, and Region II would be half as wide. The random intervals obtained above would have their lengths changed. Those corresponding to Eqn. (34) would be about half as long for the same probability on the RHS. For averages of 16, if possible, the intervals corresponding to Eqn. 34 would be about one fourth as long.

8. EXAMPLES BASED ON A NEW SCATTEROMETER DESIGN

8.1 Theoretical Considerations. There are two sources of variability in the backscatter values that could be obtained by a scatterometer. These are (1) the variability in the estimates of the received power as a result of the combined effects of self-noise in the receiver and Raleigh-fading for the backscattered power and (2) the uncertainties in the calculation of the rest of the terms in the radar equation that convert the estimate of the backscattered power to the estimate of the normalized backscattering cross section, σ^o.

The theory for the variability of the estimates of the received power is well in hand, but the calculation of the effects of the rest of the terms in the radar equation poses some important questions.

The radar equation can be simplified for the purposes of this analysis to the form given by Eqn. (56)

$$\sigma^o = P_R \, R \tag{56}$$

In Eqn. (56), the random variable, P_R, is well understood from a probabilistic and statistical point of view. The random variable, R, is not. This term, R, depends on the calculation of the spacecraft's position, velocity and attitude at each time that an estimate of σ^o is obtained. The spacecraft may be a little bit ahead, or behind, a little bit to the right, or left, and a little bit higher, or lower, than the calculated position of its center of mass. It may be traveling a little bit faster

or a little bit slower than calculated. Also the calculated angular displacements in roll, pitch and yaw may be a little bit high or a little bit low.

All of these uncertainties enter into the calculation of R, and, according to present analysis methods, result in additional variability in the estimates of σ^o. For analysis purposes, assume that (56) can be represented by two parts as in Eqns. (57) and (58).

$$P_R = P_M + t_P SD(P_M) \tag{57}$$

$$R = R_M + t_R SD(R_M) \tag{58}$$

In Eqns. (57) and (58), t_p is known to be a normally distributed random variable with a zero mean and unit standard deviation. The nature of the estimation process for the received power assures that each and every value of P_R, and hence t_p, is totally uncorrelated with all other values. It is generally assumed that t_R has this same property in that it would also be a normally distributed random variable with a zero mean and unit variance.

However, t_R need not necessarily have the property that successive values of t_R are independent in the probability sense. As reviewed by Douglas, et al. (1987) who describe difficulties in calculating the orbit of a satellite, the residual errors in the calculation of R could be systematic, but unknown, and slowly varying along the orbit. About 2.5 seconds is required to obtain the eight measurements to be grouped eventually to form the four backscatter values estimated for the 25 by 25 km areas on

each side of the subsatellite track. There is one possibility that t_R may be substantially constant over the time interval from T_1 to T_3 in Fig. 2 so that the unknown errors may be highly correlated from one estimate to the next. A partial correlation is also possible. The present probability model assumes that successive values of t_R are independent.

Eqns. (56), (57) and (58) combine to yield Eqn. (59),

$$\sigma^o = P_M R_M + t_p SD(P_M) R_M + t_R SD(R_M) P_M + t_p t_R SD(P_M)\ SD(R_M) \qquad (59)$$

which can be rewritten as Eqn. (60) if the last term is omitted.

$$\sigma^o = \sigma_M^o + t_p SD(\sigma_p^o) + t_R SD(\sigma_R^o) \qquad (60)$$

From (60), the following can be derived.

$$\mathcal{E}(\sigma^o) = \sigma_M^o \qquad (61)$$

$$\mathcal{E}(\sigma^o - \sigma_M^o)^2 = \mathcal{E}(t_p SD(\sigma_p^o) + t_R SD(\sigma_R^o))^2 \qquad (62)$$

$$= VAR(\sigma_p^o) + VAR(\sigma_R^o)$$

8.2 A noise only model. Table 1 has been summarized for 10 selected incidence angles about 5^o apart across the swath. The table contains the values of α, β and γ as defined in Section 2.1 that would be appropriate if R in Eqn. (56) were a constant. Other quantities of interest are also tabulated. For example, if $|t_2| = |t_1| = 1$ with $\beta/2\,\alpha^{\frac{1}{2}}$ neglected and for high values of the backscatter, the random interval defined by Eqn. (50) can be found approximately in decibels in terms of the first two columns after the tabulated values of α. Receiver noise and Rayleigh fading alone make the random interval based on the estimate, σ^o, at most $\pm$ 0.25 dB and as small as $\pm$ 0.12 dB. In what follows the square root of γ will also be of interest. The last three columns provide information on the values of σ^o such that the asymptotic behavior can be used to sufficient accuracy.

8.3 Position, velocity and attitude errors. The effects of the errors in the calculation of R when combined with the types of variability represented by Table 1 are shown in Table 2. If α_1, β_1 and γ_1 are from Table 1 and α_2, β_2 and γ_2 are from Table 2, then the second term in Eqn. (62) would be given by Eqn. (63), which follows from the properties of normally distributed random variables.

$$\mathrm{VAR}(\sigma_R^o) = (\alpha_2 - \alpha_1)(\sigma_M^o)^2 + (\beta_2 - \beta_1)\sigma_M^o + (\gamma_2 - \gamma_1) \qquad (63)$$

A comparison of Tables 2 and 1, shows that the largest changes are in the values of α_2 compared to α_1. The ratios α_2/α_1 for the incidence angles in the table are given by the values in parentheses following the incidence angle as: 15.6^o(10.83), 19.9^o(22.88), 24.7^o(22.55), 31.4^o(19.42), 35.4^o(13.95),

TABLE 1a SELECTED SCATTEROMETER DESIGN VALUES FOR COMMUNICATION NOISE AND RECEIVER NOISE (ACTUAL VALUES HAVE BEEN MULTIPLIED BY THE POWER OF 10 SHOWN).

θ	$\alpha(X\ 10^3)$	$(1+\alpha^{\frac{1}{2}})^{-1}$(dB)	$(1-\alpha^{\frac{1}{2}})^{-1}$(dB)	$\beta(X10^4)$	$\gamma(X10^6)$	$\gamma^{\frac{1}{2}}(X10^3)$	$\gamma^{\frac{1}{2}}$(dB)
15.6	1.766	-0.18	+0.19	24.74	974.8	31.22	-15.06
19.9	0.7204	-0.12	+0.12	13.36	809.7	28.46	-15.45
24.7	0.7666	-0.12	+0.12	4.425	82.26	9.07	-20.42
31.4	0.8822	-0.13	+0.13	1.617	9.262	3.04	-25.17
35.4	1.272	-0.15	+0.16	1.083	2.705	1.64	-27.85
41.0	1.477	-0.16	+0.17	0.544	0.5756	0.759	-31.20
46.0	1.888	-0.18	+0.19	0.4228	0.2643	0.514	-32.89
50.5	1.729	-0.18	+0.18	0.3045	0.1512	0.389	-34.10
55.7	2.234	-0.20	+0.21	0.3685	0.1675	0.409	-33.88
59.1	3.234	-0.24	+0.25	0.5809	0.2993	0.547	-32.60

TABLE 1b, SELECTED SCATTEROMETER DESIGN VALUES FOR COMMUNICATION NOISE AND RECEIVER NOISE (ACTUAL VALUES HAVE BEEN MULTIPLIED BY THE POWER OF 10 SHOWN).

θ	$\beta/2\alpha^{\frac{1}{2}}(X10^{3})$	$\gamma-\beta^{2}/4\alpha(X10^{6})$	$(\gamma-\beta^{2}/4\alpha)^{\frac{1}{2}}(X10^{3})$
15.6	29.4	108.3	10.4
19.9	24.9	190.3	13.8
24.7	7.99	18.40	4.29
31.4	2.72	1.852	1.36
35.4	1.52	0.400	0.632
41.0	0.708	0.0747	0.273
46.0	0.487	0.0276	0.166
50.5	0.366	0.0171	0.131
55.7	0.390	0.0155	0.124
59.1	0.511	0.0384	0.196

TABLE 2a SELECTED SCATTEROMETER DESIGN VALUES FOR THE COMBINED EFFECTS OF COMMUNICATION NOISE, RECEIVER NOISE, POSITION, VELOCITY AND ATTITUDE ERRORS. (ACTUAL VALUES HAVE BEEN MULTIPLIED BY 10 TO THE POWER SHOWN).

θ	$\alpha(X10^3)$	$(1+\alpha^{\frac{1}{2}})^{-1}$(dB)	$(1-\alpha^{\frac{1}{2}})^{-1}$(dB)	$\beta(X10^4)$	$\gamma(X10^6)$	$\gamma^{\frac{1}{2}}(X10^3)$	$\gamma^{\frac{1}{2}}$(dB)
15.6	19.125	-0.56	+0.65	25.17	991.7	31.49	-15.02
19.9	16.48	-0.52	+0.60	13.575	822.5	28.68	-15.42
24.7	17.29	-0.54	+0.61	4.497	83.54	9.14	-20.39
31.4	17.13	-0.54	+0.61	1.642	9.405	3.067	-25.13
35.4	17.75	-0.54	+0.62	1.100	2.748	1.658	-27.80
41.0	18.41	-0.55	+0.63	0.553	0.5849	0.7648	-31.16
46.0	19.375	-0.57	+0.65	0.430	0.2688	0.5185	-32.85
50.5	19.919	-0.57	+0.66	0.310	0.1539	0.3923	-34.06
55.7	21.64	-0.60	+0.69	0.37595	0.1709	0.4134	-33.83
59.1	23.76	-0.62	+0.73	0.5929	0.3055	0.5527	-32.57

TABLE 2b, SELECTED SCATTEROMETER DESIGN VALUES FOR THE COMBINED EFFECTS OF COMMUNICATION NOISE, RECEIVER NOISE, POSITION, VELOCITY AND ATTITUDE ERRORS. (ACTUAL VALUES HAVE BEEN MULTIPLIED BY 10 TO THE POWER SHOWN).

θ	$\beta/2\alpha^{\frac{1}{2}}(X10^{3})$	$\gamma-\beta^{2}/4\alpha(X10^{6})$	$(\gamma-\beta^{2}/4\alpha)^{\frac{1}{2}}(X10^{3})$
15.6	9.10	908.9	30.15
19.9	5.29	794.5	28.19
24.7	1.710	80.61	8.98
31.4	0.627	9.011	3.00
35.4	0.413	2.578	1.606
41.0	0.204	0.5434	0.7372
46.0	0.154	0.2449	0.4949
50.5	0.110	0.1418	0.3766
55.7	0.128	0.1546	0.3932
59.1	0.192	0.2685	0.5182

$40.0^{o}(12.46)$, $46^{o}(10.26)$, $50.5^{o}(11.52)$, $55.7^{o}(9.69)$ and $59.1^{o}(7.35)$. The asymptotic random intervals vary from -0.52 and +0.60 dB to -0.62 and +0.73 dB in Table 2.

If the successive values of t_R are independent in the probability sense, then the full table extension of Table 2 as the values vary slowly along the orbit could be used for all of the preceding analysis, and in particular Eqns. (4), (22), (24), (27), (31), (34), (50), (51) and (52) would be theoretically correct.

8.4 Time correlated random variables. For a particular sequence of 25 by 25 km areas a particular distance cross track along the swath, suppose that successive values of t_R at the times t_1, $t_1 + \Delta t$ and so on as in, say, (60) are given by

$$t_R(t_1),\ t_R(t_1 + \Delta t),\ t_R(t_1 + 2\Delta t),\ \ldots\ t_R(t_1 + n\Delta t)$$

It is possible for the successive values of t_R to have a unit variance, zero mean normal PDF for a long enough sample, but the successive values can be highly correlated such that

$$\mathcal{E}(t_R(t_1),\ t_R(t_1 + n\Delta t)) \neq 0 \tag{64}$$

and instead

$$\mathcal{E}\ (t_R(t_1),\ t_R(t_1 + n\Delta t)) = \rho(n\Delta t) \tag{65}$$

where ρ is the correlation coefficient.

The next simplest model of the error structure for R would then be a stationary Gaussian random process similar to the linear model for ocean waves sampled as a function of time at a

fixed point, but with a longer (?), or different, time scale. For the four beams involved, the model might have to be extended to a vector Gaussian process. Very little is known about how this could be done, but the off nadir altimeter effects and the altimeter attitude data might provide guidance.

It might be possible to investigate whether or not the errors in R are time correlated along the orbit once the scatterometer is in orbit if the mesoscale variability in the wind vectors for each area sampled is not too great. The small scale variability of the wind will be described next. The analysis will be completed after this complication is described.

8.5 Model errors, synoptic scales and mesoscales. The concept of a model for σ^o_M or as an extended concept the model for backscatter involving $\tilde{U}$, χ and θ in Eqns. (7) and (8), is needed to recover vector winds from backscatter data. The area inside the 25 by 25 km area defining the array of the sampled backscatter values that is actually illuminated by the radar to obtain the backscatter estimate is much smaller than 625 km^2, and the wind over this smaller area has a considerable amount of mesoscale variability from one 25 by 25 km area to the next. The concept of a synoptic scale perturbed from one area to the next by mesoscale wind fluctuations is useful. Although the larger ocean gravity waves may not change appreciably, the Bragg scatterers will respond to these fluctuations. These concepts have been explored more fully by Pierson (1983a), Pierson, et al. (1984) and summarized in Pierson, et al. (1986). Basically on an i, j grid of 25 by 25 km areas, the departures from a synoptic

scale wind $\bar{U}_S$, χ_S could be represented by the pattern shown below near an arbitrary origin.

$\bar{U}_S + \Delta U_{0,2}$; $\chi_S + \Delta\chi_{0,2}$	$\bar{U}_S + \Delta U_{1,2}$; $\chi_S + \Delta\chi_{1,2}$	$\bar{U}_S + \Delta\chi_{2,2}$; $\chi_S + \Delta\chi_{2,2}$
$\bar{U}_S + \Delta U_{0,1}$; $\chi_S + \Delta\chi_{0,1}$	$\bar{U}_S + \Delta U_{1,1}$; $\chi_S + \Delta\chi_{1,1}$	$\bar{U}_S + \Delta U_{2,1}$; $\chi_S + \Delta\chi_{2,1}$
$\bar{U}_S + \Delta U_{0,0}$; $\chi_S + \Delta\chi_{0,0}$	$\bar{U}_S + \Delta U_{1,0}$; $\chi_S + \Delta\chi_{1,0}$	$\bar{U}_S + \Delta U_{2,0}$; $\chi_S + \Delta\chi_{2,0}$

The concurrent variability in the actual wind, the random variability of t_p and the two possibilities (at least) for the variability of t_R make it difficult to determine whether or not the different values of σ^o are independent random variables or correlated as a function of time and adjacent sampled areas of the ocean.

Errors in the model are, at present, mostly systematic and not random. Whatever these errors are, they must be modeled in terms of σ^o_M, not σ^o. Simply increasing VAR(σ^o_M) by changing α , β and γ does not help because this changes the theoretical behavior of the radar and not the model. Errors in the theoretical model for backscatter from waves need to be treated some other way after the gross errors in the model for σ^o_M are removed.

8.6 A test for t_R constant over short orbit segments. Statistics can be computed from sample values of σ^o that may reveal whether or not successive values of σ^o are highly correlated for some subset of the sample values. For a given antenna and row of 25 by 25 km areas parallel to the subsatellite track, the wind vectors may be slowly varying enough and the mesoscale variability may be small enough to verify the assumption that the values of t_R are highly correlated. The failure of the test does not show that the t_R are uncorrelated since mesoscale effects may mask the hypothesis. The test would then show that other sources of variability dominate even if the t_R are correlated and that the correlation can be neglected.

For a sequence of n areas parallel to the subsatellite track, with n perhaps as large as 5 or 10, and for the same polarization and antenna, the available random variables would be

$$\sigma_1^o, \sigma_2^o, \sigma_3^o, \ldots\ldots \sigma_n^o$$

Suppose that t_R is constant for the n samples. Then from Eqn. (60), the expected value of σ^o is given by Eqn. (66).

$$\mathcal{E}(\sigma^o) = \sigma_M^o + t_R SD(\sigma_R^o) \tag{66}$$

It follows that if

$$\bar{\sigma}_1^o = \frac{1}{n} \sum_1^n \sigma_i^o \tag{67}$$

then

$$\mathcal{E}(\bar{\sigma}_1^o) = \sigma_M^o + t_R SD(\sigma_R^o) \tag{68}$$

and that

$$\mathcal{E}\,(\sigma^{o} - \bar{\sigma}_1^{o})^2 = \frac{n-1}{n}\,\mathrm{VAR}(\sigma_p^{o}) \tag{69}$$

so that

$$S_1^2 = \frac{1}{n-1}\sum_{1}^{n}\,(\sigma_i^{o} - \bar{\sigma}_i^{o})^2 \tag{70}$$

has an expected value of VAR(σ_p^{o}) and is an unbiased estimate of VAR(σ_p^{o}). This ought to be close to

$$S_{1*}^2 = \alpha_1(\bar{\sigma}_1^{o})^2 + \beta_1\,\bar{\sigma}_1^{o} + \gamma_1 \tag{71}$$

If, on the other hand, t_p and t_R are independent for this sample, then

$$\bar{\sigma}_2^{o} = \frac{1}{n}\sum_{1}^{n}\,\sigma_i^{o} \tag{72}$$

is the sample mean such that

$$\mathcal{E}\,(\bar{\sigma}_2^{o}) = \sigma_M^{o} \tag{73}$$

Also

$$S_2^2 = \frac{1}{n-1}\sum_{1}^{n}\,(\sigma_i^{o} - \bar{\sigma}_2^{o})^2 \tag{74}$$

is the unbiased sample variance. The quantity S_2^2 has an expected value equal to the variance of σ^{o} and is an unbiased estimate of VAR(σ_M^{o}) which ought to be close to

$$S_{2*}^2 = \alpha_2(\bar{\sigma}_2^{o})^2 + \beta_2\,\bar{\sigma}_2^{o} + \gamma_2 \tag{75}$$

from Eqn. (62).

The different samples of size n do not contain any information on whether either $\bar{\sigma}_1^o$, S_1^2 and S_{1*}^2 or $\bar{\sigma}_2^o$, S_2^2 and S_{2*}^2 were sampled, but the statistics could contain this information. Only one sample mean is known and only one sample variance is known. The sample mean can be substituted into both Eqns. (67) and (71).

If S_2^2 and S_{2*}^2 are close together, with perhaps S_2^2 larger than S_{2*}^2 then successive values of σ^o are probably independent, and Table 2 is appropriate. If S_1^2 and S_{1*}^2 are close together and if S_{2*}^2 is seven to twenty times larger than S_1^2, then successive values of t_R are highly correlated. Locally, the sampling variability is described by Table 1, but the expected values of the estimates do not equal the values for the model and can be biased either high or low.

Thus, if the above statistics yield values for estimates of the variance perhaps 50% higher (or perhaps two to three times larger), but not seven to twenty times larger, than those in Table 1, the independence of successive values of t_R is questionable. The use of Table 2 to recover the winds poses problems because the errors in the recovered winds from the MLE are systematic locally and not independent. This contingency needs to be treated theoretically and modeled. A test of the hypothesis can be made rather quickly and the contingent plans implemented if needed.

It is also possible that improved methods for reducing the additional sources of variability included in Table 2 may be

developed so that the values of α in that table may be reduced considerably prior to the launch of the spacecraft. All of the results presented prior to Part 8 are subject to revision if successive values of t_R are not independent in the probability sense.

8.7 The Amazon rain forest. The SEASAT-SASS antenna pattern was calibrated against homogenious and isotropic backscatter from the Amazon rain forest. These values would not vary because of mesoscale fluctuations in the wind over the ocean as described in Section 8.5. The test described in Section 8.6 can easily be applied over fairly long orbit segments so as to be able to determine whether or not the added effects in Table 2, compared with Table 1, contribute to the variability of the sample values of the backscatter.

9. EXAMPLES BASED ON TABLE 2 FOR RANDOM INTERVALS AND RESULTS FOR A CANDIDATE MODEL FUNCTION

9.1 Assumptions. In this part, it will be assumed, subject to revision, that Table 2 represents the parameters, α, β and γ, for the various tabulated incidence angles. What could happen if Table 1 should have been used along with slowly varying values of t_R will be mentioned at times.

9.2 Random intervals. Tables 3.1 to 3.10 provide values for the end points of the random intervals with various probabilities of including the model value, σ^o_M, given a sample value of σ^o. The calculations are based on the ten sets of values of α, β and γ for the ten different incidence angles in Table 2.

The first column is the value of t appropriate to the sample value, σ^o. The integral from t to ∞ is the probability that σ^o_M is zero (it cannot be negative).

The sample value of σ^o is in the second column. The column headed by 5% is the lower bound on a range of values for σ^o_M such that the value in that column and the value in the 95% column provide an interval that has a 90% chance of including the value of σ^o_M.

The 15.87% and 84.13% columns are for $|t_1|=|t_2| = 1$. The intervals defined by these end points have a 68.26% chance of enclosing the value of σ^o_M.

From Table 3.1 for the first row, a few of the statements that can be made are:

(1) If $\sigma^o = 0.18$, the probability that $\sigma_M^o \equiv 0$ is negligible.

(2) $P(0.1155 < \sigma_M^o < 0.2713) = 0.90$

(3) $P(0.1387 < \sigma_M^o < 0.2389) = 0.6826$

In contrast, if the sample value is 0.06 (i.e. $\sigma^o = 0.06$), the probability that σ_M^o could be identically zero can be found in the tables for the normal PDF. Also

(4) $P(0.0077 < \sigma_M^o < 0.0576) = 0.90$

and so on.

If the sample value is 0.012, the probability that $\sigma_M^o \equiv 0$ is not negligible. Also

(5) $P(0 < \sigma_M^o < 0.0705) < 0.90$

and

(6) $P(0.0705 < \sigma_M^o < \infty) = 0.05$

If $\sigma^o = -0.06$, none of the intervals exist. The probability that $\sigma_M^o \equiv 0$ is almost but not quite 1.00 as calculated from t and the probability that σ_M^o is greater than zero is less than 0.05.

In terms of the analysis given in Section 5.4, the bottom four rows show the values of σ^o such that, in order, the lower bounds on the 90% and 68.26% intervals become zero and the upper

TABLE 3.1 STATISTICS FOR RANDOM INTERVALS AND MAXIMUM LIKELIHOOD ESTIMATES (TIMES 10^2) $\theta = 15.6^0$, $\alpha = 0.019125$ $\beta = 0.002517$, $\gamma = 0.0009917$

t	SAMPLE σ^0	5%	15.87%	84.13%	95%	MLE
5.72	18.0	11.55	13.87	23.09	27.13	17.54
5.33	16.8	10.50	12.77	21.74	25.65	16.36
4.95	15.6	9.44	11.67	20.40	24.18	15.19
4.57	14.4	8.38	10.56	19.05	22.71	14.01
4.19	13.2	7.32	9.46	17.71	21.24	12.83
3.81	12.0	6.25	8.35	16.38	19.78	11.65
3.43	10.8	5.17	7.23	15.05	18.33	10.48
3.05	9.6	4.08	6.11	13.72	16.87	9.30
2.67	8.4	2.98	4.99	12.40	15.45	8.12
2.29	7.2	1.88	3.86	11.08	14.02	6.99
1.91	6.0	0.77	2.72	9.77	12.61	5.76
1.52	4.8	-	1.58	8.46	11.20	4.59
1.14	3.6	-	0.43	7.16	9.80	3.41
0.76	2.4	-	-	5.87	8.41	2.23
0.38	1.2	-	-	4.59	7.05	1.06
0	0	-	-	3.31	5.69	0
-0.38	-1.2	-	-	2.04	4.35	0
-0.76	-2.4	-	-	0.78	3.01	0
-1.14	-3.6	-	-	-	1.05	0
-1.53	-4.8	-	-	-	0.41	0
-1.91	-6.0	-	-	-	-	0
1.654	5.18	0	NA	NA	NA	
1.000	3.14	NA	0	NA	NA	
-1.000	-3.14	NA	NA	0	NA	
-1.654	-5.18	NA	NA	NA	0	

NA is "not applicable"

TABLE 3.2 STATISTICS FOR RANDOM INTERVALS AND MAXIMUM LIKELIHOOD ESTIMATES (TIMES 10^2) $\theta = 19.9^o$, $\alpha = 0.01648$, $\beta = 0.0013575$, $\gamma = 0.0008225$

t	SAMPLE σ^o	5%	15.87%	84.13%	95%	MLE
6.29	18.0	12.22	14.32	22.42	25.84	17.64
5.86	16.8	11.15	13.21	21.09	24.40	16.46
5.44	15.6	10.08	12.10	19.76	22.96	15.28
5.02	14.4	9.00	10.98	18.44	21.53	14.10
4.60	13.2	7.91	9.86	17.12	20.10	12.92
4.18	12.0	6.82	8.73	15.81	18.67	11.74
3.77	10.8	5.72	7.60	14.50	17.27	10.56
3.55	9.6	4.61	6.47	13.19	15.87	9.38
2.93	8.4	3.49	5.33	11.89	14.48	8.20
2.51	7.2	2.37	4.19	10.59	13.09	7.02
2.09	6.0	1.23	3.04	9.30	11.72	5.84
1.67	4.8	0.008	1.88	8.02	10.35	4.66
1.26	3.6	-	0.71	6.74	9.00	3.48
0.84	2.4	-	-	5.48	7.66	2.29
0.42	1.2	-	-	4.21	6.34	1.12
0.00	0	-	-	2.96	5.02	0
-0.42	-1.2	-	-	1.72	3.72	0
-0.84	-2.4	-	-	0.48	2.44	0
-1.26	-3.6	-	-	-	1.16	0
-1.67	-4.8	-	-	-	-	0
1.654	4.72	0	NA	NA	NA	
1.000	2.87	NA	0	NA	NA	
-1.000	-2.87	NA	NA	0	NA	
-1.654	-4.72	NA	NA	NA	0	

NA is "not applicable"

TABLE 3.3 STATISTICS FOR RANDOM INTERVALS AND MAXIMUM LIKELIHOOD ESTIMATES (TIMES 10^2) $\theta = 24.7^o$, $\alpha = 0.01729$, $\beta = 0.0004497$, $\gamma = 0.00008354$

t	SAMPLE σ^o	5%	15.87%	84.13%	95%	MLE
5.91	5.40	3.58	4.24	6.79	7.87	5.29
5.51	5.04	3.26	3.91	6.39	7.44	4.93
5.12	4.68	2.94	3.58	5.99	7.01	4.58
4.72	4.32	2.62	3.24	5.60	6.59	4.22
4.33	3.96	2.29	2.91	5.20	6.15	3.87
3.94	3.60	1.96	2.57	4.80	5.72	3.52
3.54	3.24	1.63	2.23	4.41	5.29	3.16
3.15	2.88	1.30	1.89	4.01	4.87	2.81
2.76	2.52	0.96	1.55	3.63	4.45	2.46
2.36	2.16	0.63	1.20	3.23	4.03	2.10
1.97	1.80	0.28	0.86	2.85	3.62	1.75
1.58	1.44	-	0.51	2.47	3.21	1.39
1.18	1.08	-	0.16	2.08	2.80	1.04
0.79	0.72	-	-	1.70	2.40	0.69
0.39	0.36	-	-	1.13	1.80	0.33
0.00	0	-	-	0.95	1.61	0
-0.39	-0.36	-	-	0.57	1.21	0
-0.79	-0.72	-	-	0.19	0.83	0
-1.18	-1.08	-	-	-	0.25	0
-1.58	-1.44	-	-	-	0.07	0
-1.97	-1.80	-	-	-	-	0
1.654	1.50	0	NA	NA	NA	
1.000	0.91	NA	0	NA	NA	
-1.000	-0.91	NA	NA	0	NA	
-1.654	-1.50	NA	NA	NA	0	

NA is "not applicable"

TABLE 3.4 STATISTICS FOR RANDOM INTERVALS AND MAXIMUM LIKELIHOOD ESTIMATES (TIMES 10^3) $\theta = 31.4^o$, $\alpha = 0.01713$ $\beta = 0.0001642$, $\gamma = 9.405 \cdot 10^{-6}$

t	SAMPLE σ^o	5%	15.87%	84.13%	95%	MLE
5.87	18.0	11.89	14.11	22.68	26.32	17.62
5.48	16.8	10.83	13.00	21.35	24.87	16.44
5.09	15.6	9.75	11.89	20.02	23.43	15.26
4.70	14.4	8.67	10.77	18.70	21.99	14.08
4.30	13.2	7.59	9.65	17.37	20.56	12.90
3.91	12.0	6.50	8.52	16.06	19.14	11.72
3.52	10.8	5.40	7.40	14.74	17.71	10.54
3.13	9.6	4.29	6.27	13.43	16.31	9.36
2.74	8.4	3.17	5.13	12.13	14.91	8.18
2.35	7.2	2.05	3.99	10.83	13.52	7.00
1.96	6.0	0.91	2.83	9.54	12.13	5.87
1.57	4.8	-	1.60	8.25	10.77	4.64
1.17	3.6	-	0.52	6.97	9.41	3.46
0.78	2.4	-	-	5.70	8.06	2.28
0.39	1.2	-	-	4.44	6.73	1.10
0.00	0	-	-	3.18	5.40	0
-0.39	- 1.2	-	-	1.93	4.10	0
-0.78	- 2.4	-	-	0.69	2.80	0
-1.17	- 3.6	-	-	-	1.52	0
-1.57	- 4.8	-	-	-	0.26	0
1.654	5.04	0	NA	NA	NA	
1.000	3.07	NA	0	NA	NA	
-1.000	-3.07	NA	NA	0	NA	
-1.654	-5.04	NA	NA	NA	0	

NA is "not applicable".

TABLE 3.5 STATISTICS FOR RANDOM INTERVALS AND MAXIMUM LIKELIHOOD ESTIMATES (TIMES 10^3) $\theta = 35.4^o$, $\alpha = 0.01775$, $\beta = 0.00011$, $\gamma = 2.478 \cdot 10^{-6}$

t	SAMPLE σ^o	5%	15.87%	84.13%	95%	MLE
7.24	12.0	8.36	9.66	14.88	17.17	11.74
6.76	11.2	7.66	8.93	13.99	16.18	10.95
6.27	10.4	6.96	8.20	13.09	15.20	10.17
5.79	9.6	6.26	7.46	12.19	14.22	9.38
5.31	8.8	5.55	6.73	11.30	13.25	8.59
4.83	8.0	4.84	5.99	10.41	12.28	7.81
4.34	7.2	4.12	5.25	9.53	11.32	7.02
3.86	6.4	3.40	4.50	8.64	10.36	6.24
3.38	5.6	2.67	3.75	7.76	9.41	5.45
2.90	4.8	1.94	3.00	6.88	8.46	4.66
2.41	4.0	1.20	2.24	6.01	7.52	3.88
1.93	3.2	0.45	1.48	5.16	6.59	3.09
1.45	2.4	-	0.72	4.28	5.67	2.30
0.97	1.6	-	-	3.43	4.75	1.52
0.48	0.8	-	-	2.57	3.85	0.73
0.00	0	-	-	1.73	2.96	0
-0.48	-0.8	-	-	0.89	2.07	0
-0.97	-1.6	-	-	0.06	1.20	0
-1.45	-2.4	-	-	-	0.35	0
1.654	2.73	0	NA	NA	NA	
1.000	1.66	NA	0	NA	NA	
-1.000	-1.66	NA	NA	0	NA	
-1.654	-2.73	NA	NA	NA	0	

NA is "not applicable".

TABLE 3.6 STATISTICS FOR RANDOM INTERVALS AND MAXIMUM LIKELIHOOD ESTIMATES (TIMES 10^4) $\theta = 41^o$, $\alpha = 0.01841$, $\beta = 5.53 \times 10^{-5}$, $\gamma = 5.849 \cdot 10^{-7}$

t	SAMPLE σ^o	5%	15.87%	84.13%	95%	MLE
6.28	48.0	31.97	37.73	60.64	70.64	46.87
5.86	44.8	29.17	34.80	57.05	66.70	43.73
5.44	41.6	26.36	31.86	53.46	62.78	40.58
5.02	38.4	23.53	28.92	49.88	58.87	37.44
4.60	35.2	20.69	25.97	46.32	54.98	34.30
4.18	32.0	17.83	23.00	42.76	51.10	31.16
3.77	28.8	14.95	20.03	39.22	47.24	28.01
3.35	25.6	12.05	17.04	35.68	43.41	24.87
2.93	22.4	9.13	14.04	32.16	39.59	21.73
2.51	19.2	6.18	11.03	28.66	35.80	18.58
2.09	16.0	3.21	7.99	25.17	32.04	15.44
1.67	12.8	0.21	4.95	21.70	28.31	12.30
1.26	9.6	-	1.88	18.24	24.61	9.16
0.84	6.4	-	-	14.81	20.94	6.02
0.42	3.2	-	-	11.40	17.31	2.88
0.00	0	-	-	8.00	13.72	0
-0.42	-3.2	-	-	4.64	10.17	0
-0.84	-6.4	-	-	1.30	6.66	0
-1.26	-9.6	-	-	-	3.19	0
1.654	12.58	0	NA	NA	NA	
1.000	7.65	NA	0	NA	NA	
-1.000	-7.65	NA	NA	0	NA	
-1.654	-12.58	NA	NA	NA	0	

NA is "not applicable".

TABLE 3.7 STATISTICS FOR RANDOM INTERVALS AND MAXIMUM LIKELIHOOD ESTIMATES (TIMES 10^3) $\theta = 46^o$, $\alpha = 0.019375$, $\beta = 0.000043$, $\gamma = 2.688 \times 10^{-6}$

t	SAMPLE σ^o	5%	15.87%	84.13%	95%	MLE
5.79	3.0	1.93	2.31	3.85	4.53	2.92
4.82	2.5	1.49	1.86	3.29	3.91	2.43
3.86	2.0	1.05	1.39	2.73	3.30	1.94
2.89	1.5	0.597	0.929	2.17	2.69	1.45
1.93	1.0	0.137	0.459	1.62	2.10	0.960
1.157	0.6	-	0.078	1.19	1.63	0.568
0.965	0.5	-	-	1.08	1.51	0.4695
0	0	-	-	0.546	0.940	0
-0.965	-0.5	-	-	0.002	0.383	0
-1.544	-0.8	-	-	-	0.057	0
1.645	0.853	0	NA	NA	NA	
1.000	0.518	NA	0	NA	NA	
-1.000	-0.518	NA	NA	0	NA	
-1.645	-0.853	NA	NA	NA	0	

NA is "not applicable".

TABLE 3.8 STATISTICS FOR RANDOM INTERVALS AND MAXIMUM LIKELIHOOD ESTIMATES (TIMES 10^3) $\theta = 50.5^o$, $\alpha = 0.019917$, $\beta = 0.000031$, $\gamma = 1.539 \times 10^{-7}$

t	SAMPLE σ^o	5%	15.87%	84.13%	95%	MLE
6.12	2.4	1.57	1.87	3.06	3.59	2.34
5.10	2.0	1.23	1.50	2.61	3.09	1.95
4.08	1.6	0.872	1.14	2.16	2.60	1.55
3.06	1.2	0.512	0.765	1.72	2.11	1.16
2.04	0.8	0.144	0.389	1.28	1.64	0.769
1.02	0.4	-	0.007	0.840	1.17	0.377
0	0	-	-	0.412	0.709	0
-1.02	-0.4	-	-	-	0.265	0
1.645	0.645	0	NA	NA	NA	
1.000	0.392	NA	0	NA	NA	
-1.000	-0.392	NA	NA	0	NA	
-1.645	-0.645	NA	NA	NA	0	

NA is "not applicable".

TABLE 3.9 STATISTICS FOR RANDOM INTERVALS AND MAXIMUM LIKELIHOOD ESTIMATES (TIMES 10^3) $\theta = 55.7^o$, $\alpha = 0.021640$ $\beta = 0.000037595$, $\gamma = 1.709 \times 10^{-7}$

t	SAMPLE σ^o	5%	15.87%	84.13%	95%	MLE
5.81	2.4	1.53	1.84	3.10	3.68	2.33
4.84	2.0	1.18	1.48	2.65	3.17	1.94
3.87	1.6	0.833	1.11	2.20	2.67	1.55
2.90	1.2	0.476	0.741	1.75	2.18	1.16
1.94	0.8	0.111	0.367	1.31	1.70	0.765
1.161	0.48	-	0.064	0.956	1.31	0.452
0.967	0.4	-	-	0.869	1.22	0.373
0	0	-	-	0.438	0.757	0
-0.967	-0.4	-	-	0.0140	0.307	0
-1.549	-0.64	-	-	-	0.0434	0
1.645	0.680	0	NA	NA	NA	
1.000	0.413	NA	0	NA	NA	
-1.000	-0.413	NA	NA	0	NA	
-1.645	-0.680	NA	NA	NA	0	

NA is "not applicable".

TABLE 3.10 STATISTICS FOR RANDOM INTERVALS AND MAXIMUM LIKELIHOOD ESTIMATES (TIMES 10^3) $\theta = 59.1^o$, $\alpha = 0.02376$, $\beta = 0.00005929$, $\gamma = 3.055 \times 10^{-7}$

t	SAMPLE σ^o	5%	15.87%	84.13%	95%	MLE
5.43	3	1.84	2.25	3.95	4.74	2.90
4.52	2.5	1.41	1.80	3.38	4.10	2.41
3.62	2.0	0.98	1.35	2.81	3.47	1.93
2.71	1.5	0.535	0.886	2.25	2.84	1.44
1.81	1.0	0.083	0.421	1.69	2.23	0.948
1.085	0.6	-	0.045	1.25	1.74	0.557
0.905	0.5	-	-	1.14	1.62	0.460
0	0	-	-	0.59	1.02	0
-0.905	-0.5	-	-	0.056	0.456	0
-1.629	-0.9	-	-	-	0.010	0
1.645	0.909	0	NA	NA	NA	
1.000	0.553	NA	0	NA	NA	
-1.000	-0.553	NA	NA	0	NA	
-1.645	-0.909	NA	NA	NA	0	

NA is "not applicable".

bounds on the 68.26% and 90% intervals become zero. All of the probability statements in Section 5.4 can be made for the various values of the random variable, σ^o, based on statistics calculated from this random variable as derived in Section 7.

The last column in each table provides the values of the maximum likelihood estimates for each sample value of σ^o. Each estimate is slightly less than the value of σ^o. If the estimate, σ^o, is negative, the maximum likelihood estimate of σ_M^o must be zero.

There is a theoretical inconsistency in the definition of the maximum likelihood estimate as in Eqn. (24). If there is a finite probability that $\sigma_M^o \equiv 0$, since the PDF is otherwise continuous, the MLE strictly defined ought to be zero. In another sense the PDF is maximized for two different value of σ^o and the realistic choice is the one tabulated.

Figs. 4a to 4g are graphs of these values for incidence angles of 15.6^o, 19.9^o, 24.7^o, 31.4^o, 41.0^o, 50.5^o and 59.1^o. The graphs are entered with the sample value of σ^o on the vertical scale and the curves then define the various random intervals with the indicated probabilities of enclosing the value of σ_M^o as given on the horizontal axis. Supplementary values in dB are also shown for each graph.

For Fig. 4a, the sample values range from 0.20 (-6.99 dB to) zero (- ∞ dB) to -0.10 (dB not defined). If σ^o has the value given by $1.654\,\gamma^{\frac{1}{2}}$, the 90% random interval has a range from - ∞ to somewhat greater than -10 dB. Trying to understand backscatter

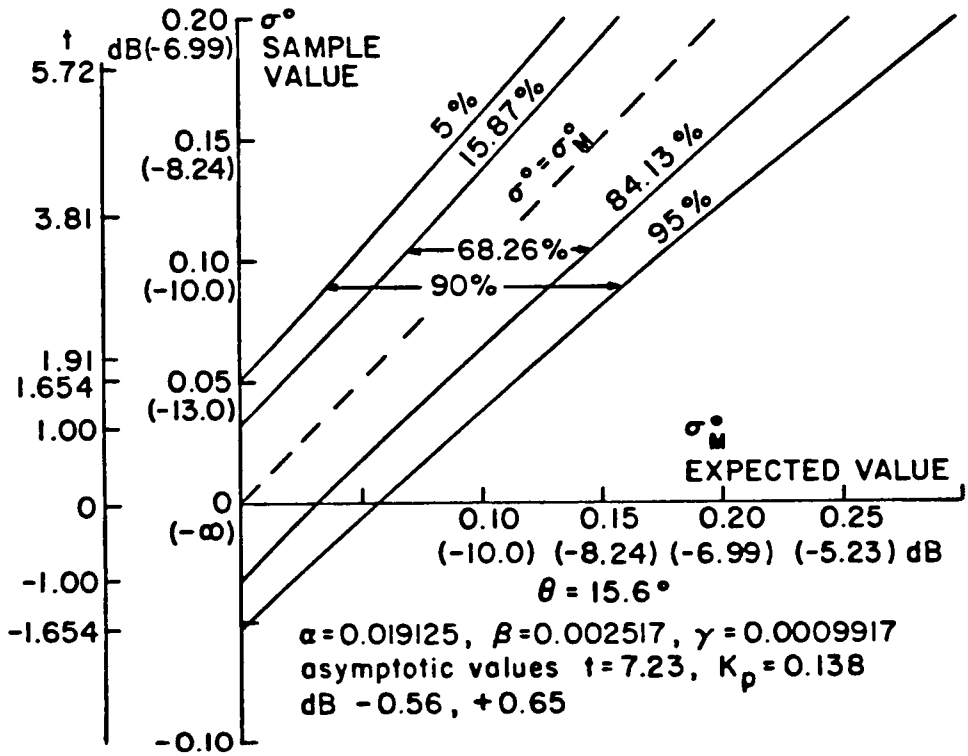

Fig. 4a Random Intervals with Probabilities of 68.26% and 90% of Enclosing the Model Value for σ°_{M} 15.6° and the Values of α, β and γ in Table 2. Linear scales (Values in dB are Shown in Parentheses).

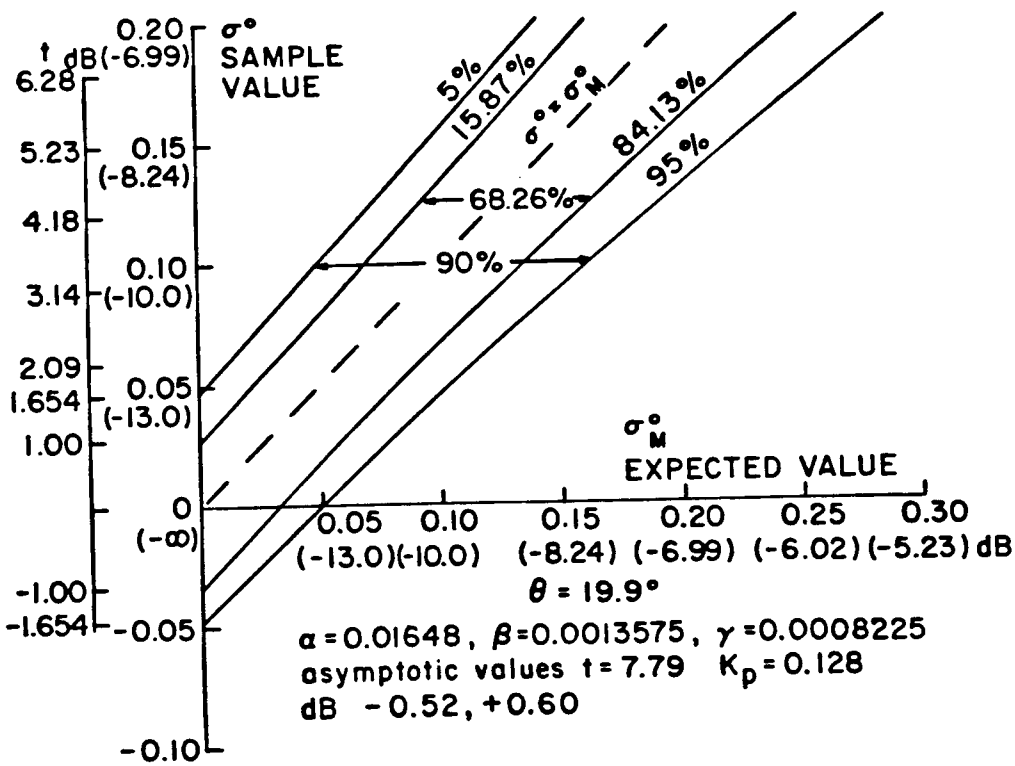

Fig. 4b Same as Fig. 4a Except for $\theta = 19.9^{\circ}$.

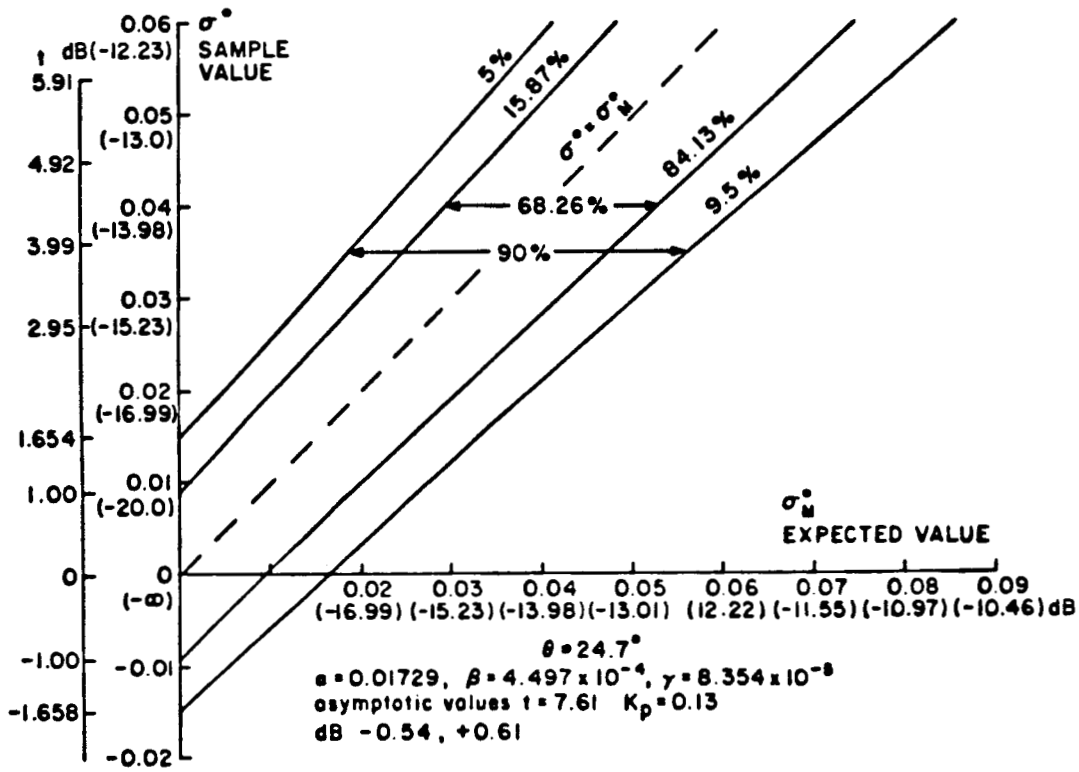

Fig. 4c Same as Fig. 4a Except for $\theta = 24.7^{\circ}$.

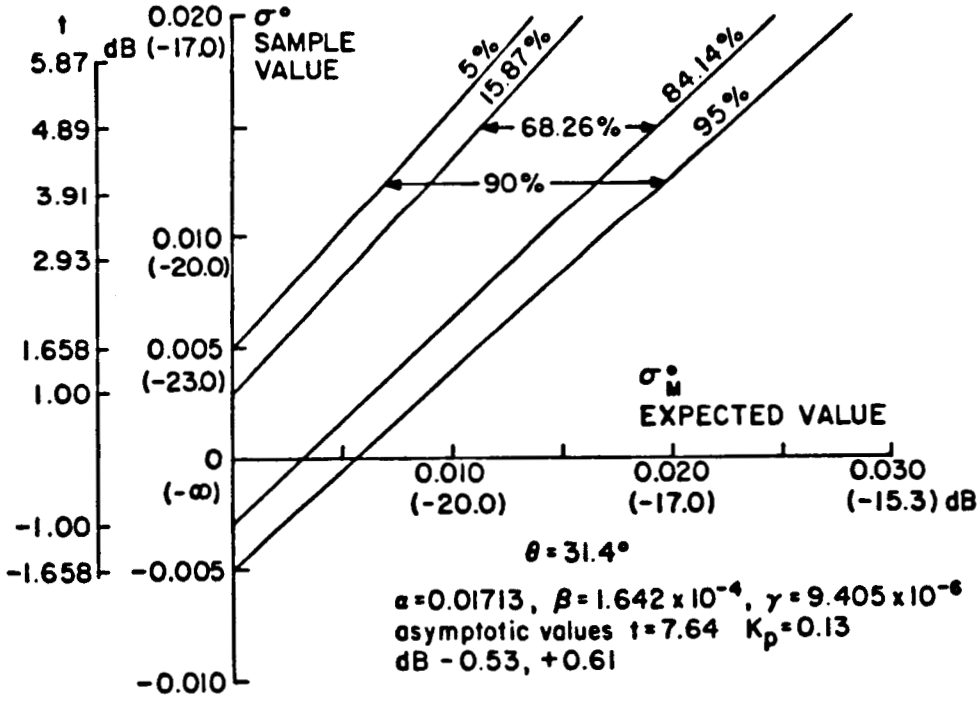

Fig. 4d Same as Fig. 4a Except for $\theta = 31.4^{\circ}$.

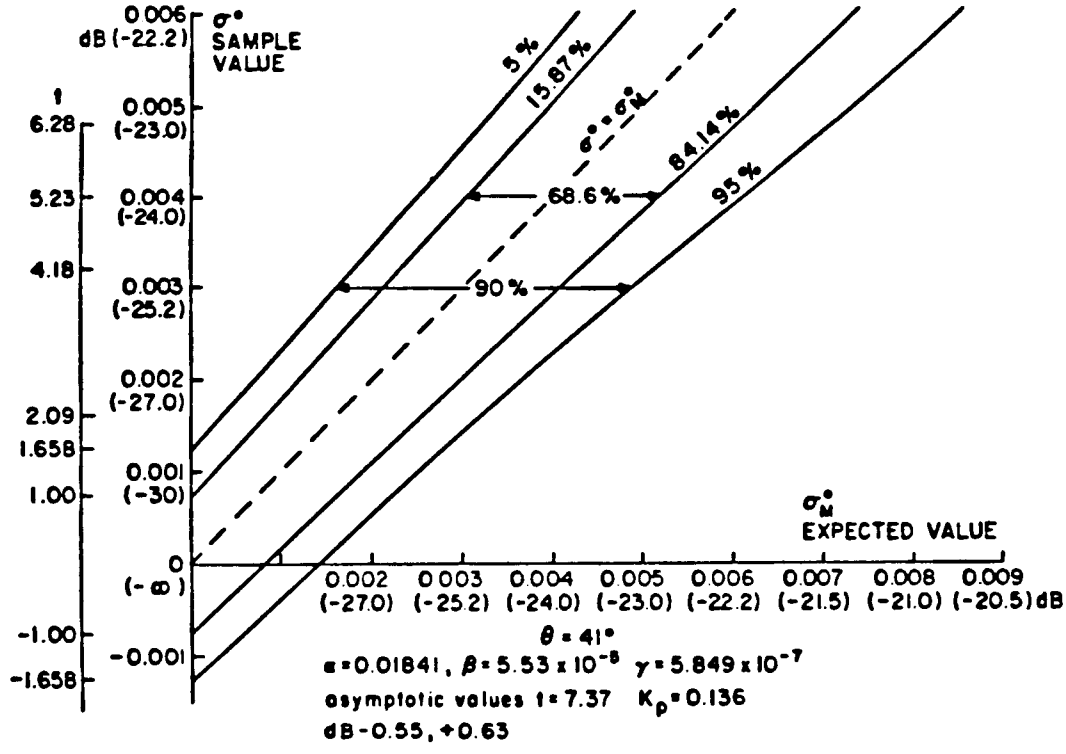

Fig. 4e Same as Fig. 4a Except for $\theta = 41.0^{\circ}$.

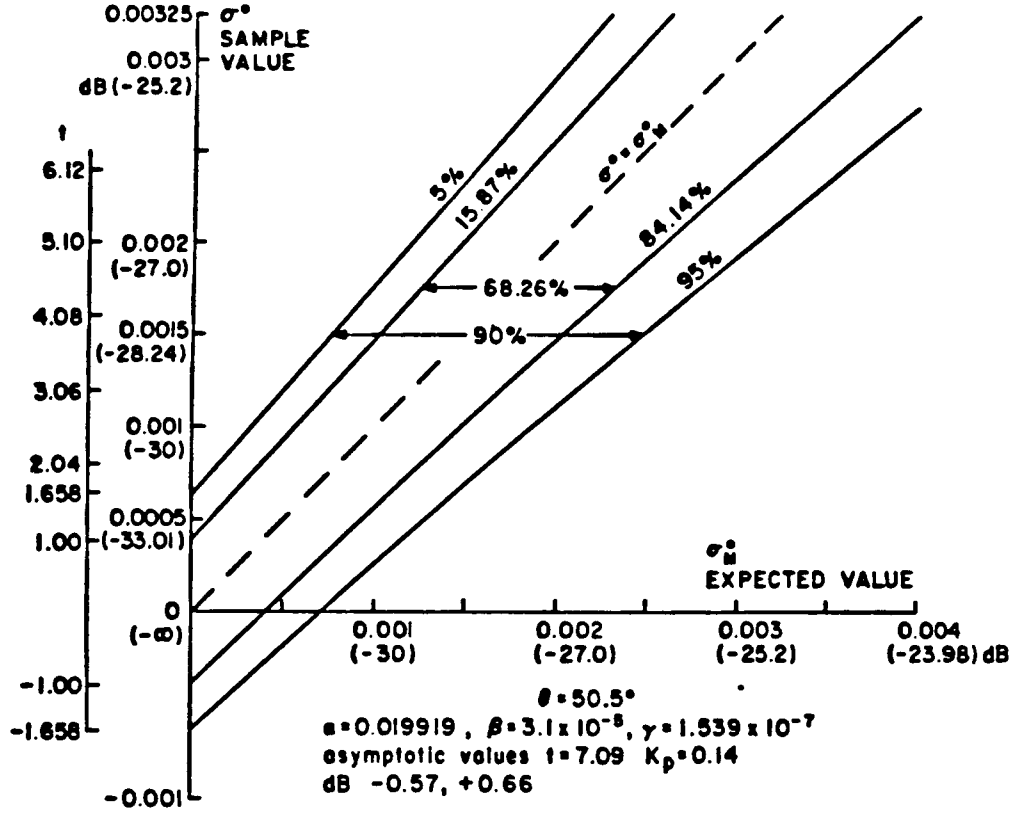

Fig. 4f Same as Fig. 4a Except for $\theta = 50.5^{\circ}$.

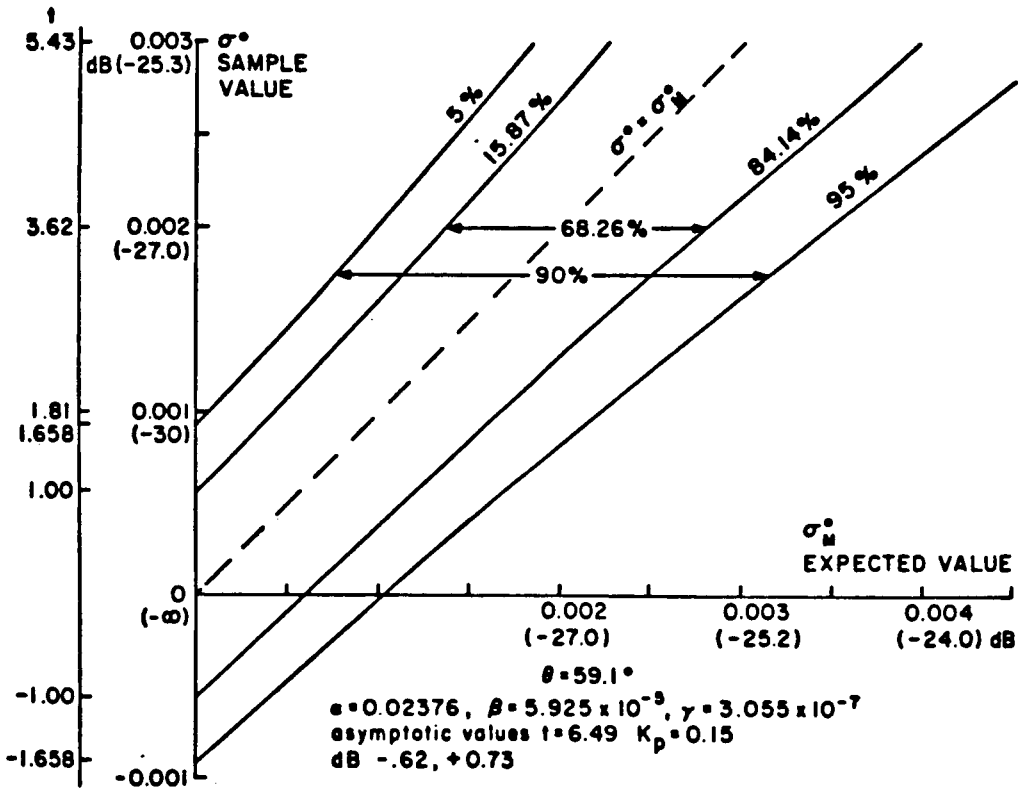

Fig. 4g Same as Fig. 4a Except for $\theta = 59.1^{\circ}$.

values in terms of decibels or logarithms of σ^o and σ_M^o can be difficult at times.

These seven graphs at first glance appear to be very much alike, but closer inspection shows them to be quite different. The ranges of σ^o and σ_M^o are different. The intercepts with the σ^o axis, which depend on $\gamma^{\frac{1}{2}}$ are different and the lengths of the random intervals increase at different rates depending on the size of α.

Since γ decreases by only 1.5 to 2% when Table 1 is compared to Table 2, had Table 1 been used to construct the graphs, the four curves would have had slopes closer to unity and the lengths of the random intervals would not increase as rapidly as they do in these figures. The variability introduced by the uncertainty in the quantity, R, is thus important for high values of σ^o (and σ_M^o), in a relative sense, as determined especially by α, and by β and γ.

9.3 Interpretation in terms of a candidate model. For illustrative purposes, the candidate model will be the one given by Donelan and Pierson (1987). The curves for the model are from Fig. 7 of this reference. Figs. 5a and 5b are for a water temperature of 0^oC and incidence angles respectively of 20^o, 40^o and 60^o and 30^o and 50^o. Figs. 5c and 5d are for a water temperature of 30^o and the same incidence angles as in the previous two figures. The slight differences in incidence angle between Table 2 and these values have been neglected. All four of these figures are based on the sampling variability of one single 25 by 25 km area for vertical polarization.

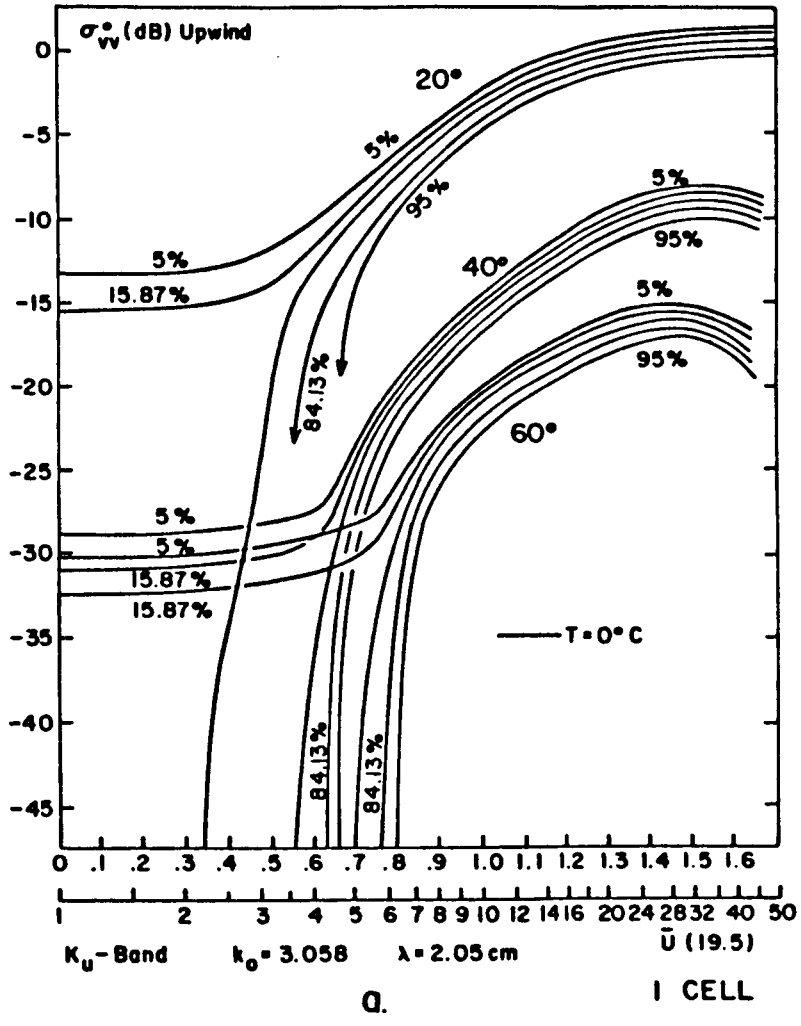

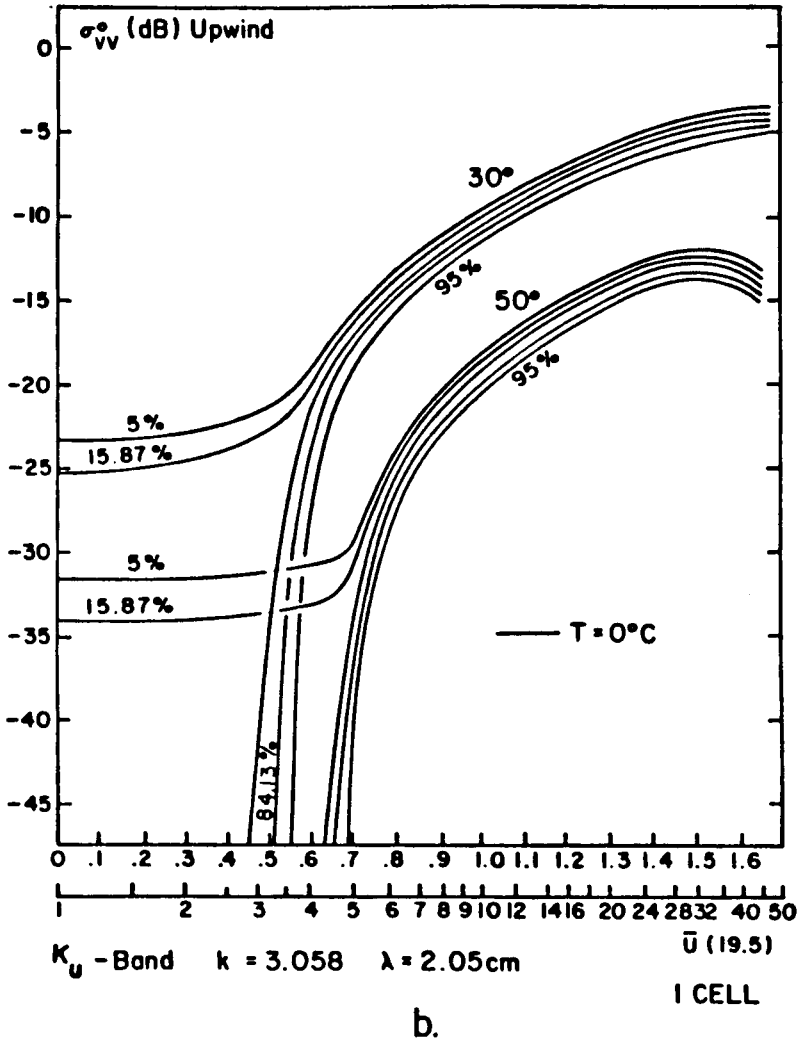

Fig. 5a Curves for 5%, 15.87%, 84.13% and 95% Based on Table 2 for One 25 by 25 Km Area for an Assumed Model for Incidence Angles of 20°, 40° and 60° and a Water Temperature 0°C. For Interpretation, See Text.

Fig. 5b Same as Fig. 5a Except for Incidence Angles of 30° and 50° and a Water Temperature of 0°C.

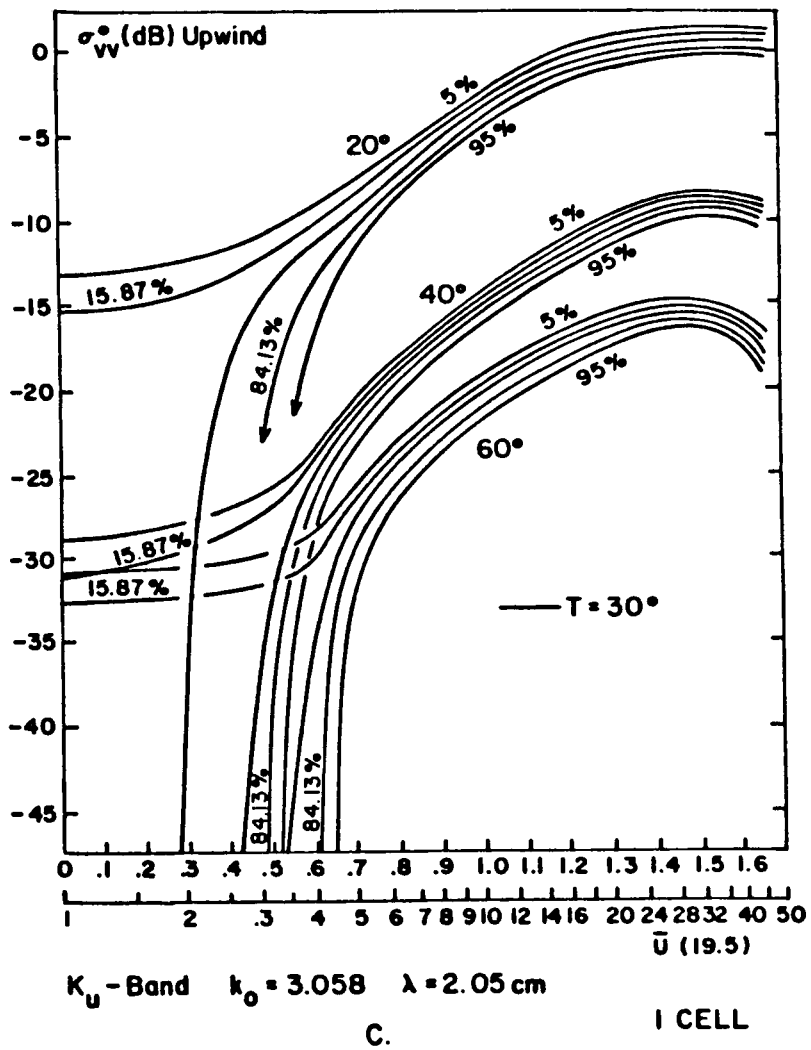

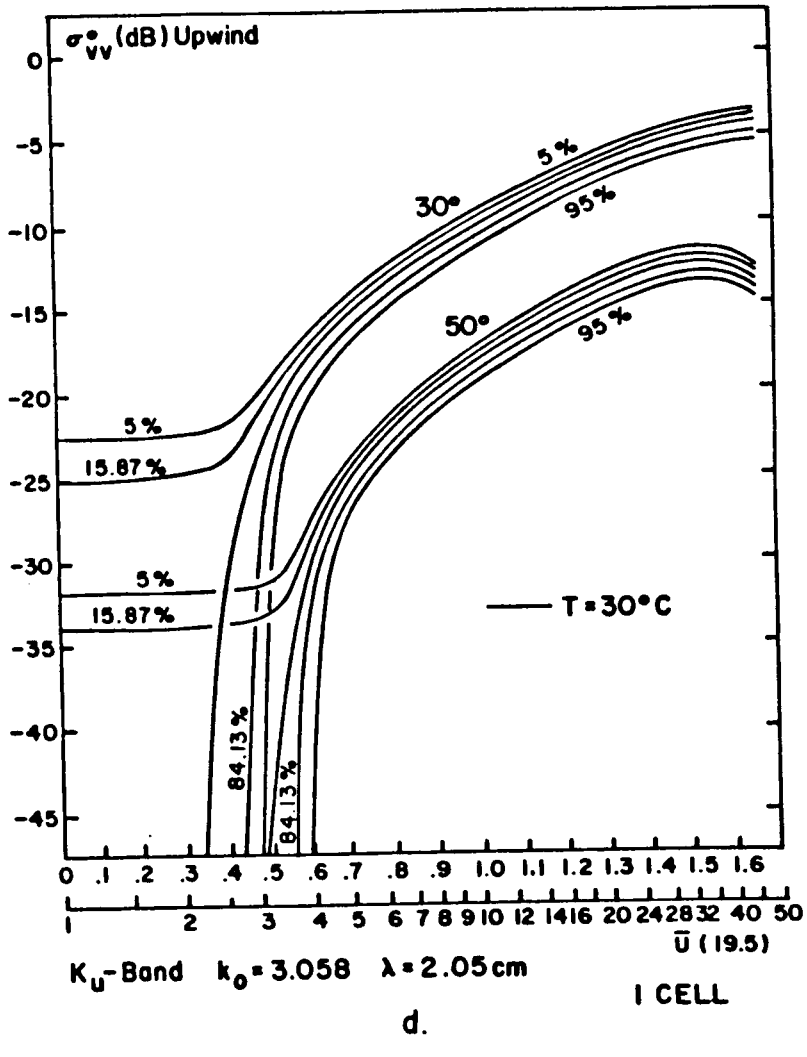

Fig. 5c Same as Fig. 5a Except for Incidence Angles of 20°, 40° and 60° and a Water Temperature of $30^{\circ}C$.

Fig. 5d Same as Fig. 5a Except for Incidence Angles of 30° and 50° and a Water Temperature of $30^{\circ}C$.

Figs. 6a to 6d show the result of averaging the σ^o values from four 25 by 25 km areas in a row parallel to the subsatellite track. The four incidence angles and the four values of α, β and γ would be averaged also. The values of α, β and γ have been divided by four based on (27).

For purposes of discussion, it will be assumed that the model is correct. The results are for either one 25 by 25 km area at the indicated incidence angle and temperature as in Figs. 5a to 5d or for a row of four areas parallel to the subsatellite track as in Figs. 6a to 6d. The values of α, β and γ from Table 2 have been used for the incidence angles closest to those in these figures.

For each incidence angle in Figs. 5a to 5d there are five curves. The center curve is for the model, and it is surrounded by the four curves labled 5%, 15.83%, 84.13% and 95%. The backscatter estimate is assumed to be for an upwind look. The conclusions of Donelan and Pierson that the backscatter can become undetectable before the wind becomes zero, that there is no power law and that backscatter may saturate and then decrease for high enough winds are illustrated by this set of four figures.

The interpretation of each one of the eight figures depends on the meaning of the vertical axis. If $\sigma^o_{VV(dB)}$ for upwind represents the model value, then entering with the wind speed on the horizontal axis provides the model value for σ^o_M on the vertical axis. Eqn. (12) can then be used to calculate the scatter of the random variable σ^o about the value of σ^o_M and graph the four curves with the assigned probabilities for Figs. 5a to 5d. Thus

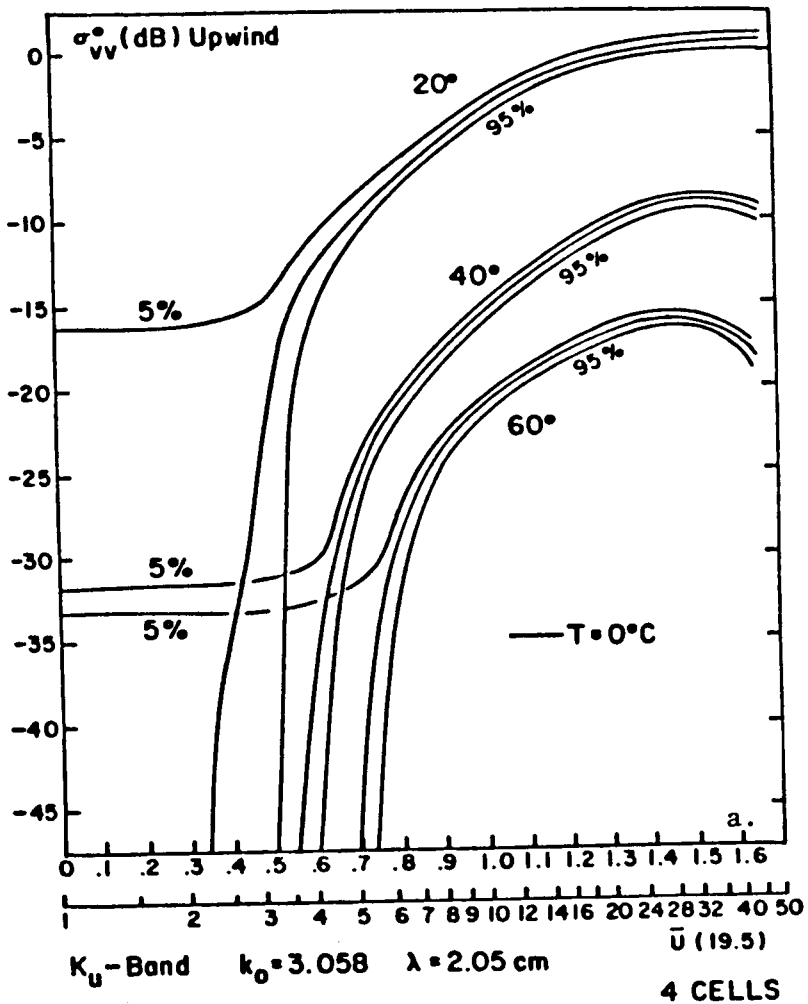

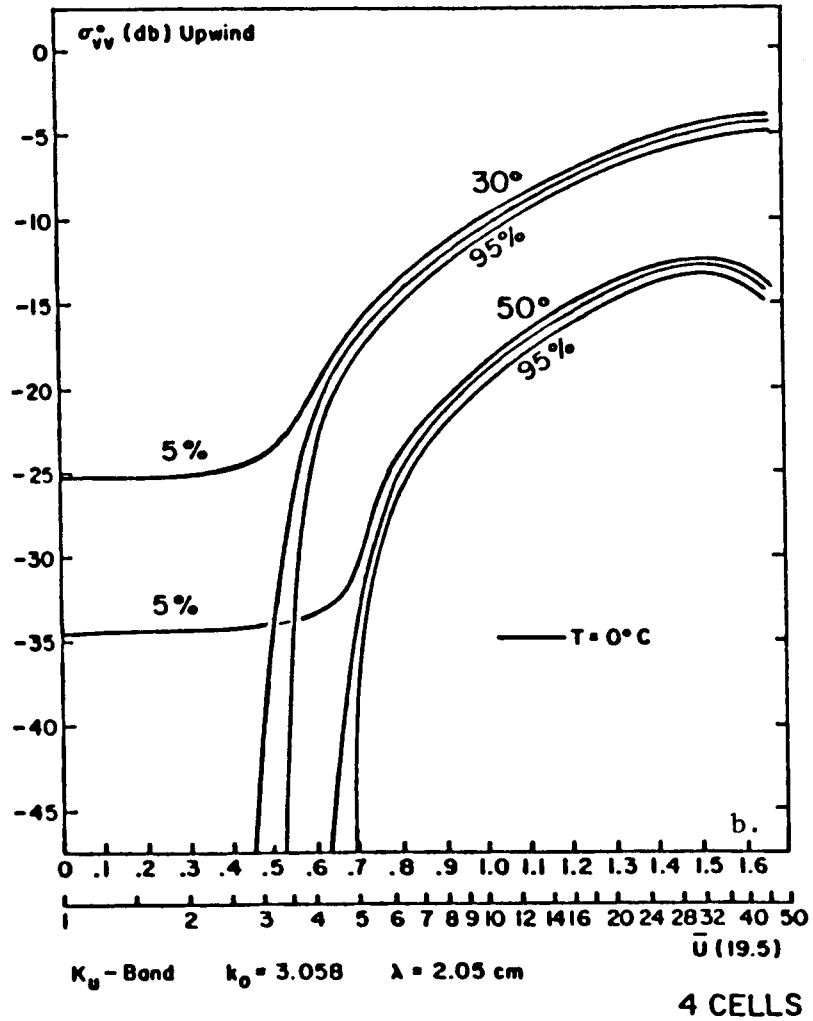

Fig. 6a Curves for 5% and 95% Based on Table 2 for the Average of Four Adjacent 25 by 25 Km Areas at the Same Incidence Angle for Incidence Angles of 20°, 40° and 60° and a Water Temperature of $0^{\circ}C$. For Interpretation, See Text.

Fig. 6b Same as Fig. 6a Except for Incidence Angles of 30° and 50° and a Water temperature of $0^{\circ}C$.

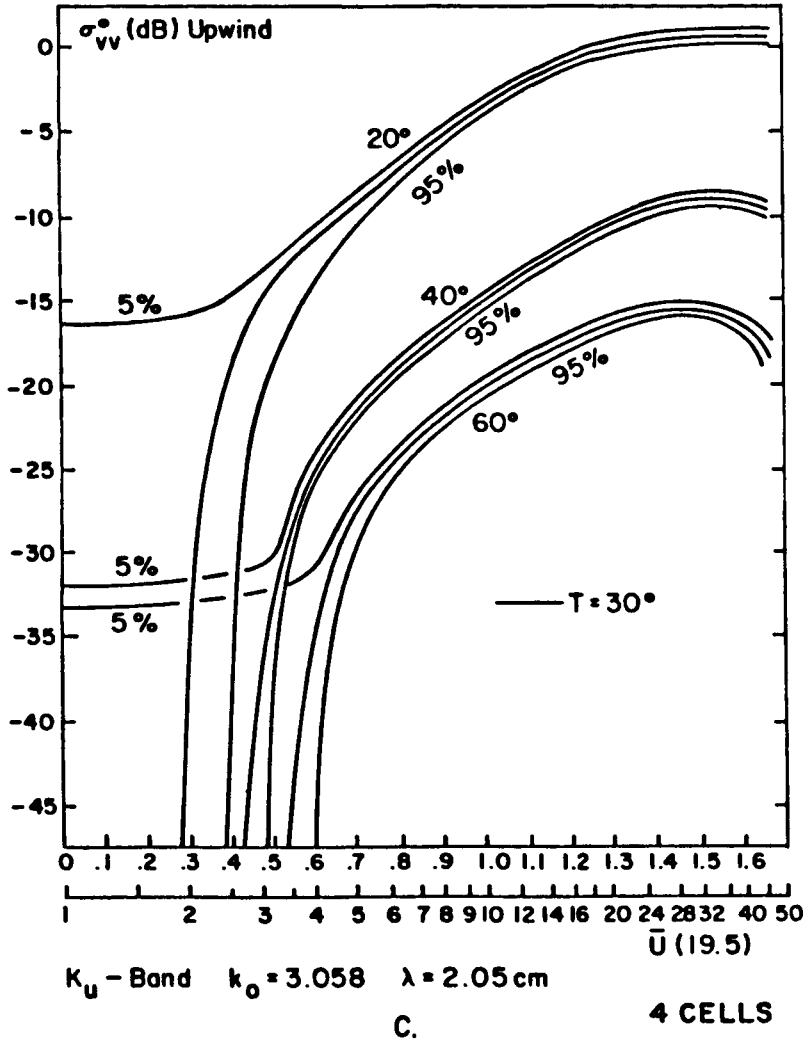

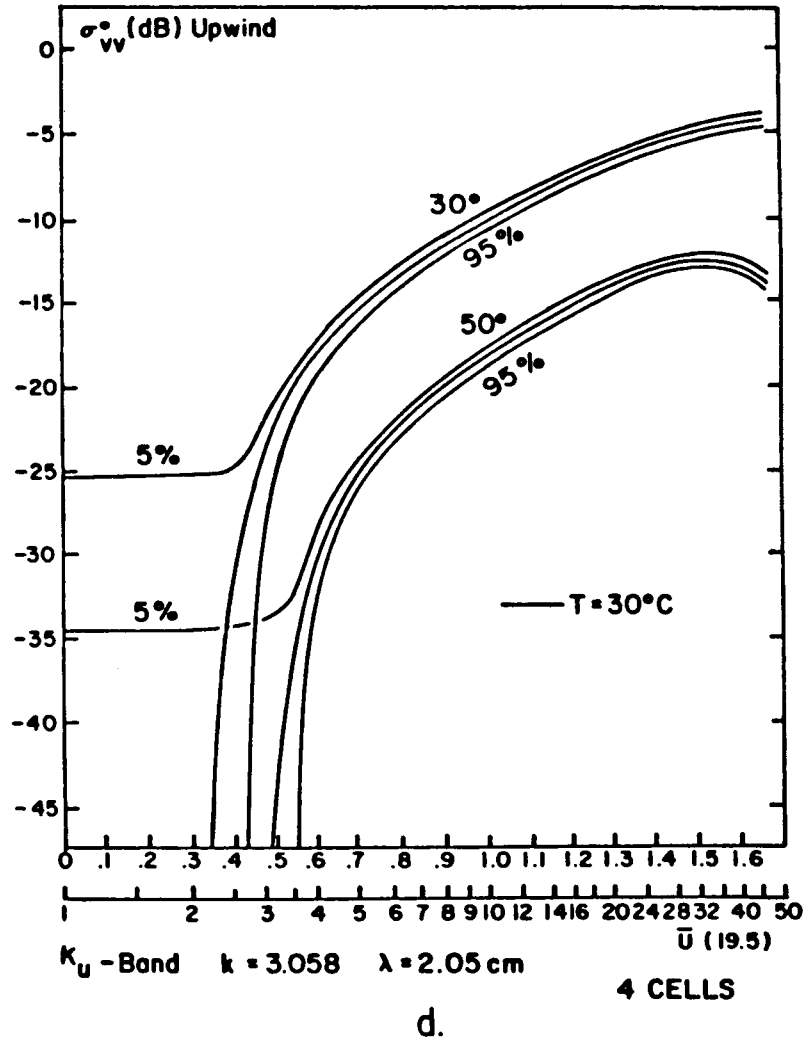

Fig. 6c Same as Fig. 6a Except for Incidence Angles of 20°, 40° and 60° and a Water Temperature of 30°C.

Fig. 6d Same as Fig. 6a Except for Incidence Angles of 30° and 50° and a Water Temperature of 30°C.

for Fig. 5a if the wind is, say, 10 m/s for an incidence angle of 40^{o}, the random variable, σ^{o} will be between about -14 dB and -17 dB 90% of the time. For Figs. 6a to 6d, Eqn. (27) yields a reduced variance and standard deviation, and this new value is used in (12) to calculate the 5% and 95% curves. At 10 m/s for, example, in Fig. 8a at a 40^{o} incidence angle, the random variable will be within a range from about -15.4 dB to about -16.8 dB 90% of the time.

For all eight figures for low enough wind speeds, there is no backscatter predicted by the model above -47.5 dB. In the model being used as an example, the prediction is that there is no backscatter from the waves for winds below a certain water temperature dependent wind speed. Below this threshold wind speed the model value for σ^{o}_{M} is zero. In Figs. 5a to 5d, the 5% and 15.87% curves are drawn for 1 m/s at the values $1.645\gamma^{\frac{1}{2}}$ and $\gamma^{\frac{1}{2}}$ in dB. In Figs. 6a to 6d, the 5% curve is at $1.645(\gamma/4)^{\frac{1}{2}}$ and is thus 3 dB lower for low winds than the corresponding curve in Figs. 5a to 5d.

The 84.13% and 95% curves in the various Figs. 5a to 5d go to minus infinity dB at those points on the $\bar{U}$, axis in the appropriate Figure from Figs. 4a to 4g where these curves intersect the σ^{o}_{M} axis for one 25 by 25 km area. For low winds with σ^{o} in antilog form, the 90% range of values of σ^{o} would be from the appropriate antilog in the figure as an upper bound to its negative value as a lower bound.

The lower left region for each incidence angle has the property that positive sample values of the backscatter from ac-

tual data plotted in dB against meteorologically obtained winds would scatter all over the region. This feature of actual data is well illustrated in Schroeder, et al. (1982). Negative values were discarded.

For the range of wind speeds that were used for the study of the SEASAT SASS data, it would be possible to draw a number of different power laws within the 5% to 95% curves for Figs. 5a to 5d. Graphs such as these figures about model lines as power laws would still form the same patterns for the low wind, low σ^o areas, and thus light winds would still be uncertain, but well within present design requirements, except, perhap, for cold water.

For one 25 by 25 km area (1 cell), Figs. 5a to 5d show that if the incidence angle and water temperature are known, 90% of the sample values of σ^o will occur somewhere in the region below the 5% curve and above, or to the left, of the 95% curve. Were both the value of σ^o and the wind speed known the plotted point ($\bar{U}$, σ^o) would usually not fall on the model curve for σ^o_M.

For four cells in a row parallel to the subsatellite track, the advantage of an average (if the wind does not change too much) is evident in Figs. 6a to 6d. Ninety percent of the points ($\bar{U}$, $\bar{\sigma}^o$) scatter in a much narrower range about the model curve and the area in the lower left for each incidence angle is made smaller.

Figures similar to these eight figures could also have been prepared for averages of two σ^o values parallel to the subsatel-

lite track. The values of α, β and γ would be reduced by a factor of two. The asymptotic values in Table 2 would all be reduced. The value of $\gamma^{\frac{1}{2}}$ would also be reduced. As an example, for, say a 35.4^{o} incidence angle, instead of -0.54 and +0.62 dB, the asymptotic values would be -0.39 and +0.43 and $\gamma^{\frac{1}{2}}$ in dB would be -29.3 instead of -27.8, dB.

Each of these figures for a particular incidence angle could be extended to a three variable plot of $\sigma_M^o + |t_2|SD(\sigma_M^o)$, σ_M^o and $\sigma_M^o - |t_1|SD(\sigma_M^o)$ versus $\bar{U}$ and χ. For a fixed $\bar{U}$, the resulting surface for σ_M^o would vary as sketched in Figs. 5 and 6 and the upper and lower ranges for the scatter in σ^o would follow the undulations of the surface.

If the vertical scale on these eight figures represents the sample value, either σ^o or $\bar{\sigma}^o$, there is the temptation to enter one of these figures, with the sample value, find the values for the 5% and 95% curves, for example, and the corresponding wind speeds and conclude that, if looking upwind, there is a 90% chance that the wind speed is between these two values. As a first approximation, this proceedure yields a range of wind speeds that is not quite correct because the slopes of the curves are continuously changing with increasing wind speed.

Figs. 7a to 7d illustrate a correct way to interpret these figures given a sample value of either σ^o or $\bar{\sigma}^o$. Since the incidence angle is known, the values of α, β and γ are known. The random interval with, say, a 90% chance of enclosing the value, σ_M^o can be computed, and the values for the end points will intersect the curve for σ_M^o in the various ways sketched in the

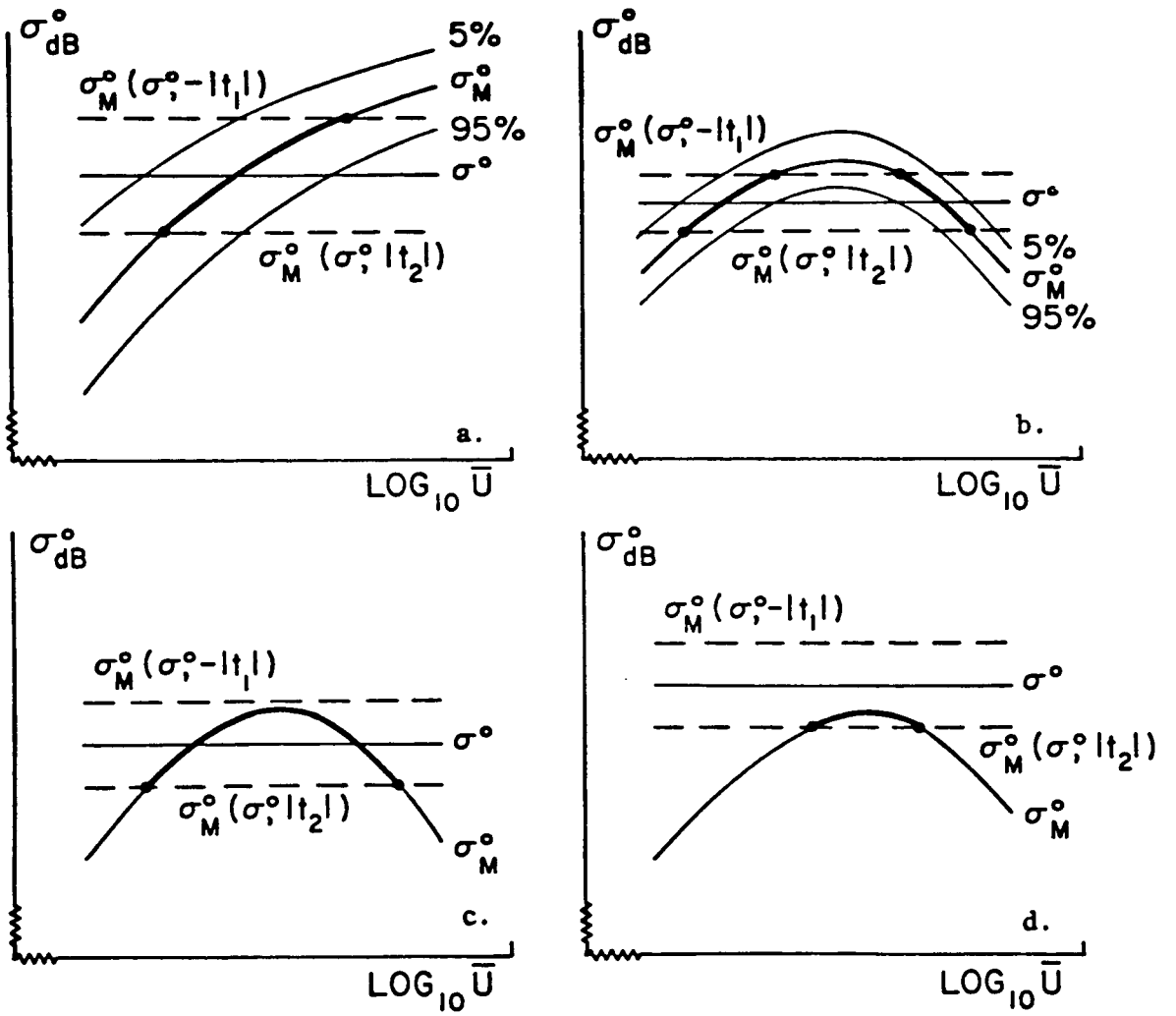

Fig. 7a) An Example of the Use of a 90% Random Interval for a Portion of one of the Sets of Curves in Either Fig. 5 or 6. Not to Scale;
b) The Use of a 90% Random Interval if the Model Values Saturate and Then Decrease;
c) The Use of a 90% Random Interval Near the Roll-Over Portion of a Model, the 5% and 95% Curves Have No Meaning;
d) A Possible 90% Random Interval Near the Maximum of the Roll-Over for a Model, the 5% and 95% Curves Have No Meaning.

figures, if the lower bound lies above the 5% curve for the chosen incidence angle and sample value.

Fig. 7a illustrates the condition that the sample value is low enough so that the possible effect of saturation and roll-over for the model need not be considered. The upper and lower bounds on the random interval with a 90% chance of containing the value, σ^o_M, intersect the model curve at two points and the possible values of σ^o_M, 90% of the time, will be on the heavy portion of the curve shown in Fig. 7a. Compared with the points where the line for σ^o intersects the 5% and 95% curves, the bounds on the range of wind speeds are broader.

Should the effect of roll-over be even more pronounced than modeled in Figs. 5 and 6, three possibilities are shown in Figs. 7b, 7c and 7d. For Fig. 7b, there are two possible ranges of values for σ^o_M and two possible ranges of wind speed. For Fig. 7c, a very broad range of wind speeds is possible near the maximum of the model curve.

Fig. 7d is an interesting result. The sample value can be higher than the model value such that only the lower bound intersects the σ^o_M curve. If the model is correct, the range of wind speeds can be much smaller compared with Fig. 7c.

The lower left corner for each incidence angle in Figs. 5 and 6, is difficult to interpret for low winds and low backscatter estimates because of the distortion introduced by the logarithmic scales. Figs. 8a to 8d show how the sample values can be used for linear scales. For Figs. 8a to 8d, the main part

of the figure is the same. The curves for σ^o equal to σ^o_M and the 5% and 95% bounds are sketched, but would need to be calculated carefully. Only the values of σ^o and the lines for the end points of the random interval with, say, a probability of 90% of enclosing the value, σ^o_M, change.

For the model being used for an example, the value of σ^o_M goes to zero at some water temperature dependent wind speed, designated by $\bar{U}_T$. For wind speeds less than $\bar{U}_T$, since there is no backscatter from the waves, the random variability is determined solely by the value of γ in Table 2. Ninety percent of the sample values will scatter somewhere in the rectangular area bounded by $0 < \bar{U} < \bar{U}_T$ and $+ 1.645\gamma^{\frac{1}{2}}$ and $- 1.645\gamma^{\frac{1}{2}}$ if $\bar{U}$ is less than $\bar{U}_T$.

For Fig. 8a, the sample value, σ^o, lies just above this rectangular area, but the lower bound is within this area. Nevertheless, the values for the upper and lower bounds on the random interval intersect the curve for σ^o_M at two points corresponding to speeds greater than $\bar{U}_T$. The range of wind speed for a 90% interval would be quite small.

For Fig. 8b, the sample value is below the 5% line, the lower bound for σ^o_M is zero and the upper bound for σ^o_M exists. The 90% range on $\bar{U}$ is from zero to this upper bound.

In Fig. 8c, the sample value is zero. An upper bound for σ^o_M exists. The range of wind speeds is from zero to the speed determined by the upper bound.

In Fig. 8d, the sample value is negative. The upper bound still exists and the wind speed range is from zero to this upper

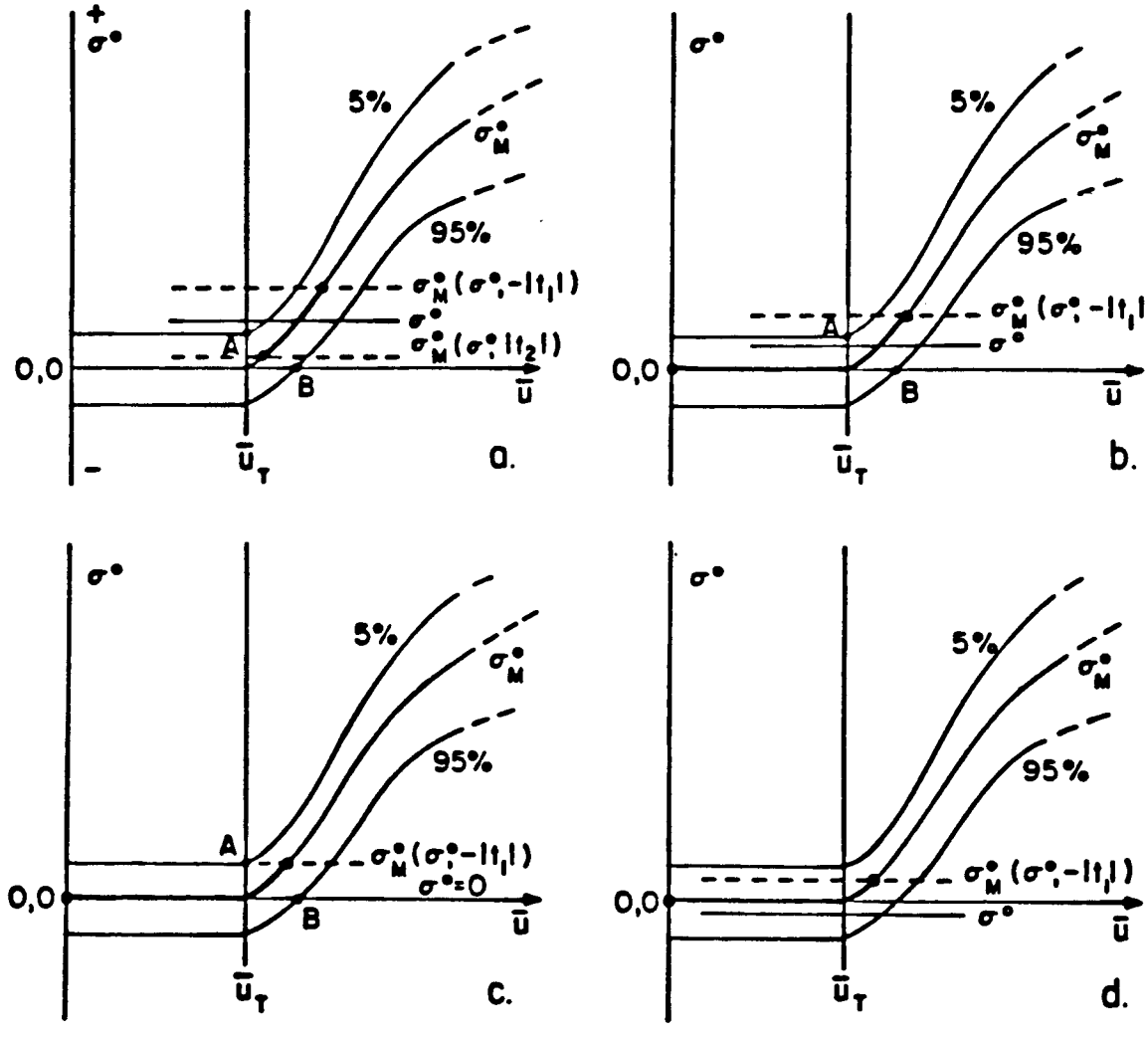

Fig. 8a) The Use of the 90% Random Interval With Linear Scales for Values Near the Water Temperature Dependent Threshold Wind for a Sample Value Greater Than the 5% Curve;
b) Same as a Except for a Positive Sample Value Below the 5% Curve;
c) Same as a Except for a Sample Value of Zero. The Points Marked A and B Correspond to the Intercepts of the Lower and Upper Bounds with the σ^o and σ^o_M Axes of Fig. 4;
d) Same as a Except for a Negative Sample Value. For b, c and d, the Interval for σ^o_M is From Zero to the Upper Bound and the Probability is 95%.

bound.

9.4 The effect of constant orbit errors for fairly long times. If the statistical test given in Part 8.6 shows that the values of t_R are sensibly constant over a fairly large portion of a sampled area of the ocean, Figs. 5 and 6 would not be applicable. There would be a curve on each of these figures for each incidence angle somewhat above or somewhat below the curve for σ_M^o (perhaps similar to a curve for σ_M^o for a slightly different incidence angle) that would correspond to Eqn. (75). The sample values would scatter about this curve with standard deviations calculated from Table 1 for the area of the ocean being sampled. The values of t_R need not be the same for the eight different antennas on the spacecraft. The analysis carried out above could perhaps be modified to account for this effect. The overall outcome for this possibility would be that wind recoveries could be systematically biased from one area of the ocean to another, especially for moderate and high winds.

10. MAXIMUM LIKELIHOOD ESTIMATES FOR $\bar{U}$ AND χ.

10.1 Wind speed and direction conventions. Let the 45^{o} antenna in Fig. 2 for vertical polarization be pointing at an angle of χ_o clockwise relative to north. The values of χ in (7) and (8) are to be added to χ_o to obtain the wind direction relative to north. The result is the direction from which the wind is blowing in degrees measured clockwise from north. For the two beams at 45^{o}, in Fig. 2 the wind direction is simply $\chi_o + \chi$ if χ is known.

When the beam at 115^{o} to the subsatellite track samples the 25 by 25 km area a few minutes later, if the wind direction relative to the 45^{o} beam was 0^{o}, then the wind direction relative to the 115^{o} beam would be -70^{o} or 290^{o}. Similarly, for the 135^{o} beam, the direction relative to this beam would be -90^{o}. It is important that these sign conventions be correctly accounted for in the interpretation of the data. A transformation of variables to refer all directions to the 45^{o} beam is accomplished by using $\chi - 70^{o}$ and $\chi - 90^{o}$ as the case may be in (7) or (8).

10.2 Theories and models. There have been numerous efforts to apply electromagnetic theory combined with various properties of the waves on the ocean to the prediction of the backscatter that would be estimated by a scatterometer, or any other properly designed and calibrated radar. The problem is very complex since there are many physical processes involved, some of which may not even have been considered.

So as to avoid still more complicated notation, subscripts will be added to (7) and (8) to distinguish among the four different measurements. A theory, or a model, essentially attempts to predict the quantity σ^o_M as a function of $\bar{U}$, χ and θ as defined in Section 2.1.

To determine the wind speed and direction, the information available for a 25 by 25 km area can be summarized as follows:

σ^o_{VV1} is the estimate for vertical polarization from the 45^o forward beam with θ_1, α_1, β_1 and γ_1 known and a predicted expected value from the theory, or model, given by $\sigma^o_{VV}(\bar{U}, \chi, \theta_1)$ which should equal the expected value of this estimate.

σ^o_{HH2} is the estimate for horizontal polarization from the 45^o forward beam with θ_2, α_2, β_2 and γ_2 known and a predicted expected value from the theory, or model, given by $\sigma^o_{HH}(\bar{U}, \chi, \theta_2)$ which should equal the expected value of this estimate.

σ^o_{HH3} is the estimate for horizontal polarization from the 115^o aft beam with θ_3, α_3, β_3 and γ_3 known and a predicted expected value from the theory, or model, given by $\sigma^o_{HH}(\bar{U}, \chi - 70^o, \theta_3)$ which should equal the expected value of this estimate.

σ^o_{VV4} is the estimate for vertical polarization from the 135^o aft beam with θ_4, α_4, β_4 and γ_4 known and a predicted expected value from the theory, or model, given by $\sigma^o_{VV}(\bar{U}, \chi - 90^o, \theta_4)$ which should equal the expected value of this estimate.

Each of the four expected values for the model backscatter is different because for the same wind speed, the model varies as a function of θ and χ, for the same χ, the model varies as a function of wind speed and θ and for the same θ the model varies as a function of wind speed and χ. (There may be other physical quantities involved whose effects have already been accounted for.) Since however θ is known, a known value of χ will determine a unique wind speed from the model, and a known value of $\bar{U}$ will determine four, or fewer, unique values of the wind direction from the model even for just one of the estimates.

10.3 Maximum likelihood estimates of $\bar{U}$ and χ. Since the expected values and variances of the four different estimate of the backscatter are all different, the four different estimates, σ^o_{VV1}, σ^o_{HH2}, σ^o_{HH3} and σ^o_{VV4} are each a sample of size one from populations defined by (4) such that the expected values and variances are all different.

The joint probability density function for the four sample values is the product of four probability density functions similar to (4) but with different expected values and variances. These depend on different known values for θ, α, β and γ as in Eqn. (76) where the expected values and variances are now predicted by the theory, or model. The four sample values are independent in the probability sense.

$$f(\sigma^o_{VV1}, \sigma^o_{HH2}, \sigma^o_{HH2}, \sigma^o_{HH3}, \sigma^o_{VV4}) = f(\sigma^o_{VV1}) \cdot f(\sigma^o_{HH2}) \cdot f(\sigma^o_{HH3}) \cdot f(\sigma^o_{VV4}) \tag{76}$$

Since the expected values for the four backscatter estimates are now given by a model, the maximum likelihood estimates of $\bar{U}$ and χ can be found by maximizing the right hand side of Eqn. (76) by varying $\bar{U}$ and χ because σ^o_{VV1}, σ^o_{HH2}, σ^o_{HH3} and σ^o_{VV4} are the known random variables. The steps are similar to those for Eqn. (24) except that the model, or theory, has imposed a further restriction on the expected values and variances, or standard deviations, that can be used to maximize the probability.

The result is given by Eqn. (77) as $\bar{U}$ and χ are varied.

$$
\begin{aligned}
MLE(\bar{U}, \chi) = MAX - \Bigg\{ & \frac{(\sigma^o_{VV1} - \sigma^o_{VV}(\bar{U}, \chi, \theta_1))^2}{VAR(\sigma^o_{VV}(\bar{U}, \chi, \theta_1))} + \frac{(\sigma^o_{HH2} - \sigma^o_{HH}(\bar{U}, \chi, \theta_2))^2}{VAR(\sigma^o_{HH}(\bar{U}, \chi, \theta_2))} \\
& + \frac{(\sigma^o_{HH3} - \sigma^o_{HH}(\bar{U}, \chi-70^o, \theta_3))^2}{VAR(\sigma^o_{HH}(\bar{U}, \chi-70^o, \theta_3))} + \frac{(\sigma^o_{VV4} - \sigma^o_{VV}(\bar{U}, \chi-90^o, \theta_4))^2}{VAR(\sigma^o_{VV}(\bar{U}, \chi-90^o, \theta_4))} \\
& + \ell n\,((VAR(\sigma^o_{VV}(\bar{U}, \chi, \theta_1))/(\alpha_1(\sigma^o_{VV1})^2 + \beta_1\,\sigma^o_{VV1} + \gamma_1))) \\
& + \ell n\,((VAR(\sigma^o_{HH}(\bar{U}, \chi, \theta_2))/(\alpha_2(\sigma^o_{HH2})^2 + \beta_2\,\sigma^o_{HH2} + \gamma_2))) \\
& + \ell n\,((VAR(\sigma^o_{HH}(\bar{U}, \chi-70^o, \theta_3)/(\alpha_3(\sigma^o_{HH3})^2 + \beta_3\sigma^o_{HH3} + \gamma_3))) \\
& + \ell n\,((VAR(\sigma^o_{VV}(\bar{U}, \chi-90^o, \theta_4)/(\alpha_4\,(\sigma^o_{VV4})^2 + \beta\,\sigma^o_{VV4} + \gamma_4)))\Bigg\}
\end{aligned}
\qquad (77)
$$

The one half in Eqn. (24) has been omitted above because it is irrelevant. It could also have been omitted in Eqn. (24).

Eqn. (77) can have more than one local maximum. A computer search for these maxima can find them quickly. The power law assumption that was used for the model for backscatter during the SEASAT-SASS program and the use of only two backscatter values most of the time, such as σ^o_{VV1} and σ^o_{VV4} with the other terms omitted in (77), yields four maxima for many sample values corresponding to four different wind vectors such as $\bar{U}_1$, χ_1; $\bar{U}_2$, χ_2; $\bar{U}_3$; χ_3 and $\bar{U}_4$, χ_4 with wind vectors, one per quadrant, relative to χ_o. The subject is discussed in considerable detail in Pierson (1983b). The design in Figs. 1 and 2 is a simpler one than the one analysed by Pierson and Salfi (1982) when the NOSS (National Oceanographic Satellite System) was under consideration. It is not essential to know the inverse of, say,

$$\sigma^o_{VV} = \sigma^o_{VV}(\bar{U}, \chi, \theta) \tag{78}$$

in terms of

$$\bar{U} = \bar{U}(\sigma^o_{VV}, \chi, \theta) \tag{79}$$

analytically in order to determine the maximum likelihood estimates of $\bar{U}$ and χ.

The maximum of the local maxima for Eqn. (77) may provide a unique wind vector most of the time. The beam at 115^o for the example chosen above will almost always eliminate two of the four "X" type SASS solution. Differences betweeen horizontally polarized backscatter and vertically polarized backscatter could

eliminate one of the remaining two.

It is also possible to extend these results to, say, four 25 by 25 km areas that form a 50 by 50 km area. Eqn. (77) would then contain four times as many terms, one for each 25 by 25 km area. Averaging, as described above, could help reduce the computational load.

11 SYSTEM AND MODEL VALIDATION

11.1 Comparison with conventional wind measurements. Once the MLE has obtained values of $\bar{U}$ and χ, the resulting wind vector can be compared with a wind measured by conventional means in terms of an effective neutral wind computed from the conventional measurement for an assigned height, say 19.5 or 20 m, and the $\bar{U}$ from a boundary layer model for the same height. The usual procedure is to make scatter plots of the two different speeds and the two different directions. It was difficult to obtain comparison data for high winds for the SEASAT-SASS program. Also certain kinds of systematic errors are not immediately obvious in such analyses.

The system and model validation for some future scatterometer may be easier than it was for the SEASAT-SASS because of the expanded network of deep ocean data buoys deployed by the National Data Buoy Center. It is planned to have these data buoys obtain five consecutive 10 min wind averages followed by an 8 min average to allow for data transmission each hour. Scatterometer data can be co-located with a data buoy in both time and space, and the data buoy winds can be averaged for as long a time as appropriate to obtain a more representative wind, if needed. Gilhousen (1986) has reported on the present accuracy of wind measurements by the National Data Buoys.

There are plans to try to modify 18 National Data Buoys during the next few years so as to accomplish this change (Personal communication, J. Wilkerson 1987). With two 600 km wide swaths perhaps as many as 80% of the buoys will be in the swath twice each day so that in about one year there will be over 9000 data buoy reports to be compared with SCAT recoveries. The various incidence angles will range over about 25^{o} so that 360 comparisons per incidence angle should be possible.

Nevertheless, scatter plots of $\bar{U}$(SCAT) versus $\bar{U}$(BUOY) and χ(SCAT) versus χ(BUOY) will produce points that do not lie on the line of perfect fit. The reasons for this are many such as:

(1) The model, or theory, is wrong.
(2) The values of σ^{o} are estimates and do not equal the expected value predicted by a correct model.
(3) The conventional measurements have systematic and sampling variability "errors".

For the final validation of any model, it is essential to be able to compare the winds recovered from the backscatter estimates with the winds measured by a conventional system. The sources of "bias" and errors must be identified, and the effects of sampling variability for both the scatterometer winds and the conventional winds must be accounted for separately.

The maximum likelihood estimates of $\bar{U}$ and χ when compared with the $\bar{U}$ and χ obtained from a data buoy provide not only these comparisons but also ways to compare the backscatter estimates from the scatterometer with the model backscatter values

recovered from the maximum likelihood estimate and the backscatter values that would be computed from the model from the data buoy winds with due consideration of the "errors" and sampling variability of the data buoy winds.

For a given 25 by 25 km area that contains a data buoy, and for other areas that surround it, the available data (with the incidence angle known) consist of the following:

$\bar{U}_B$, χ_B from the buoy.

$\bar{U}$, χ from the maximum likelihood estimate.

$\sigma^o_{VV}(U_B, \chi_B), \sigma^o_{HH}(\bar{U}_B, \chi_B), \sigma^o_{HH}(\bar{U}_B, \chi_B), \sigma^o_{VV}(\bar{U}_B, \chi_B)$ computed from the model and the buoy wind for the appropriate wind direction relative to each beam.

$\sigma^o_{VV}(\bar{U}, \chi)$, $\sigma^o_{HH}(\bar{U}, \chi)$, $\sigma^o_{HH}(\bar{U}, \chi)$, $\sigma^o_{VV}(\bar{U}, \chi)$ from the wind speed and direction recovered from the maximum likelihood estimate.

σ^o_{VV1}, σ^o_{HH2}, σ^o_{HH3}, σ^o_{VV4} the random variables obtained by the scatterometer for the area.

To avoid complicated subscripts, the values are ordered in the same sense as the first four terms in Eqn. (77). The data for a large number of data buoy reports can be stratified according to $\bar{U}_B$ and θ for comparison purposes as the data set increases. Other buoy data such as wave spectral data, air temperature and water temperature will also be needed.

In general, $\bar{U}_B$, χ_B will not agree exactly with $\bar{U}$, χ from the maximum likelihood estimate, nor will the triplets of backscatter values for a given scatterometer beam such as $\sigma^o_{VV}(U_B, \chi_B)$, $\sigma^o_{VV}(\bar{U}, \chi)$ and σ^o_{VV1} agree with each other.

The ability to construct a random interval from the value of σ^o_{VV1} (and all other estimates) that contains the expected value of the backscatter with a known probability provides a new way to study the data set. If $\sigma^o_{VV}(\bar{U}_B, \chi_B)$ and $\sigma^o_{VV}(\bar{U}, \chi)$ do not lie in this random interval an appropriate fraction of the time, say, 0.6826, if $|t_1| = |t_2| = 1$ is used, with due consideration of buoy contributions, then the model is not predicting the expected value of the backscatter and needs to be improved.

Suppose, for example, that about 100 sets of data for reported buoy winds are collected. These would be 200 vertically polarized and 200 horizontally polarized sets of data for comparison. The binomial distribution would be applicable. For two standard deviations, there ought to be somewhere between 124 and 150 values from the model as calculated from $\bar{U}_B$ and χ_B and, perhaps, from the MLE values $\bar{U}$ and χ that fall within the appropriate random intervals.

If much fewer than 124 successes occur, the result is strong evidence that the model has not correctly treated all of the various properties of the waves that produce backscatter and accounted for those effects that cause the backscatter to vary that are not directly related to the local wind speed and direction.

If the number of successes is very much over 150, say, 175 to 200, so that the random interval nearly always encloses the model values computed from $\bar{U}_B$ and χ_B, then the random variation of the estimates of the backscatter is so great that there may be no skill in the recoveries of the winds from the backscatter data. The requirements for $\pm$ 2 m/s or 10% for speed and corres-

ponding direction requirements will then have to be checked carefully.

11.2 Comparisons of maximum likelihood estimates when conventional data are unavailable. Woiceshyn, et al. (1986) and Woiceshyn, et al. (1987) have uncovered many systematic sources of error in the wind recoveries from the SASS-1-SOS model and wind recovery algorithm simply from the study of the SASS wind data alone. Some way to compare various theoretical backscatter models without conventional wind data so that the best one could be further improved would be useful.

Difficulties with the SASS-1-SOS wind recovery algorithm that were revealed by the study of Mode 4 data consisted of (1) systematic differences between the values of $\bar{U}$ for vertical polarization and horizontal polarization for high winds with the horizontally polarized wind speeds much higher (as much as 9 m/s) than the vertically polarized wind speeds and (2) systematic patterns in the wind direction recoveries such that for some wind speeds, wind directions for χ(i.e. relative to χ_o) were dominant for 45^o, 135^o, 225^o and 315^o and for other wind speeds only directions of either 0^o and 180^o or 90^o and 270^o were dominant. The wind speed discrepancies need to be eliminated for a future model and the systematic direction biases would cause difficulties for any data assimilation method that depended heavily on correct wind directions. It would be possible to monitor the wind recoveries from a model and to determine areas of the ocean and wind speed ranges for which these various discrepancies occur.

Woiceshyn, et al. (1986) compared winds recovered from pairs of vertically polarized backscatter estimates 90^{o} apart with winds recovered from pairs of horizontally polarized backscatter estimates 90^{o} apart for the same location on the ocean for the available Mode 4 data from the SEASAT-SASS. The SASS-1 model function was used with the SOS wind recovery algorithm, Jones, et al. (1982). Except for the logarithmic terms in (77), pairs of backscatter estimates about 90^{o} apart often yield the same results for both the SOS and the MLE. Differences are described in Pierson (1984) for the SASS-1 model function. Other slight differences will be investigated in terms of the design features of a scatterometer in a subsequent section.

If the backscatter model that was chosen would have the property that horizontally polarized backscatter predicts higher winds than vertically polarized backscatter, the four backscatter estimates make it possible to detect this kind of discrepancy and to understand it so that the model can be corrected. Also consistently erroneous wind directions can be found and corrected.

11.3 Detecting large wind speed discrepancies between models for vertically and horizontally polarized data. Although it is not essential to know the inverse of Eqn. (78) as in Eqn. (79), enough can be learned about such inverses for any of the models described above to make it possible to describe the properties of the backscatter estimates in terms of these inverses for analysis purposes.

Also if the sample values equal the model values, (77) is identically zero. Were it not for the terms involving the natural logarithms, the value of zero would be a maximum. The logarithmic terms are a logical consequence of the definition of a maximum likelihood estimate, and the actual maximum will be somewhat greater than zero and not at the value for an input without sampling variability. Maximum likelihood estimates are not necessarily unbiased. The effect of the logarithmic terms appears to be rather small, and it will be neglected in this section, to be discussed in more detail in terms of design data.

Fig. 9a illustrates possible backscatter curves versus χ for some fixed value of $\bar{U}$ for one of the outer 25 by 25 km areas of the swath. The figure is schematic so that no scale is given for the vertical axis. The upper continuous curve shows the variation of vertically polarized backscatter versus χ for some fixed value $\bar{U}_1$, for the incidence angle appropriate to the area. The incidence angles for the forward 45° beam and the aft 135° beam are nearly equal so that the slight difference can be neglected for illustrative purposes. The next continuous curve from the top shows the variation of horizontally polarized backscatter versus χ for $\bar{U}_1$ for the 115° beam for a lower incidence angle appropriate to that beam. The lowest continuous curve is for horizontal polarization versus χ at the incidence angle for the 45° beam for $\bar{U}_1$. The two dashed curves correspond to the values predicted by the model in use for $\bar{U}_1$ for horizontal polarization.

For the area under consideration, four estimates of the backscatter will be obtained. Suppose that the wind is from

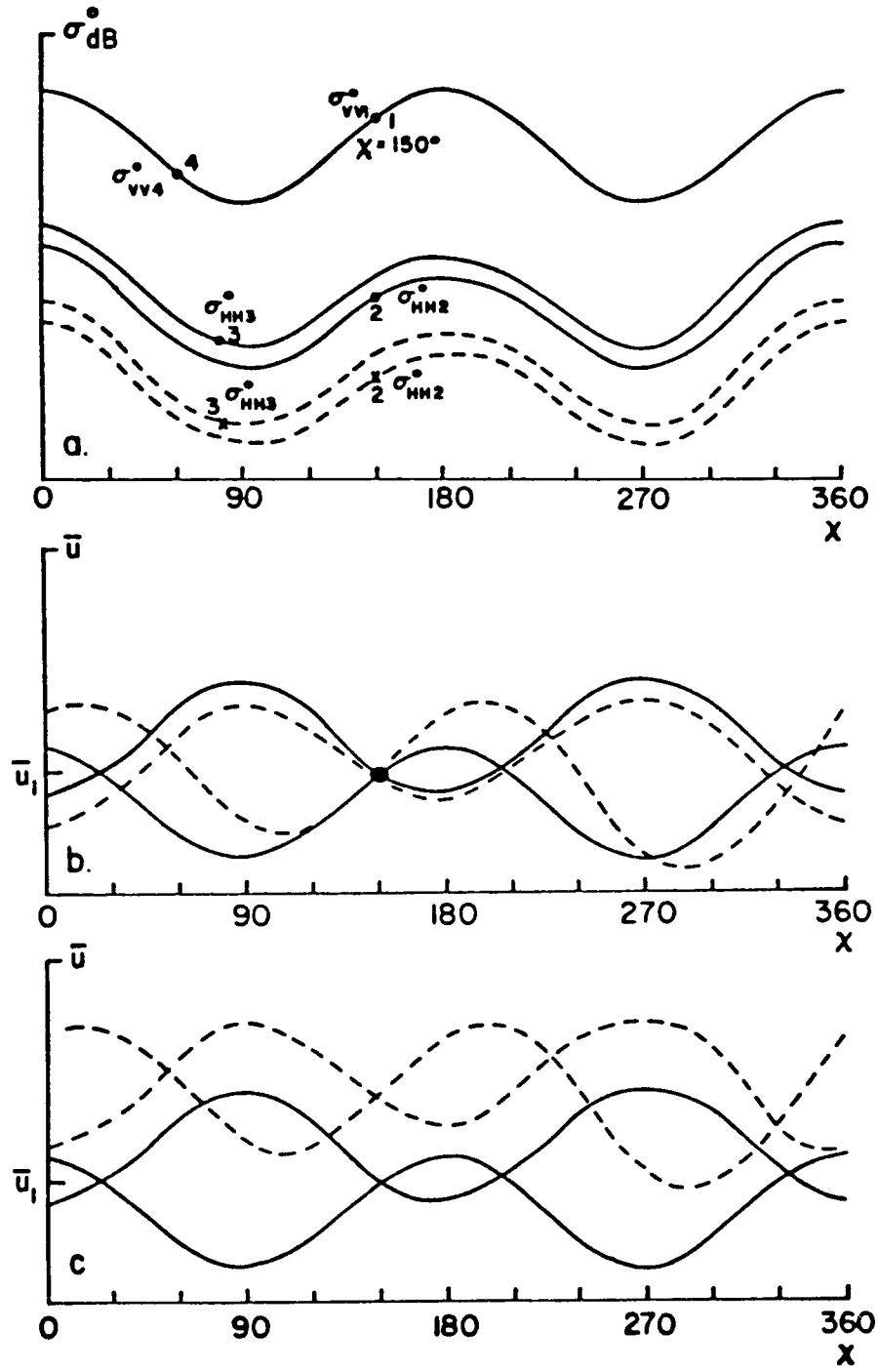

Fig. 9 Model Errors that Result From an Incorrect Model for Horizontal Polarization:

a) Backscatter Versus Aspect Angle for a Fixed $\bar{U}$ for Vertical and Horizontal Polarization with the Continuous Curves Representing a Correct Model and the Dashed Curves Representing an Incorrect Model for Horizontal Polarization;

b) Results for the MLE if the Incorrect Dashed Curves Were Correct;

c) Results for the MLE if the Correct Curves are the Continuous Curves for Horizontal Polarization and the dashed incorrect curves are used. (See Text).

C -2

150^{o}. The forward vertically polarized estimate will have an expected value given by the point labeled, 1, and will depart in a random way from the point shown according to Eqn. (12). The forward horizontally polarized value will scatter in the same way about the point labeled, 2. The point labeled, 3, is for the 115^{o} beam for horizontal polarization, and corresponds to a wind direction relative to that beam from 80^{o}. The point labeled, 4, corresponds to the 135^{o} beam and falls at a wind direction of 60^{o} relative to that beam. The two points shown by the x's are for the model predictions for horizontally polarized backscatter.

Fig. 9b illustrates what numerical results could be obtained under the assumption that the two lower dashed curves for horizontal polarization and the upper continuous curve for vertical polarization were correct. The figure is schematic and no vertical scale is needed. Consider the evaluation of the terms involving σ^{o}_{VV1} in Eqn. (77). the continuous curve with a minimum at 0^{o}, a maximum at 90^{o} and so on, is the graph of the inverse of Eqn. (78) as in Eqn. (79) as χ is varied.

If the wind direction was from the direction, χ, relative to χ_{o}, then the wind speed would have to be the value graphed so that the corresponding backscatter value from Fig. 9a would have been the measured value. If the wind direction in Fig. 9a is changed, the inverse curve will change by moving up or down relative to $\tilde{U}_{1}$. Relative to χ_{o} for inverse curves for the 45^{o} beam, all inverse curves have a minimum at 0^{o}, a maximum near 90^{o}, a minimum at 180^{o}, and a maximum near 270^{o} with similar properties,

properly phase shifted, for all of the other inverse curves. For error free data, they must intersect at the input wind speed and direction for a model and its inverse.

The model values always equal the value of σ^{o}_{VV1} (with its sampling variability) on this curve. Thus whatever the estimate of σ^{o}_{VV1}, there will be a locus of points in the $\bar{U}$, χ plane such that these two terms in (77) are zero. Were (77) evaluated at points in the $\bar{U}$, χ plane not on the curve the numerical values would rapidly become more and more negative. The smaller the standard deviation of the estimate the more rapidly the ridge-like form following the curve becomes very negative.

The continuous curve with a maximum near 0^{o} and a minimum at 90^{o} corresponds to the value labeled σ^{o}_{VV4} for the upper curve of Fig. 9a. Were (77) evaluated for the two values of σ^{o}_{VV1} and σ^{o}_{VV4} four peaks would appear at the four points where the two curves cross. These four values of wind speed and corresponding directions, one in each quadrant, represent the usual four vector winds recovered by the operational mode of the SEASAT-SASS. Only those points where the curves cross are consistent with a possible vector wind for the area sampled.

The dashed curve with the minimum of the two minima at 290^{o} (360^{o}-70^{o}) represents the inverse curve for the horizontally polarized measurement from the beam at 115^{o}. The minima for this curve are different because in Fig. 9a upwind horizontal polarization is shown to be stronger than downwind horizontal polarization. The shift away from 90^{o} to the forward beam to 70^{o} away from the forward beam produces the result that although this

dashed curve passes through the point corresponding to $\bar{U}_1$ at 150^o, it is far from the speeds and directions for which the pair of curves for the vertically polarized values crossed for the values near 30^o and 210^o. Two of the peaks in the value of (77) would be greatly reduced by this third contribution to the evaluation.

The remaining dashed curve is for the horizontally polarized estimate, σ^o_{VV2}. It again passes through the value $\bar{U}_1$ at 150^o. The four curves in the vicinity of a direction of 330^o come close together, but do not all pass through a common point. If (77) has a low value at this point, it could be quite a bit higher than the value at 150^o and $\bar{U}_1$. Contours for Eqn. (77) for an appropriate area of the $\bar{U}$, χ plane could be revealing for a chosen model and for known design values of α, β and γ. Had the measurements had no sampling variability and had the model been correct, Eqn. (77) would have its maximum at the assumed input, $\bar{U}_1$, 150^o.

Fig. 9b also illustrate an important feature of Eqn. (77). Sampling variability effects have been neglected. Each of the estimates for the area under analysis is subject to the effect of sampling variability as in Eqn. (12). The random variables, say, t_1 to t_4 have an equal chance of being either positive or negative, and thus each of the four curves in Fig. 9b has an equal chance of shifting up or down. There are 16 possibilities as shown in Table 4.

If all four curves shift upward, they could all still intersect at nearly the same wind direction, but at a higher value than $\bar{U}_1$. If all four curves shift downward, the result would be

TABLE 4. COMBINATIONS SUCH THAT σ_{VV1}, σ_{HH2}, σ_{HH3} AND σ_{VV4} CAN BE GREATER THAN (+) OR LESS THAN (-) THE EXPECTED VALUE IN THE ORDER GIVEN.

+	+	+	+
+	+	+	-
+	+	-	+
+	+	-	-
+	-	+	+
+	-	+	-
+	-	-	+
+	-	-	-
-	+	+	+
-	+	+	-
-	+	-	+
-	+	-	-
-	-	+	+
-	-	+	-
-	-	-	+
-	-	-	-

a lower wind at nearly the same direction.

Other kinds of shifts could also result in points in the $\bar{U}$, χ plane such that the four curves come close together and produce a large value for the maximum of the maxima of the MLE. Large values for the maximum of the maxima of the MLE do not always mean that the speed and direction recovered by the MLE are more accurate than smaller values for the maximum of the maxima.

The shifts in the curves as a result of these random effects can at times produce an incorrect wind speed and direction. For Fig. 9b, the cluster of crossing curves that produce intersections near 330^{o} as a result of shifts because of the random variability could move more closely together and perhaps even merge into one point.

Since the dashed curves for horizontal polarization in Fig. 9a are assumed to be incorrect, the pattern shown in Fig. 9b will not occur.

If, in fact, the variation of horizontally polarized backscatter is shown by the two continuous curves in Fig. 9a for a wind speed of $\bar{U}_1$ and if the model is using the values for the dashed curves for a wind speed of $\bar{U}_1$ the result would be very different from the curves shown in Fig. 9b as shown in Fig. 9c. The effect of an incorrect model would be to shift the two curves for the horizontally polarized value for the inverse curves from σ^{o}_{HH2} and σ^{o}_{HH3} upward in the $\bar{U}$, χ plane by many m/s because the horizontally polarized backscatter values that were actually obtained would be higher than the model predicts for $\bar{U}_1$. Whatever

the maximum of the maxima of Eqn. (77) would be, it would have to be very small compared to values that would be obtained for (77) from Fig. 9b. There is no point in the $\bar{U}$, χ plane where all four curves come close to the value $\bar{U}_1$ and 150^o. This would be an operational clue that something was not being accounted for correctly by the model.

Without any knowledge of the actual wind from a conventional source, the two backscatter estimates for horizontal polarization could be used to recover (for this example, others would differ) four vector winds, and the two vertically polarized estimates could be used to recover four more. The differences in the speeds, which will be large, for the four horizontally polarized winds and the four vertically polarized winds provide data to permit adjusting the model so that the recovered winds will be more nearly in agreement.

It could also be possible that the curve for vertical polarization is too high and would need to be lowered. A few conventional winds included in a set of such calculations can quickly provide information on which way the model needs to be adjusted especially if the random intervals derived above are used to determine how far off the model is compared to the desired result. The sampling variability of any new design needs to be known so that statistics can be calculated to determine whether the effect is real or the result of sampling variability.

There are four possible ways to pair the four estimates that would be obtained such that the two estimates that are used are either 70^o or 90^o apart for antenna pattern 1 in Fig. 2. Each

one can be identified in Fig. 9c for the example under analysis. Each pair would permit the rapid recovery of four wind vectors (or two or three as special cases) with, usually, one per quadrant relative to χ_o. As in Fig. 9c, there would be 12 plus 2 (usually 16) quite different speeds and directions. For each pair, the MLE speeds and directions can be used to compute the backscatter from the model that ought to have been the expected value for the other two backscatter estimates that were not used. If the random intervals defined by (34), (50) and (51), do not enclose these model values for an appropriate percentage of data sets for a given incidence angle, the data alone are sufficient to reveal the inadequacy of the model.

11.4 Detecting model errors that result from incorrect upwind-crosswind and downwind-crosswind differences. Fig. 10 illustrates the reason for the SEASAT-A SASS-1 model function to have the propensity to recover the two types of wind direction recoveries that were unrealistic as described by Woiceshyn, et al. (1987). It extends the concept to winds that could be recovered by this new instrument if the model used had similar errors. Fig. 10a illustrates two possible models for the variation of backscatter with aspect angle. For vertical polarization at a fixed wind speed for the upper two curves, one is continuous and one is dashed. The curves can be used for the 45^{o} and 135^{o} beam. The next two, one dashed and one continuous, are for the 115^{o} degree beam for horizontal polarization, and the lowest two are for the 45^{o} beam for horizontal polarization.

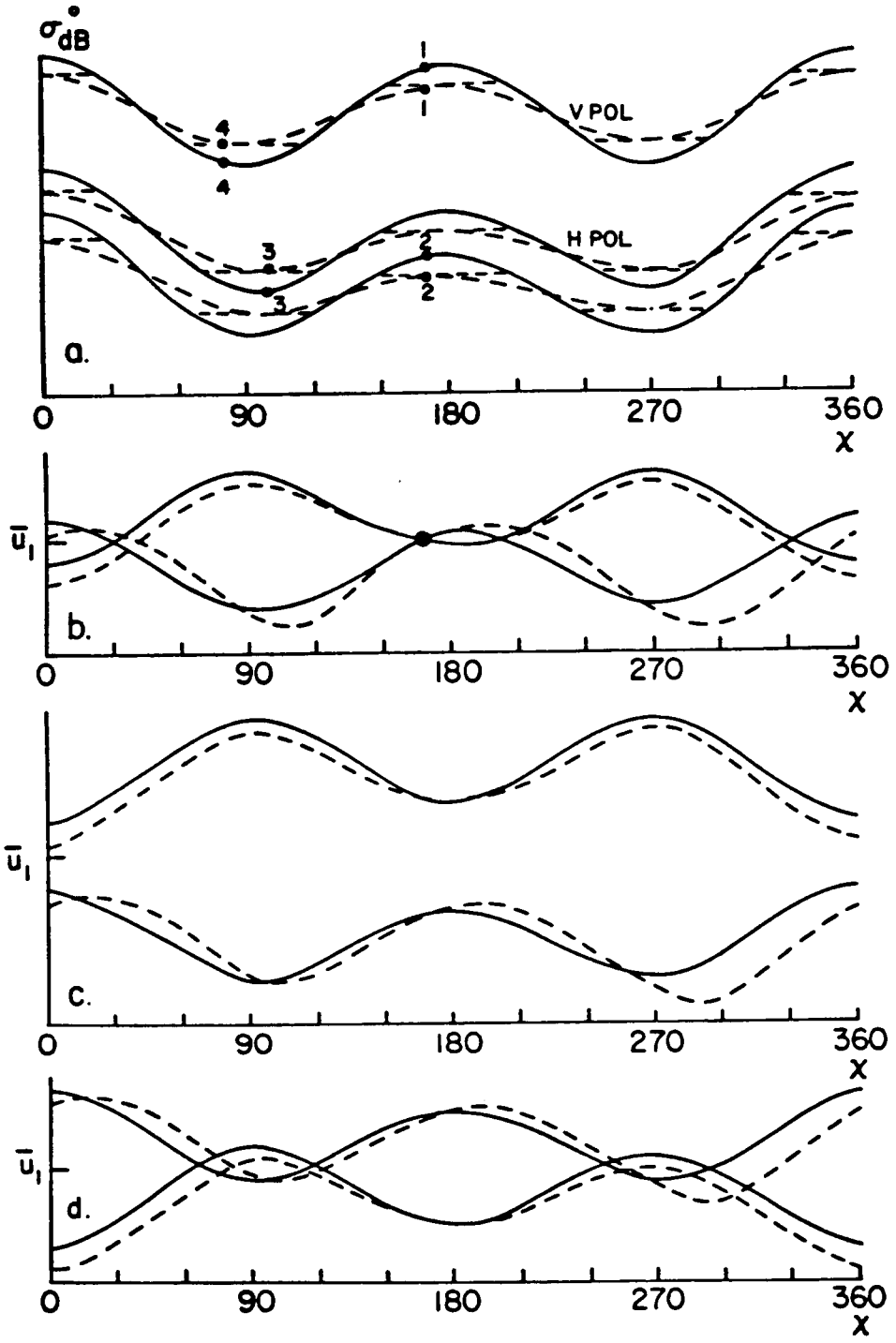

Fig. 10 Model Errors that Result From Incorrect Upwind-Crosswind and Downwind-Crosswind Differences:
a) Backscatter Versus Aspect Angle for Two Possibilities and the Four Expected Values for Each,
b) Continuous Curves Correct and Used to Recover Winds,
c) Continuous Curves Correct, Model Uses Dashed Curves for Expected Values,
d) Dashed Curves Correct, Model Uses Continuous Curves for Expected Values.

The figures are schematic. No vertical scales are needed. It is assumed that the wind is $\bar{U}_1$ from 170° and four expected values are shown for the continuous curves and four for the dashed curves. The estimates will scatter about the expected values as in (12).

Fig. 10b is the result of assuming that the continuous curves is Fig. 10a are correct and are used to recover winds from actual data (with sampling variability neglected). Fig. 10c is the result of assuming that the continuous curves correspond to the real data, and the model is the dashed curves. Fig. 10d is the result of assuming that the dashed curves provide the actual data, and the continuous curves are the model.

The difference between the various continuous and dashed curves for Fig. 10a is that the upwind-crosswind and downwind-crosswind differences in the backscatter are greater for the continuous curves than for the dashed curves. A larger upwind-downwind difference is also shown for the horizontally polarized aspect angle variation.

Fig. 10b is what would be expected in the absence of sampling variability if the model were correct. The continuous curves are for vertical polarization and the dashed ones are for horizontal polarization. The greater upwind-downwind difference for horizontal polarization, plus the 115° degree beam, helps to make the one point in the $\bar{U}$, χ plane where all four curves pass through $\bar{U}$ and 170° distinct from other possibilities.

Fig. 10c is the result obtained if the dashed curves in Fig.

10a are for the model and the continuous curves are for the actual conditions. The "true" backscatter values for both vertical polarization and horizontal polarization at the assumed direction of 170^{o} are too high compared to the model values for the vertically polarized beam at 45^{o} and the horizontally polarized beam at 45^{o}. The vertically polarized value for the beam at 135^{o} (at 80^{o} for χ) and the horizontally polarized beam at 115^{o} (at 100^{o} for χ) are too low compared to the model.

When the model is used to try to recover the wind speeds and directions, the inverse curves for the 45^{o} beam, both horizontal and vertical have to move up relative to $\bar{U}_1$ and the inverse curves for the 115^{o} (horizontal) and 135^{o} beam (vertical) have to move down. As shown in Fig. 10c, the upper and lower pairs of curves might not intersect at all. A maximum likelihood estimate based on the vertically polarized data alone would yield very weak maxima for (77) as would the two curves for horizontal polarization. The value of the maxima from (77) for all four input backscatter values would also be low.

There would most likely be two maxima for (77) one near 0^{o} and the other near 180^{o} for the conditions shown. A true wind near 90^{o} would place the lower curves in Fig. 10c well above the upper curves and give maxima for (77) near 90^{o} and 270^{o}.

Horizontal lines are shown on Fig. 10a from the maxima and minima of the dashed curves to the point of intersection with the continuous curves. For any set of data recovered by NSCAT such that the wind direction for, say, the 45^{o} beam lies within the range of these horizontal lines, the backscatter values obtained

by the scatterometer will be higher (or lower) that than those for the model because the up wind-crosswind and down wind-crosswind differences are larger than the model predicts. For this example, backscatter values larger than the model predicts for the upper continuous and dashed curves would occur. The range is $\pm$ 25° to 30° about the maxima and minima of the various pairs of curves, and unless the wind direction is somewhere near 45°, 135°, 225°, or 310° plus or minus the range for which the actual backscatter exceed the maxima and minima of the model, the result will always be like Fig. 10c, except that the curves will move closer together. For $\pm$ 25° about the maxima and minima, 200° degrees of possible directions will all be recovered by (77) as pairs (or single values for one of two directions) at either 0° and 180° or 90° and 270°. Even if backscatter values are recovered within the range of possible values required by the model, the values will correspond to wind directions closer to 0°, 90°, 180° and 270°, and all recovered winds directions would be closer to 0°, 90°, 180° and 270° than the correct directions. Those points near where the continuous and dashed curves cross would be the only wind direction that would be nearly correct.

Fig. 10d is the reverse of Fig. 10c. The continuous curves in Fig. 10a are the model values and the dashed curves are the actual values that could be recovered for some fixed wind speed, $\bar{U}_1$, as a function of aspect angle. For an assumed wind direction of 170°, the inverse curves for the 45° beams must move down because the actual backscatter values are lower than those for the model. Those for the 115° and 135° beams must move up because the actual backscatter values are greater than those

for the model. Eqn. (77) might recover a wind speed and direction somewhere near 115^{o} and 250^{o}. The vertically polarized pair of backscatter values alone would yield four winds with directions near 65^{o}, 120^{o}, 245^{o} and 290^{o}. The horizontally polarized pair would yield winds with directions near 80^{o}, 115^{o}, 255^{o} and 305^{o} as sketched.

From Fig. 10a, it would never be possible to obtain backscatter estimates that correspond to the values required by the model for the ranges of wind directions shown by the horizontal dashed lines. The ranges of wind directions that would be obtained by (77) must be for the open spaces between the horizontal lines of Fig. 9a.

Even if a single vector, $\tilde{U}(?), \chi(?)$ is selected by (77), it will be far from the correct value for an extensive range of possible correct wind direction. The wind directions will be concentrated within a small range of directions centered near 45^{o}, 135^{o}, 225^{o} and 315^{o}. The illustration consequently explains the results of Woiceshyn, et al. (1987) in terms of the SASS-1 model function and pairs of vertically polarized or horizontally polarized backscatter estimates 90^{o} apart from the SEASAT-SASS. For the SASS-1 model function, the disparity because of the model was even more concentrated near 45^{o}, 135^{o}, 225^{o} and 315^{o} than Fig. 10 illustrates.

11.5 Additional considerations. Figs. 9 and 10 illustrate another important feature for attempts to develop a good model for backscatter from waves and to relate the backscatter to the local wind speed and direction. Any model can be used to

simulate backscatter values and the effects of sampling variability can be simulated by Monte Carlo methods. Since the model is also used to recover the winds, results such as Fig. 9c, 10c or 10d cannot be simulated unless deliberate kinds of differences between the model used to generated simulated backscatter estimates and the model used to recover the winds are introduced. If this were done, there is hardly any need to introduce sampling variability. Curves such as those in Figs. 9 and 10 quickly reveal the inconsistencies that will be the result.

Unless the effects of sampling variability completely dominate differences between the model used and what is obtained by a scatterometer, a subset of the data for incidence angles nearest to 20°, 25°, 30°, 35° and so on for the 45° forward beam for every fifth point parallel to the subsatellite track could quickly reveal the kinds of inconsistencies considered for Figs. 9 and 10. The random intervals that can be computed for each of the four estimates per 25 by 25 km area can also quickly reveal whether or not unique functions such as Eqns. (7) and (8) exist as functions of $\bar{U}$ and χ with the alternative that a much more complicated model needs to be considered.

The pattern shown by Fig. 10c can be quickly detected by a validation procedure when a scatterometer becomes operational. The recovered winds will have directions near 0° and 180° as illustrated (or 90° and 270° as a second possibility). The model values for the backscatter for each beam can be found for these winds. The four sample values each have an appropriate random

interval. If these random intervals do not enclose the model values (they may be very, very far apart), then the first type of error illustrated by Fig. 10a is evident.

In contrast, the pattern shown by Fig. 10d is more difficult to detect. The sample values occur for the model curves, but not at a correct aspect angle. A test similar to the one for Fig. 10c would not reveal any inconsistency. A running count of recovered wind directions for selected incidence angles and recovered wind speeds could eventually show the concentration of directions near 45^{o}, and so on, and the absence of directions near 0^{o}, 90^{o} and so on.

Figs. 9 and 10 also illustrate an advantage of the sampling pattern that was used as opposed to the alternative described in Part 1.2. For the alternative pattern there would be only one inverse curve with maxima at 90^{o} and 270^{o}. Two others would have minima near 110^{o} and 290^{o}, and the last one would have minima near 90^{o} and 270^{o}. Three of the inverse curves would track the same general region of the $\bar{U}$, χ plane. Only one inverse curve could intersect these three curves at four possible wind directions. If this one curve is high or low as a result of sampling variability, there will be a correlation between the errors in the recovered wind speeds and the recovered wind directions. Also the upwind-downwind difference for horizontally polarized backscatter for high winds and high incidence angles for the forward 45^{o} beam for the illustrated sampling pattern could at times eliminate a false solution by patterns such as those in Figs. 9 and 10.

Results similar to the above analysis were obtained by Pierson and Salfi (1982) for the study of the NOSS. There are numerous examples of curves similar to Figs. 9b and 10b. The kinds of errors found by Woiceshyn, et al. (1986) and Woiceshyn, et al. (1987) were not known at that time.

11.6 Additional applications of the random intervals. If the logarithmic terms in (77) are omitted, and if t_1, t_2, t_3 and t_4 represent the sampling variability of the four backscatter random variables as in (12), the substitution of four values for (12) into (77) yields

$$\text{MLE } (\bar{U}, \chi) \overset{\sim}{=} - (t_1^2 + t_2^2 + t_3^2 + t_4^2) \qquad (80)$$

which suggests that the MLE varies something like a gamma (or Chi Square) PDF. This is not correct for reasons given in section 11.3. The minimization of (77) juggles these four quantities relative to the "true" wind by allowing one term to become larger if other terms can be made even smaller.

However, the calculation of the MLE involves the separate calculation of each of the first four terms in the sum. These are usually combined to give single values for the maxima of (77). The numerical values of the first four terms in (77) contain information that is not in their sum especially if the values are computed in terms of a standard deviation in the denominator before squaring so as to obtain the signs of the t's.

The values from the model can be computed from each of the MLE estimates of $\bar{U}$, χ but upon substitution into (77) the same values for the four t_i's would result. Thus if one of the values

of t_i is outside of the range $\pm$ 1.645, the 90% random interval for the corresponding sample value will not include the model value. The MLE's will not be sensitive to some of the combinations of sign shown in Table 4, but they can be sensitive to forced maxima such that the four inverse curves do not come close to intersecting at a point in the $\bar{U}$, χ plane.

For each of the four values of the t_i, a success can be defined as a values within $\pm$ 1.645 and a failure as a value outside of this interval. The probability of a success if the "true" wind were known for a "true" model would be 0.90 and the probability of a failure if the "true" wind were known for a "true" model would be 0.10. For four values of the t_i, the result can be interpreted in terms of the binomial distribution as in Table 5.

For, say, 10,000 successive recoveries of maximum likelihood estimates, the successes will be biased high compared to the "true" values. This would decrease the probabilities for two or fewer successes. If, then, many more than 486 recoveries have only 2 successes, or if many more than 36 recoveries have only one success, of if there are many more than one recovery without a success, for all of the maximum likelihood estimates, further study of the model is needed. Repeated values for the maximum of the first four terms in the MLE less than $-4,(1.645)^2 = -10.8241$ virtually assure that the model is incorrect. Also for all of the maximum likelihood estimates for a given cell, a simple count of the successes and failures provides a ranking for the wind speeds and directions that may be helpful in removing ambiguous

TABLE 5 PROBABILITIES FOR A BINOMIAL PROBABILITY DENSITY FUNCTION FOR A SAMPLE OF FOUR SUCH THAT THE PROBABILITY OF SUCCESS IS 0.90.

P(4 successes)	=	0.6561
P(3 successes, 1 failure)	=	0.2916
P(2 successes, 2 failures)	=	0.0486
P(1 success, 3 failures)	=	0.0036
P(4 failures)	=	0.0001
Sum	=	1.0000

solutions, especially if patterns emerge as a function of the quadrant for each wind.

11.7 Applications to the SEASAT-SASS data. Except for two features, the Mode 4 backscatter data from the SEASAT-SASS are similar to the data that would be obtained by this new design. The SASS data can be co-located in sets of four backscatter estimates, two for vertical polarization and two for horizontal polarization, that are about 90^{o} apart. The cell centers do not occur as close together as those for the new design. Except for the availability of the beam at 115^{o}, which often eliminates two of the four ambiguities, the SASS data are similar to the new data if α, β, γ and θ are known.

However, any candidate model for backscatter can be tested against the above analysis and the model deficiencies, if any, can be found. There are ways to obtain a candidate model based on the SASS data for Mode 4 that can be compared with improved versions of the models described above.

12 RESOLUTION AND WAVENUMBER ALIASING

12.1 Twenty five kilometer resolution. For 25 kilometer resolution, the scatter in the sample values of the four backscatter estimates will be similar to those shown in Fig. 5 for any wind direction. The maximum likelihood values for the wind speeds and directions would scatter approximately as the distance between the 5% and 95% curves. For winds below about 20 m/s the errors in the wind recoveries compared to data buoy winds would not be too great, especially if refinements are introduced for low winds. Any mesoscale variability as described in Part 8.5 would be masked by the effects of variability in the backscatter estimates. There would be eight terms to be evaluated in Eqn. (77) except that the logarithmic terms will be shown to be negligible in Part 13, to follow, so that they can be omitted.

12.2 Fifty kilometer resolution. Averages of the values for two adjacent areas parallel to the subsatellite track can be formed and grouped to represent an area 50 km by 50 km. The effects of sampling variability would be reduced as described above. With the logarithmic terms omitted, there would be eight terms in the applicable version of (77). How much this would reduce the scatter in the wind recoveries could be determined for any candidate model function.

12.3 One hundred kilometer resolution. From Fig. 5, the recoveries for high winds will not be very good for twenty five kilometer resolution. They may still not be good enough for

fifty km resolution. There is the possibility that horizontally polarized backscatter will not behave in the same way as vertically polarized backscatter and will continue to increase on past those speeds in these figures for winds as high as to be anticipated for the most intense extratropical cyclones in the historical record. If horizontally polarized backscatter behaves differently, more accurate high winds might be recoverable. The winds over the Antarctic Ocean from August to October may be the highest to be expected.

Improved computer based numerical weather predictions are one of the primary uses for the scatterometer winds. The present numerical models have yet to achieve 100 km resolution in the horizontal, and this, or even coarser resolution, is adequate for these models except near fronts. The high winds in an intense extratropical cyclone can easily extend over areas of 1500 kilometers in diameter, and a 100 km resolution for these winds would be an important contribution.

Sixteen 25 by 25 km areas grouped in sets of four see (Fig. 1) parallel to the subsatellite track would be the starting point. The values parallel to the track would be averaged and the four slightly different values of α, β and γ would be averaged and then be reduced by a factor of 4. The MLE would then be computed by using 16 terms (see Part 13). What would result for averages of four at upwind was discussed for Figs. 5a to 5d. These ranges of uncertainty as in Fig. 6 are probably better than the winds reported by ships of opportunity (Dischel and Pierson (1986)). If the model should verify approximately as shown, the

most extreme winds will be recovered with considerable accuracy.

12.4 Wave number aliasing and filtering. At any nominal scatterometer resolution, there will be contributions to the estimates of the vector wind from both the sampling variability of the backscatter estimates and from the mesoscale variability for each of the actual ocean areas sampled by a given antenna. These perturbations will alias into lower wavenumbers. The usual assimilation procedures for winds in numerical models will suppress these aliases to some extent. For some applications of these data, aliasing can be reduced by considering 125 km resolution involving twenty five 25 by 25 km areas with the recovered wind located at the center square. The 125 km resolution areas could be overlapped by 62.5 km to produce a smooth wind field. Again, special attention is needed near fronts.

The various tests described for the 25 by 25 km areas can all be extended in a straight forward way to these coarser resolution wind recoveries. The random intervals become much shorter, and the tests will reveal whether or no the coarser resolution results are good. Many of the hypotheses and tests described above can be modified to include the possibility that locally the values of t_R are nearly constant.

13. FURTHER CONSIDERATION OF THE MAXIMUM LIKELIHOOD ESTIMATES.

13.1 Discussion. The use of maximum likelihood estimators to obtain estimates of the unknown parameters from a random sample with an assumed probability density functions is a powerful method. For moderate and large samples, it often yields an estimator similar to the method of moments except that it is biased. Eqn. (77) is an application of the maximum likelihood concept in a way that is quite different from the usual applications of the concept.

There are other ways to estimate $\bar{U}$ and χ, and the superiority of the MLE for the model that will eventually be used is still to be proven. Tables 3.1 to 3.10 gave values for the MLE to be compared with $\sigma^o = \sigma^o_M$ as another choice for the estimate. The differences between σ^o_{MLE} and σ^o_M are quite small.

13.2 Maximum likelihood estimates for a wider range of σ^o. Given a random value of σ^o there are two possible estimates of the model values. One is σ^o_{MLE} and the other is σ^o_M. The quantity σ^o_{MLE} was computed in 5 dB steps from zero to -40 dB and expressed in dB for both a single estimate and averages of 4 estimates with α, β and γ reduced by a factor of 4. The values, D and $\bar{D}$ are the numerical results for

$$D = \sigma^o_{MLE(dB)} - \sigma^o_{M(dB)} \tag{81}$$

for single values of σ^o and

$$\bar{D} = \bar{\sigma}^o_{MLE(dB)} - \sigma^o_{M(dB)} \qquad (82)$$

for averages of four values. These differences (or effectively ratios) are given in Table 6 for the values of α, β and γ in Table 2. For high relative values of σ^o, the differences between the MLE and the expected value are small compared to the ranges of the random intervals that have been obtained.

A strange result is that formally Eqn. (24) for low values of σ^o can have a maximum for a negative value of σ^o_M. This can be shown by substituting $\sigma^o = 0$ into (24). The natural logarithm becomes $\ln(1 + (\beta/\gamma)\sigma^o_M + (\alpha/\gamma)(\sigma^o_M)^2)$ and for slightly negative values of σ^o_M the β/γ term dominates. The theory is then contradicted by the physics and the alternate choice, mentioned above, namely $\sigma^o_{MLE} = 0 = \sigma^o_M$ is correct.

Eqn. (77) has the disconcerting property that one of its maxima will not be exactly at the input wind speed and direction if the random variables are replaced by their expected values throughout from a model. Since the values for the maximum likelihood estimates differ in almost a negligible way from the expected values and since the random interval for a given sample value are much much larger than the difference between σ^o_{MLE} and σ^o_M, it seems that the terms in Eqn. (77) involving the logarithms can be dropped in the search for the winds that fit the model.

The new modified estimator would need a new name. What

TABLE 6a VALUES OF THE DIFFERENCES D = $\sigma^o_{MLE(dB)} - \sigma^o_{M(dB)}$ FOR THE RANDOM VARIABLE σ^o IN DB FOR INCIDENCE ANGLES, θ IN DEGREES, FROM 15.6° TO 59.1°. NEG = MLE NEGATIVE.

σ^o (dB) \ θ	15.6° D	19.9° D	24.7° D	31.4° D	35.4° D	41.0° D	46.0° D	50.5° D	55.7° D	59.1° D
0	-0.082	-0.070	-0.073	-0.073	-0.075	-0.078	-0.082	-0.084	-0.091	-0.100
-5	-0.082	-0.071	-0.073	-0.073	-0.075	-0.078	-0.082	-0.085	-0.091	-0.100
-10	-0.088	-0.071	-0.074	-0.073	-0.076	-0.078	-0.082	-0.085	-0.091	-0.100
-15	-0.223	-0.133	-0.075	-0.074	-0.076	-0.078	-0.082	-0.085	-0.092	-0.100
-20	-0.605	-0.316	-0.133	-0.074	-0.076	-0.079	-0.082	-0.085	-0.092	-0.101
-25	-2.219	-1.080	-0.363	-0.133	-0.088	-0.088	-0.088	-0.086	-0.093	-0.102
-30	NEG	-4.949	-1.136	-0.410	-0.267	-0.178	-0.133	-0.088	-0.133	-0.178
-35	NEG	NEG	-5.376	-1.308	-0.862	-0.410	-0.363	-0.267	-0.315	-0.458
-40	NEG	NEG	NEG	-7.215	-3.469	-1.427	-1.080	-0.758	-0.916	-1.550

TABLE 6b VALUES OF THE DIFFERENCES $\bar{D} = \sigma^o_{MLE(dB)} - \sigma^o_{M(dB)}$ WITH $\bar{D}$ FOR AVERAGES OF FOUR FOR THE RANDOM VARIABLE $\bar{\sigma}^o$ IN DB FOR INCIDENCE ANGLES, θ IN DEGREES, FROM 15.6^o TO 59.1^o. NEG = MLE NEGATIVE.

$\bar{\sigma}^o$ (dB) θ	15.6^o $\bar{D}$	19.9^o $\bar{D}$	24.7^o $\bar{D}$	31.4^o $\bar{D}$	35.4^o $\bar{D}$	41.0^o $\bar{D}$	46.0^o $\bar{D}$	50.5^o $\bar{D}$	55.7^o $\bar{D}$	59.1^o $\bar{D}$
0	-0.021	-0.018	-0.018	-0.018	-0.019	-0.020	-0.021	-0.021	-0.024	-0.026
-5	-0.021	-0.018	-0.018	-0.018	-0.019	-0.020	-0.021	-0.021	-0.024	-0.026
-10	-0.021	-0.018	-0.018	-0.018	-0.019	-0.020	-0.021	-0.021	-0.023	-0.026
-15	-0.021	-0.018	-0.019	-0.018	-0.019	-0.020	-0.021	-0.022	-0.024	-0.026
-20	-0.132	-0.044	-0.019	-0.019	-0.020	-0.020	-0.021	-0.022	-0.024	-0.026
-25	-1.410	-0.223	-0.044	-0.019	-0.020	-0.020	-0.021	-0.022	-0.024	-0.026
-30	-1.612	-0.758	-0.223	-0.044	-0.044	-0.020	-0.021	-0.022	-0.024	-0.026
-35	-2.011	-3.280	-0.810	-0.269	-0.188	-0.088	-0.044	-0.044	-0.044	-0.088
-40	NEG	NEG	-3.469	-0.970	-0.605	-0.269	-0.223	-0.133	-0.118	-0.316

should it be? Can it be proved to be superior to Eqn. (77)? Are the differences between the winds recovered by (77) and by (77) with the logarithmic terms omitted so small that the superiority of one over the other cannot be demonstrated by comparisons with conventionally measured winds? Answers to these questions are still to be determined.

The important and basic feature of (77) is still retained if the logarithmic terms are omitted. The denominators of the four remaining terms, and as extended to lower spatial resolution all similar terms, are a function of the model values and not the sample values. This assigns the proper weights to each term in the sum and places greater emphasis on the terms with the lowest variance.

14 SUMMARY

14.1 The probability density function for backscatter as a random variable. The PDF for backscatter estimates is very different from the usual normal PDF in that the variance is a known function of the first moment (or mean). This feature is used in several different ways to obtain statistics, with appropriate probabilities, for the interpretation of models for the expected value of the backscatter as a function of polarization, incidence angle, aspect angle and wind speed.

The backscatter values obtained by a scatterometer are random variables. These random variables may either be completely independent in the probability sense from one estimate to the next or partially correlated because the unknown errors for the calculation of σ^o as a result of orbit and attitude uncertainties are slowly varying along the orbit. A test to find out whether or not successive values of σ^o are truly independent, or partially correlated, has been devised.

Statistical estimation procedures require that all calculations be based on sample values. It is usually also required that the sample values be truly random and independent. Time series theory, which involves spectra and cross spectra, is needed if the successive random variables are not white noise; i.e. independent in the probability sense and normally distributed.

Quantities calculated from random variables that do not involve the unknown parameters of an assumed probability density function can be used to determine either point estimates for the unknown parameters or intervals with random end points with known probabilities of containing the unknown parameters. Such quantities are statistics. All of the above analysis is based on the calculation of various statistics.

14.2 Recovering wind speed and direction estimates. Given a model for the expected values of the backscatter as a function of polarization, wind speed, wind direction and incidence angle, the constraints imposed by the model are imposed on a random sample of backscatter estimates so as to maximize the probability that the independent sample values came from PDF's with expected values and variances determined by the model. The result is similar to a maximum likelihood estimate in form, but it is based on products of at least four different PDF's.

The resulting equation contains terms that involve the natural logarithm of the variance, which would follow from an exact application of probability theory. However, in general, maximum likelihood estimators can be biased. Calculations of the maximum likelihood estimates for one sample and for the average of four samples show that the maximum likelihood estimates differ negligibly from the expected value of the random variable. It is concluded that the logarithmic terms have a small effect on the estimates of $\bar{U}$ and χ and that they introduce other undesirable theoretical features. They can be left out of the equation.

15 ACKNOWLEDGEMENTS

This research was supported by the National Aeronautics and Space Administration (contract NAGW-690) and by the Jet Propulsion Laboratory (contract 957714-02/CIT/JPL). Dr Chong-Yung Chi provided the data for Tables 1 and 2.

16 REFERENCES

Bahar, E., Review of the full wave solutions for rough surface scattering and depolarization: Comparisons with geometric and physical optics, perturbation and two scale hybid solutions. J. Geophys. Res. 92, C5, 5209-5225, 1987.

Banner, M. L., and E. H. Fooks, On the microwave reflectivity of small-scale breaking water waves. Proc. R. Soc. London, Ser. A, 399, 93-109, 1985.

Chi, C. Y., D. G. Long and F. Li, Radar backscatter measurement accuracies using digital Doppler processors in spaceborne scatterometers, IEEE Trans. Geoscience and Remote Sensing GE-24, 3, 426-437, 1986.

Chi, C. Y., D. G. Long and F. Li, Round-off noise analysis for digital signal power processors using Welch's power spectrum estimation. IEEE Trans on Acoustics, Speech and Signal Processing, ASSP-35, 6, 784-795, 1987.

Dischel, R. S., and W. J. Pierson, Comparisons of wind reports by ships and data buoys. Proc. MDS '86, Marine Data Systems International Symposium, Marine Tech. Soc. Gulf Coast Section, 447-466, 1986.

Donelan, M. A., The dependence of the aerodynamic drag coefficient on wave parameters. in Proceedings of the First International Conference on Meteorology and Air Sea Interaction of the Coastal Zone, 381-387, American Meteorological Society, Boston, Mass., 1982.

Donelan, M. A., and W. J. Pierson, Radar scattering and equilibrium ranges in wind-generated waves with application to scatterometry, J. Geophys. Res. 92, C5, 4971-5030, 1987.

Douglas, B. C., D. C. McAdoo and R. E. Cheney, Oceanographic and geophysical applications of satellite altimetry. Rev. Geophys. 25, 5, 875-880, 1987.

Duffy, D. G., and R. Atlas, The impact of SEASAT-A scatterometer data on the numerical prediction of the QE-II storm, J. Geophys. Res., 91(C2), 2241-2248. 1986.

Durden, S. L., and J. E. Vesecky, A physical radar cross section model for a wind driven sea with swell, IEEE J. Oceanic Eng., OE-10(4), 445-451, 1985.

Fischer, R. E., Standard deviation of scatterometer measurements from space. IEEE Trans. Geosc. Electron, GE-10, 106-113, 1972.

Gilhousen, D. B., An accuracy statement for meteorological measurements obtained from NDBC moored buoys. Proc. MDS '86 Marine Data Systems International Symposium, Marine Tech. Soc. Gulf Coast Section, 198-204, 1986.

Guissard, A. C., Response to "Review of the full wave solutions for rough surface scattering and depolarization: Comparisons with geometric and physical optics, perturbation and two-scale hybrid solutions. J. Geophys. Res. 92, C5, 5225-5228, 1987.

Hasse, L., On Charnock's relation for the roughness at sea in Monahan, E. C. and G. MacNiocaill (eds) Oceanic Whitecaps and their Role in Air-Sea Exchange Processes, 49-55, D. Reidel Publishing Co., 1986.

Iwata, N., An algorithm of microwave backscattering from a perturbed sea surface in Toba Y and H. Mitsuyasu, eds., The Ocean Surface: Wave Breaking, Turbulent Mixing and Radio Probing, 283-286, D. Reidel Publishing Co., 1985.

Jones, W. L., L. C. Schroeder, D. H. Boggs, E. M. Bracalente, R. A. Brown, G. J. Dome, W. J. Pierson, and F. J. Wentz, The SEASAT-A satellite scatterometer: The geophysical evaluation of remotely sensed wind vectors over the ocean. J. Geophys. Res., 87(C5), 3297-3317, 1982.

Kwoh, D. S., and B. M. Lake, A deterministic, coherent, and dual-polarized laboratory study of microwave backscattering from water waves, I, Short gravity waves without wind, IEEE J. Oceanic Eng., OE-9(5), 291-308, 1984.

Lyzenka, D. R., A. L. Maffett, and R. A. Shuchman, The contribution of wedge scattering to the radar cross section of the ocean surface, IEEE Trans. Geosci. Remote Sens., GE-21(4), 502-505, 1983.

Mood, A. M., F. A. Graybeal and D. C. Boes, Introduction to the theory of statistics, Third Edition, McGraw Hill, New York, 564 pp. 1974.

Moore, R. K., and F. T. Ulaby, The radar-radiometer, Proc. IEEE 57, 4, 587-590, 1969.

Pierson, W. J. and R. E. Salfi, Monte Carlo studies of ocean wind vector measurements by SCATT: Objective criteria and maximum likelihood estimates for removal of aliases, and effects of cell size on accuracy of vector winds, NASA Contract. Rep., CR-165837-1, 282 pp. 1982.

Pierson, W. J., The measurement of the synoptic scale wind over the ocean, J. Geophys. Res., 88(C3), 1683-1708, 1983a.

Pierson, W. J. Highlights of the SEASAT-SASS program: A review in Allan, T. D. ed Satellite Microwave Remote Sensing. Ellis Harwood LTD., Chichester England, 69-86, 1983b.

Pierson, W. J., A Monte Carlo comparison of the recovery of winds near upwind and downwind from the SASS-1 model function by means of the sum of squares algorithm and a maximum likelihood estimator, NASA Contract. Rep., CR-3839, 62 pp., 1984.

Pierson, W. J., W. B. Sylvester, and R. E. Salfi, Synoptic scale wind field properties from the SEASAT-SASS, NASA Contract. Rep., CR-3810, 152 pp., 1984.

Pierson, W. J., W. B. Sylvester and M. A. Donelan, Aspects of the determination of wind by means of scatterometry and of the utilization of vector winds data for meteorological forecasts, J. Geophys. Res., 91(C2), 2263-2272, 1986.

Plant, W. J., A two-scale model of short wind-generated waves and scatterometry, J. Geophys. Res., 91(C9), 10735-10749, 1986.

Schroeder, L. C., D. H. Boggs, G. J. Dome, I. M. Halberstam, W. L. Jones, W. J. Pierson, and F. J. Wentz, The relationship between wind vector and normalized radar cross section used to derive SEASAT-A satellite scatterometer winds, J. Geophys. Res., 87, 3318-3336. 1982.

Valenzuela, G. R., Theories for the interacation of electromagnetic and oceanic waves-A review, Boundary Layer Meteorol. 13, 61-85, 1978.

Wentz, F. J., S. Peteherych, and L. A. Thomas, A model function for ocean radar cross section at 14.6 GHz, J. Geophys. Res., 89(C3), 3689-3704, 1984.

Wentz, F. J., L. A. Mattox, and S. Peteherych, New algorithms for microwave measurements of ocean winds: Applications to SEASAT and the special sensor microwave imager, J. Geophys. Res. 91(C3), 2289-2309, 1986.

Woiceshyn, P. M., S. Peteherych, M. G. Wurtele, D. H. Boggs, M. M. Borowski, G. F. Cunningham, A. Davies, and G. Muttitt, Cover photo: SEASAT scatterometer marine wind analysis, IEEE J. Oceanic Eng., OE-10(4), 342 pp, 1985.

Woiceshyn, P. M., M. G. Wurtele, D. H. Boggs, L. F. McGoldrick, and S. Peteherych, The necessity for a new parameterization of an empirical model for wind/ocean scatterometry, J. Geophys. Res., 91(C2), 2273-2288, 1986.

Woiceshyn, P. M., M. Wurtele, D. Anderson, D. Boggs, G. Cunningham, and P. Janssen, Wind field inference from ocean microwave backscatter: The problem as a whole IGARS '87, IEEE 87CH24329 Vol. II, 981-986, 1987.

NASA
National Aeronautics and Space Administration

Report Documentation Page

1. Report No.	2. Government Accession No.	3. Recipient's Catalog No.
NASA CR-4228		

4. Title and Subtitle	5. Report Date
Probabilities and Statistics for Backscatter Estimates Obtained by a Scatterometer With Applications to New Scatterometer Design Data	April 1989
	6. Performing Organization Code

7. Author(s)	8. Performing Organization Report No.
Willard J. Pierson, Jr.	
	10. Work Unit No.

9. Performing Organization Name and Address	11. Contract or Grant No.
CUNY Institute of Marine and Atmospheric Sciences The City College of New York Convent Ave. at 138th Street New York, NY 10031	NAGW-690
	13. Type of Report and Period Covered Contractor Report

12. Sponsoring Agency Name and Address	14. Sponsoring Agency Code
Oceanic Processes Branch National Aeronautics and Space Administration Washington, DC 20546-0001	EEC

15. Supplementary Notes

16. Abstract

The values of the NRCS, σ^o, obtained by a scatterometer are random variables whose variance is a known function of the expected value. The probability density function can be obtained from the normal distribution. Models for the expected value obtain it as a function of the properties of the waves on the ocean and the winds that generated the waves. Point estimates of the expected value, σ^o_M, are found from various statistics given the parameters that define the probability density function for each value. Random intervals are derived with a preassigned probability of containing the value, σ^o_M. A statistical test to determine whether or not successive values of σ^o are truly independent is derived. The maximum likelihood estimates for wind speed and direction are found, given a model for backscatter as a function of the properties of the waves on the ocean. These estimates are biased as a result of the terms in the equation that involve natural logarithms, and calculations of the point estimates of the maximum likelihood values are used to show that the contributions of the logarithmic terms are negligible and that the terms can be omitted.

17. Key Words (Suggested by Author(s))	18. Distribution Statement
Scatterometer Air-Sea Interaction Radar Backscatter Surface Winds	Unclassified - Unlimited Subject Category 32

19. Security Classif. (of this report)	20. Security Classif. (of this page)	21. No. of pages	22. Price
Unclassified	Unclassified	136	A07

NASA-Langley, 1989